

Helsinki University of Technology Department of Electrical and Communications
Engineering Laboratory of Electromechanics

Teknillinen korkeakoulu sähkö- ja tietoliikennetekniikan osasto sähkömekaniikan laboratorio
Espoo 2004

Report 72

MAGNETOELASTICITY, MAGNETIC FORCES AND MAGNETOSTRICTION IN ELECTRICAL MACHINES

Doctoral thesis

Anouar Belahcen

Dissertation for the degree of Doctor of Science in Technology to be presented with due permission of the Department of Electrical and Communications Engineering, for public examination and debate in Auditorium S4 at Helsinki University of Technology (Espoo, Finland) on the 27th of August, 2004, at 12 o' clock noon.

Helsinki University of Technology
Department of Electrical and Communications Engineering
Laboratory of Electromechanics

Teknillinen korkeakoulu
Sähkö- ja tietoliikennetekniikan osasto
Sähkömekaniikan Laboratorio

Distribution
Helsinki University of Technology
Laboratory of Electromechanics
P. O. Box 3000
FIN-02015 HUT
Tel. +358 9 451 2384
Fax. 0358 9 451 2991
E-mail: electromechanics@hut.fi

© Anouar Belahcen

ISBN 951-22-7183-4
ISSN 1456-6001

Picaset Oy
Helsinki 2004

Belahcen, A., **Magnetoelasticity, Magnetic Forces and Magnetostriction in Electrical Machines**, Doctoral thesis, Helsinki University of Technology, Laboratory of Electromechanics, Report 72, Espoo 2004, 115 p.

Keywords: magnetic force, magnetostriction, electrical machine, finite element analysis, vibration, magnetoelastic coupling.

Abstract

This thesis deals with the computation of magnetic and magnetostrictive forces, as well as with the magnetoelastic coupling in rotating electrical machines. *Magnetoelasticity* means here the interaction between the magnetic and elastic fields in the iron parts of a machine. *Magnetostriction* is the phenomenon by which an iron part changes its dimensions under the effect of a magnetic field.

The equations for magnetoelastic coupling are derived within the finite element time stepping analysis of rotating electrical machines. The elastic part of these equations is implemented into an existing program that handles the magnetic and circuit equations. Formulas for the calculation of magnetic and magnetostrictive forces are also derived. The implemented method is used to compute the vibrations of the stator core of rotating electrical machines under the effect of magnetic and magnetostrictive forces. The effect of coupling between the magnetic and elastic fields is also computed for these machines. Moreover, the effects of structural damping and of different approaches (quasi-static, dynamic, coupled and uncoupled) are illustrated.

The magnetostriction, as well as the magnetisation of electrical steel sheets, is measured within this work. The measurements are carried out using a modified version of the standard Epstein frame. The data obtained show a strong dependence on the applied mechanical stress. These results can be used not only in simulation but also for the determination of magnetoelastic coupling coefficients in some models of magnetoelasticity using coupled constitutive equations.

It is noticed that the quasi-static elastic approach is not accurate enough for the calculation of vibrations in these machines. The structural damping plays an important role in determining the amplitude of vibrations; however, within realistic values of damping, these vibrations are almost the same.

The magnetostriction damps the vibrations at some frequencies and increases them at others. The velocities of vibrations at some frequencies are found to be 8 to 9 times larger when the magnetostriction is taken into account. The magnetoelastic coupling between the displacement and the magnetic fields in the stator core of electrical machines increases the amplitudes of vibrations by about 17 % at some frequencies for the large machine, while its effect on the vibrations of the small stator is less than 0.5 %.

Preface

This work has been conducted in the Laboratory of Electromechanics at the Helsinki University of Technology within a project financed by the Academy of Finland.

First, I express my gratitude to Prof. Tapani Jokinen, former head of the Laboratory, and Prof. Asko Niemenmaa, head of the Laboratory, for giving me the chance to carry out this study at the Laboratory and under their supervision. I am also obliged to Prof. Antero Arkkio for providing me with valuable guidance and fruitful discussions.

I thank colleagues in ABB Oy and at VTT Industrial Systems for their fruitful discussions and close co-operation.

I also thank the research group “magnetostriction” from the Laboratory of Electromechanics for their close co-operation and understanding, as well as for the help they provided in getting the measurement results used in this work.

Thanks are also due to the staff of the Laboratory of Electromechanics for making the time I spent with them so pleasant and for their good humour and sound advice.

I finally thank my little daughters Delila and Amira and my wife Hannele for the understanding and patience they showed me during the years of this work.

Espoo, February 2004

Anouar Belahcen

Contents

Abstract.....	3
Preface	4
Contents	5
List of symbols and abbreviations	7
1 Introduction.....	10
1.1 Background.....	10
1.2 Aim of the research.....	12
1.3 Scope of the research.....	12
1.4 Scientific contribution	14
1.5 Conclusions	14
2 Literature review	15
2.1 Magnetoelasticity.....	15
2.2 Magnetostriction in rotating electrical machinery.....	20
2.3 Conclusions	22
3 Forces.....	23
3.1 Terminology	23
3.2 Reluctance forces.....	24
3.3 Magnetostrictive forces	26
3.4 Derivation of forces	27
3.5 The method of magnetostrictive stress	32
3.6 Maxwell stress tensor	34
3.7 Example of force calculation.....	37
3.7.1 Nodal forces	37
3.7.2 Magnetostriction forces.....	39
3.7.3 Maxwell stress method.....	42
3.8 Conclusions	45
4 Magnetoelastic coupling	46
4.1 Magnetic field.....	46
4.2 Elastic field.....	48
4.2.1 Equilibrium equations	48
4.2.2 Boundary conditions	51
4.2.3 Time discretisation	53
4.3 Magnetoelastic coupling.....	54
4.3.1 Indirect coupling	55
4.3.2 Direct coupling.....	57
4.3.3 Hybrid method.....	57
4.4 Conclusions	62
5 Measurements	63
5.1 Measurement of magnetisation.....	63
5.2 Measurement of magnetostriction	66
5.3 Calculation of single-valued curves	68
5.4 Calculation of magnetostriction from measurements.....	69
5.5 Conclusions	70
6 Validation.....	71
6.1 Structure and construction of the device	71
6.2 Measurements and simulations.....	73
6.3 Conclusions	80

7 Simulations and results	81
7.1 Synchronous machine	82
7.1.1 Quasi-static case	84
7.1.2 Dynamic case	87
7.2 Induction machine	92
7.2.1 Dynamic and coupled cases	94
7.3 Conclusions	99
8 Discussion and conclusions	100
8.1 Importance of the work	100
8.2 Accuracy matters and computation time	102
8.3 Future work	104
Appendix A: Parameters of the validation device	105
Appendix B: Result of measurements and simulations of the test device	106
Appendix C: Parameters of the analysed synchronous machine	109
Appendix D: Parameters of the analysed induction machine	110
References	111

List of symbols and abbreviations

<i>A</i>	Magnetic vector potential
<i>a</i>	Coefficient of cubic spline approximation / two dimensional Fourier series
<i>B</i>	Magnetic flux density vector, strain-displacement matrix in mechanics
<i>b, c, d</i>	Coefficient of two-dimensional Fourier series
<i>C</i>	Mechanical damping matrix, coupling matrix in magnetic problem
<i>D</i>	Electric flux density vector, coupling matrix in magnetic problem
<i>E</i>	Electric field strength, stress-strain matrix
<i>E</i>	Modulus of elasticity
<i>F</i>	Force
<i>f</i>	Force density
<i>G</i>	Coupling matrix in magnetic problem
<i>H</i>	Magnetic field strength, coupling matrix in magnetic problem
<i>I</i>	Current
<i>J</i>	Current density
<i>J</i>	Jacobian matrix in FEM
<i>K</i>	Circuit connection matrix in FEM
<i>l</i>	Length
<i>M</i>	Mass matrix
<i>m, n</i>	Spatial and temporal harmonic order
<i>N</i>	Shape function
<i>P</i>	Jacobian matrix of Newton iteration
<i>p</i>	Pole-pairs number
<i>R</i>	Resistance
<i>R</i>	Load vector in elasticity
<i>r</i>	Position, radius
<i>S</i>	Surface
<i>S</i>	Magnetic stiffness matrix
<i>T</i>	Torque, transformation matrix between two references
<i>t</i>	Time
<i>U</i>	Voltage
<i>u, v, w</i>	Displacements/ components of displacements in different directions
<i>V</i>	Volume, voltage

W	Energy, work
w	Weighting factor for numerical integration
x, y, z	Nodal coordinates
α, β	Coefficients of the Rayleigh damping
Δ	Element area in FEM
Δt	Time step
ε	Strain
κ	Mechanical damping parameter
φ	Angle
ϕ	Reduced electric scalar potential, flux, angular position
λ	Relative elongation (Magnetostriction)
ν	Reluctivity, Poisson ratio
ω	Angular velocity
ρ	Resistivity, mass density
θ	Angle
μ	Magnetic permeability
μ_0	Magnetic permeability of vacuum
$\boldsymbol{\tau}$	Maxwell stress tensor
τ	Shear stress
η, ξ	Coordinates in the reference element
γ, β	Constants defining the time integration scheme in dynamics
∇	Gradient operator
$\nabla \cdot$	Divergence operator
$\nabla \times$	Curl operator
Ω	Volume
AT	Ampere turns
det	Determinant of matrix
FE	Finite Element
FEM	Finite Element Method
DFT	Discrete Fourier Transform
ms	Magnetostriction

\dot{u}, \ddot{u} stand for, respectively, the first and second order derivatives of u with respect to time.

The subscripts x and y within a vector quantity refer respectively to the x- and y-component of that quantity in a Cartesian coordinate system.

The subscripts n and t within a vector quantity refer respectively to the normal and tangential component of that quantity with respect to a given surface.

The subscripts r and φ within a vector quantity refer respectively to the radial and circumferential component of that quantity in a polar coordinate system.

The subscript ij is used for the component in i^{th} row and j^{th} column of matrices and tensors.

The subscripts \parallel and \perp within a vector quantity refer to the components of that quantity respectively parallel and orthogonal to the direction of the flux density vector.

Superscript e within a quantity refers to the same quantity at element level.

The quantities representing vectors, tensors and matrices are denoted by bold face in the text.

1 Introduction

The aim of this chapter is to present the background of the research work reported below, as well as its scope, aims and scientific contributions in brief. The need for a study such as this is stated and the reader introduced to the main areas of the research undertaken.

1.1 Background

The magnetic and elastic properties of ferromagnetic and other materials depend on each other. The different couplings between these properties are called magnetoelastic effects. These effects can be separated into two main categories, namely direct effects and inverse effects. The best-known direct effects are the volume, Joule and dipolar magnetostriction, as well as the ΔE -effect and direct *Wiedemann effect*. In the literature, some of the inverse effects are referred to by special terms such as *Villari effect* for the inverse of Joule magnetostriction and *Matteucci effect* for the inverse of the Wiedemann effect. These terms are explained in greater detail in Chapter 2.

The magnetostriction itself, which is one of the subjects of this work, is the phenomenon by which a ferromagnetic sample deforms due to magnetic interactions that can be either within the sample itself (spontaneous magnetostriction) or caused as a consequence of an external magnetic field (forced magnetostriction). Both kinds of magnetostriction have isotropic (volume magnetostriction) and anisotropic (Joule and dipolar magnetostriction) components. The effects of the Joule and dipolar magnetostriction on the vibrations and acoustic noise of electrical machines are the only ones of interest in this work.

Rotating electrical machines are designed at many levels and from a number of different points of view. The development of powerful computation engines in previous decades allowed for the use of numerical methods in both the mechanical and electromagnetic design. The finite element method (FEM) has shown its usefulness and powerfulness as one of these methods.

Electrical machines are usually analysed separately for mechanical and electromagnetic behaviour. On the one hand, the electromagnetic analysis deals with the magnetic field in the core and air gap of the machine, as well as with related variables such as voltages, currents, power and torque. On the other hand, the mechanical analysis deals with the elasticity and mechanical structure of the machine. In this case, the vibrations of the machine, as well as the mechanical dimensioning of

different parts, are of interest. This approach is not sufficient when the design and analysis are concerned with the vibrations and noise of such a machine, or when the magnetic field is coupled with the mechanical displacement and stress. This, for example, is the case when the magnetostriction is to be taken into account or when the deformations in the stator core and teeth of the machine affect the magnetic field distribution and/or the vibrational behaviour of the stator core.

Traditionally, the problem of acoustic noise from rotating electrical machinery has been regarded as caused by separate phenomena. These phenomena are the cooling-air flow, the friction between different parts of the machine (mainly in the bearings and brushes) and the vibrations of the stator core under the effect of magnetic forces. Furthermore, the magnetostriction in the core of power transformers is known to be a major cause of low frequency acoustic noise. The effect of magnetostriction on vibrations and the acoustic noise of rotating electrical machinery has also been dealt with by some research groups. Some of the research on the subject showed that the magnetostriction might have a great effect on the vibrational behaviour of rotating electrical machines (Låftman 1995, Witczak 1996). Others believe that the magnetostriction does not have considerable effect on the noise of this kind of machinery (Delaere 2002).

A rigorous simulation tool and an extensive analysis of the effect of magnetostriction on the vibrations and the acoustic noise in rotating electrical machines are needed to confirm the previous results. Regardless of the errors induced by the FEM, it has proven to be an efficient tool when the geometry of a problem is too complicated to be handled by analytical methods. This is the case when dealing with the magnetic and mechanical aspects of electrical machines. The magnetostriction can be dealt with by including a model of it into FE analysis and solving the coupled magnetoelastic equations with a time stepping FE method.

The problem of rotating electrical machinery is a three-dimensional one, the solution of which requires huge calculation times and models that are still impossibly large. With a few simplifications, the analysis can be reduced to a two-dimensional one with acceptable accuracy. In this work, the effect of magnetostriction on the noise and vibrations in rotating electrical machines is numerically analysed by solving boundary value problems, which are integrated in time (this is known as *time stepping FE method*). The FE model is a two-dimensional one combined with the circuit equations for the windings of the machine. This work also contributes to the understanding

of magnetoelastic phenomena in magnetic material in general and in rotating electrical machines in particular.

The magnetic and magnetoelastic properties of magnetic materials differ from one material to another. Some properties, such as losses and magnetisation, are defined within existing standards, but most of the properties related to magnetoelastic coupling are not defined, neither are they known. Only old-materials measurements are available. For this reason, measurements of these properties are needed for materials that are nowadays standard.

1.2 Aim of the research

The aim of this research is to find out how the magnetostriction and magnetoelastic coupling affect the vibrations and noise of rotating electrical machines. The work consists of developing a model for the magnetostriction and the incorporation of this into an existing magnetic FE program, as well as building an elastic FE program that can be coupled with the magnetic one.

The developed simulation procedures are used to investigate the effect of magnetostriction and stator deformations on the solution of the magnetic and displacement fields of induction and synchronous machines.

Any model of magnetostriction requires magnetostriction data for the electrical steel sheets. These data are not available from the manufacturer and need to be carefully measured. The measurements needed for the acquisition of these data are also a major part of this work.

Finally, a validation device is built to estimate the validity and the accuracy of the developed magnetoelastic model. This device is constructed in such a way that it reproduces the magnetic field distribution in rotating electrical machines, but without causing the so-called Maxwell or reluctance magnetic forces.

1.3 Scope of the research

The magnetoelastic coupling is understood here as the reciprocal effect between the magnetic field and the displacement field. An obvious and direct coupling occurs through the magnetic forces as loads for the elastic field. Other kinds of coupling are the Villari effect and the effect of geometrical

changes on the magnetic field and magnetostriction. These aspects of the magnetoelasticity are explained in the appropriate chapters of this thesis.

Some assumptions and simplifications are made within this work. First, the hysteresis, anisotropy and temperature-dependency of the materials are ignored. Second, the volume magnetostriction is not taken into account and the magnetic and elastic fields are supposed to be two-dimensional. These assumptions are made for the following reasons.

The time constant of the thermal problem is larger than that of the magnetic and elastic problem; thus the thermal problem can be treated separately if necessary. The iron core of rotating electrical machines is usually manufactured in a way that minimises the anisotropic effect (transposing of iron sheets). They can be treated as isotropic with acceptable accuracy. The hysteresis is present in all iron sheets and so in rotating electrical machines. However, its treatment requires much more work and its benefit is minor for the study of noise and vibrations. These simplifications are made in accordance with the motivation of this work; namely the study of the effect of magnetostriction on noise and vibrations in rotating electrical machines.

The history and background of magnetostriction, as well as a brief literature review on the modelling of magnetostriction and its effects on the vibrations and noise of electrical machinery, are given in Chapter 2. In Chapter 3, different methods for calculating the magnetic and magnetostrictive forces are presented and used in either a simple model or a more complex calculation. The methods adopted in this work are developed in more detail. Chapter 4 deals with the methods for the magnetoelastic coupling. In this chapter, a short review of the calculation of the magnetic field in electrical machinery using the FE method and time stepping is given; the main aspects of the elastic field calculation are also presented. The coupling between these two fields is also developed within FEM. In Chapter 5, the measurement set up for the magnetic properties of electrical steel sheets is presented, together with the results of these measurements. These original results are the ones used in the calculations of Chapters 6 and 7. A validation device is constructed and measured and then simulated using the methods developed in Chapters 3 and 4. The results of these measurements and simulations are presented in Chapter 6. In Chapter 7, the simulations of a synchronous and an induction machine are presented. Conclusions are drawn in Chapter 8, where the validity of the model and the results obtained are discussed.

1.4 Scientific contribution

Both the development of magnetoelastic formulas and the construction of the simulation tools based on these formulas are original contributions to the development and understanding of magnetoelasticity, particularly in rotating electrical machines.

The stress dependency of magnetostriction is taken into account in the simulation of electrical machines and its effect on the vibrations is estimated. The stress-dependent magnetostriction is shown to increase the vibrations at almost all the frequencies. The effect of magnetostriction on the vibrations of electrical machines is established and shown to be of great importance.

The magnetoelastic coupling phenomenon is shown to exist in rotating electrical machines. The magnetoelastic coupling causes considerable changes in the velocity of vibrations of the large stator; its effect on the vibrations of the small stator is not very important. The existence of the magnetoelastic coupling phenomenon makes the traditional calculation of vibrations of electrical machines less accurate in comparison with the coupled model presented. Moreover, the simulation results show that the quasi-static elastic approximation is not sufficiently accurate to describe the vibrational behaviour of rotating electrical machines.

This work also contributes to the understanding of magnetostriction and magnetoelastic phenomena in electrical machines. The measured magnetostriction and magnetisation and their strong dependence on the applied mechanical stress are results that can be used not only in simulations as input data but also for the determination of magnetoelastic coupling coefficients in some models of magnetoelasticity using coupled constitutive equations (local coupling).

1.5 Conclusions

The background and need of this study have been stated, its aim clarified and scope set out. The scientific contributions are emphasised and explained.

Due to the controversial results on the effect of magnetostriction and magnetoelastic coupling on the vibrations of electrical machines, more research on the subject is needed. The stress dependency of magnetostriction has to be taken into account and rigorous simulation tools have to be constructed.

2 Literature review

The aim of this chapter is to introduce in more detail the phenomena related to magnetoelasticity as they are described in the literature. A review of different models of magnetostriction and magnetoelasticity is also presented in order to define the state of art in this field and the improvements needed to achieve an accurate and rigorous model of magnetostriction and magnetoelastic coupling and to acquire adequate computation tools.

2.1 Magnetoelasticity

W. P. Joule discovered the magnetostriction of iron in 1842. Since then, many phenomena related to magnetoelasticity of iron and iron alloys have been discovered and studied. Among such phenomena that may be mentioned here are volume magnetostriction, form effect, ΔE effect and the direct Wiedemann effect. These phenomena also have inverse effects, one of which is the Villari effect – the inverse of Joule magnetostriction.

Magnetostriction (du Trémolet 1993)

By *magnetostriction* is meant the deformation of a sample due to magnetic interactions. It can be divided into spontaneous and forced magnetostriction. The former is due to internal magnetic interaction in a sample, while the latter is due to magnetic interaction between the sample and an externally applied magnetic field.

When iron is cooled down from a high temperature through its Curie temperature, an anomalous isotropic expansion is observed near the Curie temperature. This slightly magnetic field-dependent anomaly associated with the magnetism of iron (and other magnetic substances) is called *volume magnetostriction*. This is the isotropic aspect of the spontaneous magnetostriction. Now, if a magnetic field is applied to the iron sample, an additional anisotropic deformation that stretches or shrinks the sample in the direction of the magnetic field is observed. This field-dependent phenomenon is called *Joule magnetostriction*; it is measured in microns per metre ($\mu\text{m}/\text{m}$) and is the anisotropic aspect of the forced magnetostriction.

There is also a deformation associated with the Joule magnetostriction in the orthogonal direction to the field. This has the opposite sign and half the amplitude and is called *transverse magnetostriction*.

The Joule and transverse magnetostriction do not change the volume of the sample. At higher magnetic fields, the Joule and transverse magnetostriction are accompanied by a small change in volume, which is the isotropic part of the forced magnetostriction.

Joule magnetostriction and transverse magnetostriction are nonlinear phenomena that reach saturation at the same level as the technical saturation of the magnetisation. Fig. 1 illustrates the spontaneous volume magnetostriction and the forced Joule and transverse magnetostriction of a spherical sample.

The above-mentioned types of magnetostriction occur at different states of magnetisation. Fig. 2 illustrates the occurrence of these phenomena at different values of the magnetic field strength. The occurrence of forced volume magnetostriction at only very high values of the magnetic field explains the exclusion of this phenomenon from the scope of this thesis.

For electrical steel and iron, the maximum value of Joule magnetostriction is of the order 1 to 10 $\mu\text{m}/\text{m}$. The highest value of magnetostriction is of the order of 1000-2000 $\mu\text{m}/\text{m}$ and occurs for the $\text{Tb}_{0.3}\text{Dy}_{0.7}\text{Fe}_2$ alloy known as Terfenol-D. The Joule magnetostriction is also stress dependent. For iron and iron alloys, this dependency is complicated and, at its extremes, changes the sign of magnetostriction so that, at high values of unidirectional stress, the magnetostriction is negative.

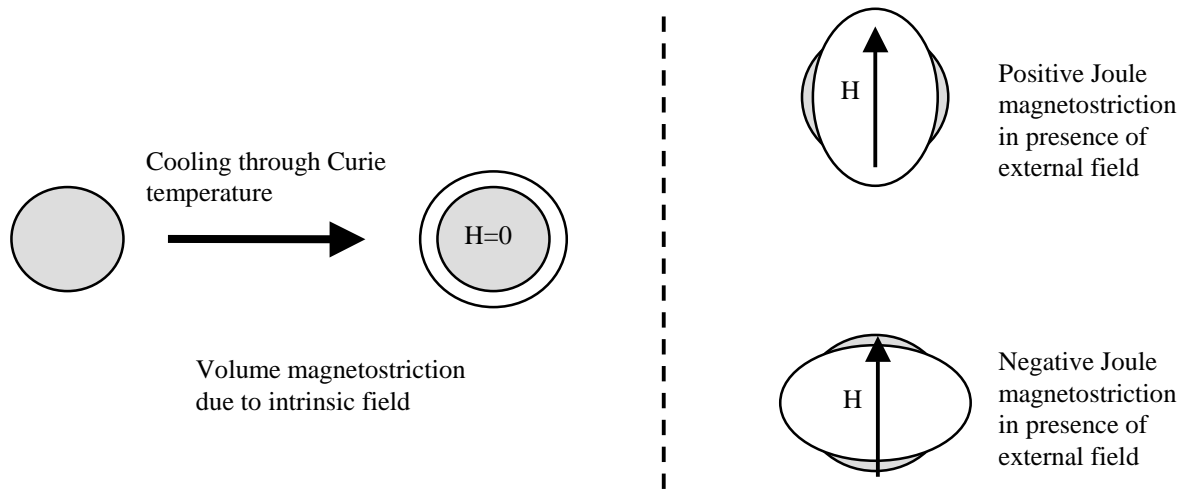


Fig. 1: Difference between volume and Joule magnetostriction in a spherical sample.

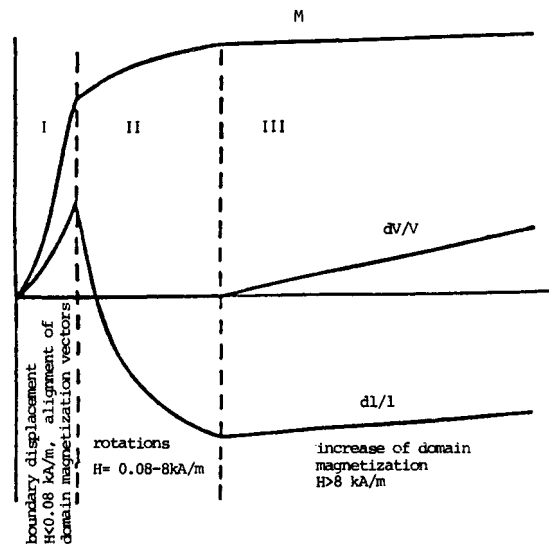


Fig. 2: Magnetisation curve and magnetostriction as a function of magnetic field strength. dV/V is the volume magnetostriction and dl/l the Joule magnetostriction (Ruuskanen 1987).

Fig. 3 illustrates the effect of mechanical stress on the magnetostriction of polycrystalline ferromagnetic metal. The meaning of the dotted line in Fig. 3 is not clear in the original reference.

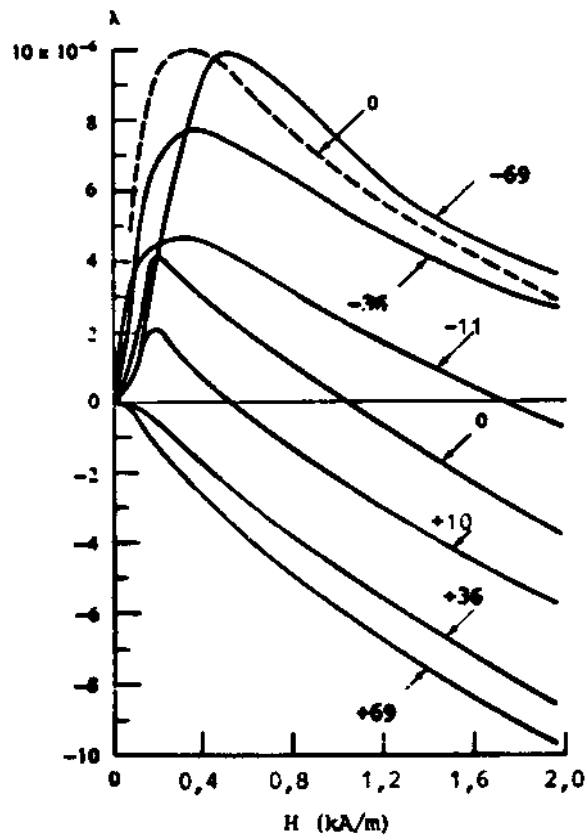


Fig. 3: Effect of mechanical stress on magnetostriction; stresses are in MPa (Ruuskanen 1987).

Villari effect or stress-dependent magnetisation (Bozorth 1951, du Trémolet 1993)

The application of a mechanical stress to magnetic material changes its magnetic properties. Such changes occur in, for example, the magnetisation curve of iron and make the magnetic induction B different for a given magnetic field at different applied stresses. This phenomenon is known as the Villari effect or inverse magnetostriction. It is illustrated in Fig. 4.

The magnetic behaviour of iron under applied mechanical stress is, by comparison with that of other magnetic materials, one of the most complicated phenomena. However, this is not a coincidence, since the magnetostrictive behaviour of iron is just as complicated as its inverse phenomena. Indeed, the Joule magnetostriction changes with applied mechanical stress. These changes are due mainly to two mechanisms: a macroscopic one due to the magnetoelastic energy, which modifies the anisotropy of the material without changing its magnetostriction coefficients, and a microscopic one due to a change in the interatomic distances and symmetry lowering. This last mechanism causes changes of the magnetostriction coefficients. Moreover, the order in which the stress is applied with respect to the magnetic field affects the final values of the magnetic induction and magnetostriction.

The other magnetoelastic phenomena mentioned above are explained in the specialised literature (Bozorth 1951, du Trémolet 1993), but are not within the scope of this study; neither are the other changes of magnetic properties with temperature. Almost all magnetic phenomena have some hysteresis; this aspect is not of concern in this work, neither is the magnetic and elastic anisotropy of the material.

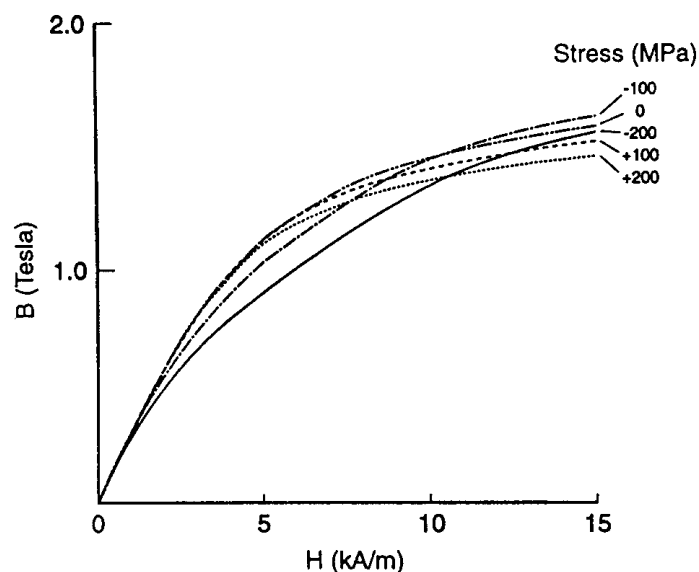


Fig. 4: Effect of mechanical stress on the magnetisation of ferromagnetic metal (Jiles 1994).

The magnetostrictive effect in magnetic materials is a useful phenomenon as it is used in actuators, transducers and devices for ultrasound generation and detection, as well as in magnetostriction motors (du Trémolet 1993). This same phenomenon becomes parasitic when the noise and vibrations of electrical machines are considered. Indeed, the low frequency monotone noise from power transformers, inductors and chokes is due mainly to magnetostriction (Thompson 1963). The effect of magnetostriction on the noise and vibrations of rotating electrical machine is still a matter of controversy.

Models of magnetostriction

The models for magnetostriction can be separated into two main frames: elongation-based and force-based. The elongation-based models use the magnetostrictive elongation as the primary quantity. In this approach, the magnetostriction data is a model of the relative elongation versus magnetic induction. The model can be a look-up table or a more or less complicated polynomial fit of measured data (Låftman 1995, Benbouzid 1997, Body 1997, Lundgren 1997, Gros 1998, Garvey 1999, Dapino 2000, Delaere 2002). The force-based models are by far the most common ones. They use magnetostrictive forces as the primary quantity. In this approach, the forces are calculated in a similar manner for both the conventional magnetic effect (called reluctance forces or Maxwell forces) and the magnetostrictive effect (called magnetostrictive forces) (Witczak 1995, 1996, Besbes 1996, 2001, Mohammed 1999, 2001, 2002, Vandeveldel 2001).

The force calculation is commonly based on the principle of virtual work locally applied to an FE mesh. This principle, also known as the local Jacobian derivative, was presented by Rafinéjad (1977) and developed by Coulomb (1983) followed by Besbes et al. (1996) and Mohammed et al. (1999). In the work of Coulomb (1983), the force is calculated as total magnetic force on rigid bodies. Bossavit (1992) is actually the first who presented the notion of force field based on the principle of virtual work. He worked out his method using the differential geometry. The merit of Besbes et al. (1996) was to rewrite the force field using vector calculus and apply them to nodal elements in 2-D problems. This method is developed further in Chapter 3.

Some force-based models use different approaches to calculate the forces; they may be based on the concept of short- and long-range forces presented by Vandeveldel (1998), for example.

More complicated models, mainly based on the work of du Trémolet (1993), have also been presented where the magnetoelastic coupling is developed from the laws of thermodynamics. The problem of this approach is that the polycrystalline iron has a structure so complicated that makes it almost impossible to deal with without strong simplifications (Beckley 2000). Other models have also been presented (Witczak 1995, 1996, Reyne 1987); they are based on different forms of the Maxwell stress tensor summarised in the work of Melcher (1981).

In most of the FE models of magnetostriction and magnetoelastic coupling encountered, the energy is separated into magnetic energy and elastic energy, the sum of which is considered as the magnetoelastic energy of the coupled system. In a recent paper, Besbes et al. (2001) presented a form of magnetoelastic energy that explicitly takes the coupling into account. This approach is quite new and its validity has to be demonstrated on simple models before it can be used for more complicated systems such as rotating electrical machines.

Models of stress-dependent magnetisation

The change in magnetisation due to applied mechanical stress has been measured and modelled by many researchers (Bozorth 1951, du Trémolet 1993, Jiles 1994, 1995, Witczak 1996). For electrical steel and iron, this behaviour is quite complicated since these materials behave in different ways at different levels of magnetisation. In general, the effect of unidirectional stress on magnetisation depends on the magnetostriction of the material (Bozorth 1951). Materials with positive magnetostriction expand under the effect of a magnetic field and their magnetisation is increased with tensile mechanical stress. Materials with negative magnetostriction contract under the effect of a magnetic field and their magnetisation decreases with tensile mechanical stress. Iron and iron alloys present both positive and negative magnetostriction, depending on the strength of the applied magnetic field. Under applied mechanical stress, their magnetisation behaves in different ways with different magnetic fields. Inversely, the magnetostriction of such a material is not only field dependent but also stress dependent, as shown in Fig. 3.

2.2 Magnetostriction in rotating electrical machinery

Witczak (1996) presented a method for calculating the magnetostrictive forces in the iron core of electrical machines. In this method, he assumed the ferromagnetic medium to be conservative, isotropic and elastically linear. He derived an expression for the tensor to be used for calculating the

magnetic forces and used it in an FE calculation of an induction machine. From his results, it appears that the magnetostrictive force density is of a larger magnitude (about 100 MN/m^3), compared to the Lorentz force density in the windings of a low-voltage induction machine (about 0.5 MN/m^3). However, the effect of these forces on the vibrations and noise of the machine has not been clarified.

He also measured the effect of an externally applied stress on the magnetisation curve of electrical steel, as well as the relative elongation (magnetostriction), under the effect of an external magnetic field. He reported data for the magnetisation curve under mechanical stress, but not those of magnetostriction under mechanical stress, as we know that magnetostriction is stress dependent.

Låftman (1995) investigated the effect of magnetostriction on the noise emitted by an induction motor. He used separate FEM packages for the mechanical and the magnetic field solution. The magnetostriction was modelled according to the strain it induces for a given value of the magnetic field distribution. These strains are obtained from measurement data of the elongation vs. magnetic field distribution. Here again the effect of stress on magnetisation and magnetostriction has not been taken into account. Låftman suggested that the magnetostriction might have a quieting effect on the noise from rotating electrical machines.

Delaere (2002) presented a method to calculate the magnetic and magnetostriction forces using the principle of virtual work combined with an alternative expression of magnetic energy. In this expression, he used the magnetic vector potential and the source term of an FE model to get the magnetic energy in terms of FE variables. The magnetostriction forces are calculated in this model as the forces needed to stretch or shrink one element into its initial form from the deformed one. The deformation itself can be calculated from a model of magnetostriction as a function of magnetic field distribution. In his work, Delaere (2002) used a polynomial fit of the magnetic flux density \mathbf{B} ; measured data, however, could also be used. The effect of mechanical stress on magnetostriction has also been disregarded here. With regard to the vibrations of rotating electrical machines, the result was that the magnetostriction does not affect the vibrations and noise of these machines.

Mohammed et al. (2002) presented a calculation of magnetic and magnetostriction forces in a permanent magnet motor. They also performed a calculation of the vibration of the stator core of such a machine and concluded that the vibrations due to magnetostriction are significant. The

magnetostriction induced asymmetry in the vibrations and enlarged the amplitude of vibrations about twice. The magnetisation and magnetostriction data used in this work are only hypothetical; they have not been measured.

Magnetostriction and magnetostrictive forces

Modelling the magnetostriction with equivalent magnetostrictive forces has a major drawback. Indeed, this method does not correctly model the mechanical stress-state of the materials. This is illustrated by the two cases of Fig. 5. In the first case the iron is prohibited from changing its dimensions by an infinitely stiff and rigid frame while in the second case the iron is free to change its dimensions without external constraints. In both cases the changes in dimensions are well described by magnetostrictive forces; however, the stress-state of iron is not correctly modelled. This effect will be explained later in Chapter 7.

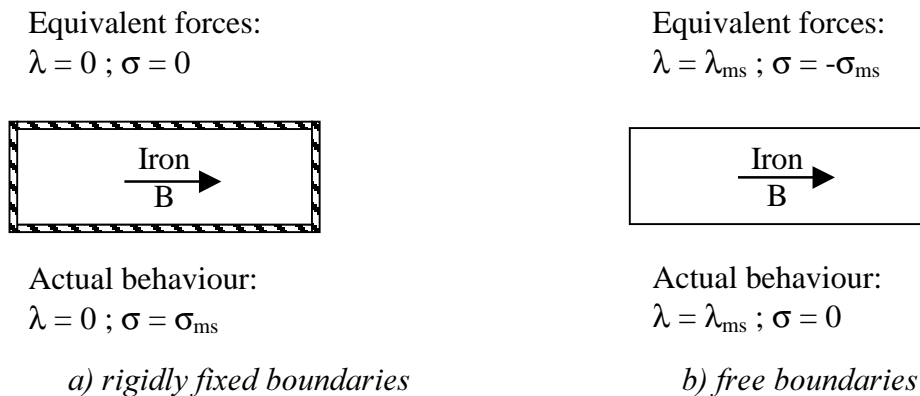


Fig. 5: Mechanical stress-state of materials under magnetostriction when forces are used to model the magnetostriction.

2.3 Conclusions

The phenomenon of magnetostriction in iron is a complicated one. The magnetostriction depends on the magnetic field as well as on mechanical stress. Most of the models presented up to now do not take this stress-dependency into account. The need for a model that takes it into account is obvious. Moreover, the results from different models are different and controversial and the data relating to the magnetostriction of electrical steel sheets are not available. More research on the subject is clearly needed.

3 Forces

The aim of this chapter is to introduce the methods used for calculating magnetic and magnetostrictive forces. The terminology related to the forces from either a magnetic or a magnetostrictive origin is clarified and existing methods of calculating such forces are presented. The methods developed and used in this work are derived in detail and discussed. Calculations on simple models are carried out to demonstrate which method is best suited to meet the objectives of this work.

3.1 Terminology

The terms *force(s)* and *force distribution(s)* are used in the literature in a sometimes-confusing way. The standard for mechanical terminology (IEC 60027-1 1992) recommends the use of *distributed forces $f(x)$* to describe mechanical actions on differential volumes or surfaces, as in body forces, surface forces or inertia forces. The same standard also defines the total force as *the integral over the volume or the surface of distributed forces*. The total force can be referred to as *force* for short. Terms like *magnetic force(s)*, *nodal force(s)* and *force distribution* are also encountered in literature dealing with magnetism and magnetic materials.

The calculation of the magnetic force acting on a ferromagnetic material without magnetostriction can be separated into two kinds: the calculation of the total force acting on a part of the machine, such as the rotor or stator, and the calculation of distributed forces, which describe the forces acting on a differential volume inside a given part. In fact, the knowledge of the force distribution is enough, since the total force can be calculated as a its volume integral.

There exist many formulations for the calculation of magnetic force (Carpenter 1959). All these formulations give the same total force acting on a part of the machine surrounded by air. However, the distributed forces are calculated differently from one formulation to another. Up to now, there is no consensus as to which of these formulations is the best, or which best describes the mechanical effect of magnetism. This abundance of formulations is a result of different models of the magnetised media (distribution of dipoles, dipoles and current, currents etc...)

3.2 Reluctance forces

The magnetic force is the rate of change in magnetic energy when the magnetic medium is undergoing an incremental displacement with the magnetic excitation held fixed (Melcher 1981).

From the above statement and the principle of energy conservation, Melcher (1981) derived an expression for the magnetic force density (Magnetic Korteweg-Helmholtz force density) and the tensor associated with it. If the magnetised iron is considered as incompressible medium having constant high permeability, the above force density reduces to a surface force density at the interface between iron and air and is equal to the normal component of Maxwell stress tensor (Carpenter 1959, Melcher 1981). The force density due to current distribution vanishes as the currents are confined to conductors and iron is supposed free of current.

The reluctance forces, also called *Maxwell forces* by reference to the Maxwell stress tensor, are these forces acting at the surfaces (or the interface) between two magnetic media with different reluctivities. It should be noticed that in this case the force distribution due to the gradient of the permeability in iron is neglected as well as the one due to the Villari effect.

For the purpose of total force calculation on a magnetised part of iron, the above Maxwell stress can be integrate on a closed surface situated in the air and surrounding the part under consideration. This method is used effectively to calculate the total force acting on the rotor of electrical machines (Arkkio 1995), as well as the torque of these machines (Arkkio 1987). Further, the radial component of the Maxwell stress tensor can be developed into the so-called two-dimensional Fourier series that can be used in the vibration analysis of rotating electrical machinery. This approach has been used by Belahcen et al. (1999) and is reported later in this chapter.

The development of the Maxwell stress tensor into a Fourier series does not have a rigorous theoretical background for the following reason: the integral of the divergence of the Maxwell stress tensors over a volume can be shown rigorously to correspond to the total force acting on this volume. Using mathematical equations, the volume integration can be reduced to surface integration of the normal component of the stress on a surface enclosing the volume under consideration. Until here, the procedure is mathematically correct. Now, taking the normal component of the stress for given force distribution is not necessary correct. In fact, the Maxwell stress tensor is derived from a

given force density and using the principle of virtual work (Melcher 1981); it is this force density that should be considered.

In an equivalent manner, as shown by Coulomb (1987), either the principle of virtual work or the local Jacobian derivative method can be used for the purpose of total force calculation. Indeed, Coulomb (1987) demonstrated that an appropriate choice of the integration path for the Maxwell stress tensor leads to the same total magnetic force as the one calculated using the virtual work principle. The torque of an electrical machine calculated in this manner is also demonstrated to agree with the one calculated from the Maxwell stress tensor.

Using the differential geometry, Bossavit (1992) introduced a method to calculate the force field in magnetised media. This method, combined with the local Jacobian derivative method has been further developed by Ren and Razek (1992) so that it gives the so-called nodal forces (distributed forces) in a FE calculation. This method is based on the differentiation of the magnetic energy of one element with respect to virtual displacements of the nodes of that element. Later, Delaere (1999) presented another version of these nodal forces. The magnetic energy was expressed in terms of FE variables, namely the magnetic vector potential and the FE current terms while in Ren's method, the energy is expressed in terms of the magnetic field strength and the magnetic induction.

Kameari (1993) also presented a method of calculating the nodal forces based on the Maxwell stress tensor. It is demonstrated that these three methods (Ren, Kameari, Delaere) are theoretically and numerically equivalent (Kameari 1993, Belahcen 2001) and the total force acting on any separate part of the machine is the same as that given by the Maxwell stress tensor method. Moreover, the Lorentz force on a current-carrying conductor can be calculated using the same method (Delaere 1999).

When dealing with the vibrations and noise of electrical machinery, distributed forces are needed. From these forces, it is possible to carry out elasticity or structural analyses by reducing these distributed forces to nodal forces. Due to the lack of accurate force distribution, and because the nodal forces are enough for structural analysis, this as well as previous work uses the method of nodal forces presented by Ren and Razek (1992) and further developed by Besbes et al. (1996) and Mohammed et al. (1999) to handle the magnetostriction also. The magnetostrictive forces calculated with this method are used in simple example in this work. However, the calculation of

magnetostriction in electrical machines (within this work) is carried out with an new alternative method presented later in this chapter, and called magnetostrictive stress method. The magnetostrictive stress method, though not very sophisticated, is more accurate within the measurements available.

3.3 Magnetostrictive forces

As explained in Chapter 2, magnetostriction (Joule magnetostriction) means changes in the dimensions of magnetic material under the effect of a magnetic field. These changes can be described in terms of applied distributed forces that produce the same changes of dimensions in magnetic material. These distributed forces are referred to in the literature as *magnetostrictive forces*. Equivalently, as presented by Bossavit (1992) and subsequently by Besbes et al. (1996) and Mohammed et al. (1999), the magnetostrictive forces can be derived directly from the concept of virtual work or the local Jacobian derivative. In this case, one should take into account the fact that the magnetisation of the magnetic material depends not only on the magnetic field strength but also on the mechanical stress that the magnetic material is under.

This observation makes it possible to calculate these forces without explicit knowledge of the magnetostrictive data of the material under consideration. This fact has been qualitatively stated by du Trémolet (1993) as a consequence of his widespread work on magnetostriction: “*The stress sensitivity of any given material may be expressed by the stress derivatives of its magnetic properties... Due to the Maxwell relations, this stress sensitivity of the magnetisation (or magnetic induction) of any ferromagnet is directly related with the field dependence of its dimensions, i.e. with its magnetostriction curve.*”

Presented for the first time by Bossavit (1992) and subsequently by Besbes et al. (1996) and Mohammed et al. (1999), the concept of virtual work is further developed in this thesis. However, the accuracy of this method relies on accurate measurements of the magnetisation of iron sheets under applied mechanical stress, not only unidirectional but also multidirectional stress. In this work, this method is used in a simple model to demonstrate the validity of that theory. For accurate calculation of magnetostrictive forces in electrical machines, the method of magnetostrictive stress is used in the simulations of Chapter 7.

3.4 Derivation of forces

In this section, the formulas related to the calculation of magnetic and magnetostriction forces are derived.

The total magnetic force \mathbf{F} acting on any part of the machine is calculated from the magnetic energy W as

$$\mathbf{F}^T = -\frac{\partial W}{\partial \mathbf{u}} \quad (1)$$

where the magnetic energy is given as

$$W = \int_{\Omega} \left(\int_0^B \mathbf{H} \cdot d\mathbf{B} \right) d\Omega \quad (2)$$

\mathbf{H} and \mathbf{B} are respectively the magnetic field strength and the magnetic flux density vectors. $\mathbf{u} = [u_l \ v_l]^T$ is the vector of virtual displacements in the considered coordinate system. For the principle of virtual work to be valid, these virtual displacements have to be flux-conserving Melcher (1981). In FE analysis this condition is satisfied by keeping the nodal values of the magnetic vector potential constants while calculating the derivative of the magnetic energy.

If we apply this method to one element (e) of a FE mesh with the area Ω^e and take \mathbf{u} as the virtual displacement of the nodes of that element, we get the contribution of one element to nodal forces

$$\mathbf{F}^{eT} = -\frac{\partial}{\partial \mathbf{u}} \int_{\Omega^e} \left(\int_0^B \mathbf{H} \cdot d\mathbf{B} \right) d\Omega^e \quad (3)$$

Equation (3) is easier to evaluate in the reference element with the area $\hat{\Omega}^e$, where the differentiation with respect to virtual displacements can be interchanged with the integration.

$$\begin{aligned} \mathbf{F}^{eT} &= -\frac{\partial}{\partial \mathbf{u}} \int_{\hat{\Omega}} \left(\int_0^B \mathbf{H} \cdot d\mathbf{B} \right) \det(\mathbf{J}) d\hat{\Omega} \\ &= -\int_{\hat{\Omega}} \frac{\partial}{\partial \mathbf{u}} \left(\int_0^B \mathbf{H} \cdot d\mathbf{B} \right) \det(\mathbf{J}) d\hat{\Omega} - \int_{\hat{\Omega}} \left(\int_0^B \mathbf{H} \cdot d\mathbf{B} \right) \frac{\partial \det(\mathbf{J})}{\partial \mathbf{u}} d\hat{\Omega} \end{aligned} \quad (4)$$

where \mathbf{J} is the Jacobian matrix of coordinate transformation and $\det(\mathbf{J})$ its determinant.

Equation (4) means that the contribution of one element (e) to the nodal force at node l is

$$F_{xl}^e = -\frac{\partial W^e}{\partial u_l}$$

$$F_{yl}^e = -\frac{\partial W^e}{\partial v_l}$$
(5)

Let us assume provisionally the constitutive equation of the material $\mathbf{H} = \nu(\mathbf{B}^2, \boldsymbol{\sigma}) \mathbf{B}$ we may write

$$\int_0^B \mathbf{H} \cdot d\mathbf{B} = \int_0^B \nu \mathbf{B} \cdot d\mathbf{B}$$
(6)

implying

$$\begin{aligned} \frac{\partial}{\partial \mathbf{u}} \left(\int_0^B \mathbf{H} \cdot d\mathbf{B} \right) &= \frac{\partial}{\partial \mathbf{u}} \left(\int_0^B \nu \mathbf{B} \cdot d\mathbf{B} \right) \\ &= \overbrace{\frac{\partial}{\partial \mathbf{B}^2} \left(\int_0^B \nu(\mathbf{B}^2, \boldsymbol{\sigma}) \mathbf{B} \cdot d\mathbf{B} \right)}^1 \frac{\partial \mathbf{B}^2}{\partial \mathbf{u}} + \overbrace{\frac{\partial}{\partial \sigma_{\parallel}} \left(\int_0^B \nu(\mathbf{B}^2, \boldsymbol{\sigma}) \mathbf{B} \cdot d\mathbf{B} \right)}^2 \frac{\partial \sigma_{\parallel}}{\partial \mathbf{u}} + \\ &\quad \overbrace{\frac{\partial}{\partial \sigma_{\perp}} \left(\int_0^B \nu(\mathbf{B}^2, \boldsymbol{\sigma}) \mathbf{B} \cdot d\mathbf{B} \right)}^3 \frac{\partial \sigma_{\perp}}{\partial \mathbf{u}} + \overbrace{\frac{\partial}{\partial \tau} \left(\int_0^B \nu(\mathbf{B}^2, \boldsymbol{\sigma}) \mathbf{B} \cdot d\mathbf{B} \right)}^4 \frac{\partial \tau}{\partial \mathbf{u}} \end{aligned}$$
(7)

The measurement of the reluctivity as function of the magnetic flux density and the unidirectional mechanical stress and its development into two dimensional Fourier series in terms of the square of the magnetic flux density and mechanical stress are described in Chapter 5.

Here, the measurement is provisionally supposed to be performed with the applied mechanical stress and using its three components $\sigma_{\parallel}, \sigma_{\perp}$ and τ , respectively parallel and orthogonal to the direction of \mathbf{B} and shear stress.

The first term of Eq. (7) can be calculated as follows

$$\begin{aligned} term1 &= \frac{\partial}{\partial \mathbf{B}^2} \left(\int_0^{\mathbf{B}^2} \frac{1}{2} \nu(\mathbf{B}^2, \boldsymbol{\sigma}) d(\mathbf{B}^2) \right) \\ &= \frac{1}{2} \nu(\mathbf{B}^2, \boldsymbol{\sigma}) \end{aligned}$$
(8)

This is half of the reluctivity of the element at the given values of flux density and mechanical stress.

The second term of Eq. (7) is

$$term2 = \left(\int_0^{B^2} \frac{1}{2} \frac{\partial v(\mathbf{B}^2, \boldsymbol{\sigma})}{\partial \sigma_{\parallel}} (d\mathbf{B}^2) \right) \frac{\partial \sigma_{\parallel}}{\partial \mathbf{u}} \quad (9)$$

The integration in Eq. (9) is done at constant stress since the measurement is performed at constant externally applied stress and the effect of stress induced by magnetostriction is not considered. The terms 3 and 4 of Eq. (7) are calculated in the same manner as term 2. The nodal forces are then

$$\mathbf{F}^{eT} = - \int_{\hat{\Omega}} \left\{ \frac{1}{2} v \frac{\partial \mathbf{B}^2}{\partial \mathbf{u}} \det(\mathbf{J}) + \frac{\partial \det(\mathbf{J})}{\partial \mathbf{u}} \int_0^{B^2} \frac{1}{2} v d\mathbf{B}^2 + \frac{\partial \sigma_{\parallel}}{\partial \mathbf{u}} \det(\mathbf{J}) \int_0^{B^2} \frac{1}{2} \frac{\partial v}{\partial \sigma_{\parallel}} d\mathbf{B}^2 + \right. \\ \left. \frac{\partial \sigma_{\perp}}{\partial \mathbf{u}} \det(\mathbf{J}) \int_0^{B^2} \frac{1}{2} \frac{\partial v}{\partial \sigma_{\perp}} d\mathbf{B}^2 + \frac{\partial \tau}{\partial \mathbf{u}} \det(\mathbf{J}) \int_0^{B^2} \frac{1}{2} \frac{\partial v}{\partial \tau} d\mathbf{B}^2 \right\} d\hat{\Omega} \quad (10)$$

For the evaluation of nodal forces, as well as for the evaluation of other terms that we will encounter in the development of the coupling between magnetic and elastic fields, it is convenient to present the reluctivity of the material as an m -dimensional cubic spline approximation with respect to the square of the flux density \mathbf{B}^2 and the components of the mechanical stress. For simplicity, and because the effect of the other stress components on the reluctivity is unknown, only the component of stress parallel to the flux density is considered. On some interval $[\mathbf{B}_k^2, \mathbf{B}_{k+1}^2] \times [\sigma_h, \sigma_{h+1}]$, the reluctivity is given by

$$v(\mathbf{B}^2, \boldsymbol{\sigma}) = \sum_{\substack{i=0,3 \\ j=0,3}} a_{khij} (\mathbf{B}^2 - \mathbf{B}_k^2)^i (\sigma - \sigma_h)^j \quad (11)$$

The integration and differentiation of the reluctivity with respect to the variables \mathbf{B}^2 or $\boldsymbol{\sigma}$ is carried out analytically using Eq. (11). In Eq. (10) there are derivatives of the flux density, the determinant of the Jacobian matrix and stresses with respect to virtual displacements. These derivatives are explicitly developed below.

The Jacobian matrix is given by

$$\mathbf{J} = \begin{bmatrix} \sum_{j=1,n} \frac{\partial N_j}{\partial \xi} x_j & \sum_{j=1,n} \frac{\partial N_j}{\partial \xi} y_j \\ \sum_{j=1,n} \frac{\partial N_j}{\partial \eta} x_j & \sum_{j=1,n} \frac{\partial N_j}{\partial \eta} y_j \end{bmatrix} \quad (12)$$

with n the number of nodes in the element, N the shape functions, ξ and η are the coordinates in the reference frame.

The determinant of the Jacobian matrix is

$$\det(\mathbf{J}) = J_{11}J_{22} - J_{12}J_{21} \quad (13)$$

and the derivative of the determinant with respect to virtual displacements (which is the same as the derivative with respect to nodal coordinates $x = x_0 + u, y = y_0 + v$) is

$$\begin{bmatrix} \frac{\partial \det(\mathbf{J})}{\partial u_i} \\ \frac{\partial \det(\mathbf{J})}{\partial v_i} \end{bmatrix} = \begin{bmatrix} \frac{\partial N_l}{\partial \xi} J_{22} - \frac{\partial N_l}{\partial \eta} J_{12} \\ \frac{\partial N_l}{\partial \eta} J_{11} - \frac{\partial N_l}{\partial \xi} J_{21} \end{bmatrix} \quad (14)$$

The flux density \mathbf{B} is calculated from the magnetic vector potential A in a standard fashion

$$\begin{bmatrix} B_x \\ B_y \end{bmatrix} = \begin{bmatrix} \frac{\partial A}{\partial y} \\ -\frac{\partial A}{\partial x} \end{bmatrix} = \begin{bmatrix} \frac{1}{\det(\mathbf{J})} \sum_{j=1,n} A_j \left[J_{11} \frac{\partial N_j}{\partial \eta} - J_{21} \frac{\partial N_j}{\partial \xi} \right] \\ \frac{1}{\det(\mathbf{J})} \sum_{j=1,n} A_j \left[J_{22} \frac{\partial N_j}{\partial \xi} - J_{12} \frac{\partial N_j}{\partial \eta} \right] \end{bmatrix} \quad (15)$$

using

$$\frac{\partial \mathbf{B}^2}{\partial \mathbf{u}} = 2\mathbf{B} \cdot \frac{\partial \mathbf{B}}{\partial \mathbf{u}} \quad (16)$$

we still need to calculate $\frac{\partial \mathbf{B}}{\partial \mathbf{u}}$, which is obtained from Eq. (15) and Eq. (14) as

$$\begin{bmatrix} \frac{\partial B_x}{\partial u_i} \\ \frac{\partial B_y}{\partial u_i} \end{bmatrix} = \begin{bmatrix} \frac{1}{\det(\mathbf{J})} \left[\sum_{j=1,n} A_j \left(\frac{\partial N_l}{\partial \xi} \frac{\partial N_j}{\partial \eta} - \frac{\partial N_j}{\partial \xi} \frac{\partial N_l}{\partial \eta} \right) - \frac{\partial \det(\mathbf{J})}{\partial u_i} B_x \right] \\ -\frac{1}{\det(\mathbf{J})} \frac{\partial \det(\mathbf{J})}{\partial u_i} B_y \end{bmatrix} \quad (17)$$

and

$$\begin{bmatrix} \frac{\partial B_x}{\partial v_i} \\ \frac{\partial B_y}{\partial v_i} \end{bmatrix} = \begin{bmatrix} -\frac{1}{\det(\mathbf{J})} \frac{\partial \det(\mathbf{J})}{\partial v_i} B_x \\ \frac{1}{\det(\mathbf{J})} \left[\sum_{j=1,n} A_j \left(\frac{\partial N_j}{\partial \xi} \frac{\partial N_l}{\partial \eta} - \frac{\partial N_l}{\partial \xi} \frac{\partial N_j}{\partial \eta} \right) - \frac{\partial \det(\mathbf{J})}{\partial v_i} B_y \right] \end{bmatrix} \quad (18)$$

The mechanical stress is given by

$$\{\boldsymbol{\sigma}\} = [\mathbf{E}]\{\boldsymbol{\varepsilon}\} \quad (19)$$

where

$$[\mathbf{E}] = \frac{E}{1-\nu^2} \begin{bmatrix} 1 & \nu & 0 \\ \nu & 1 & 0 \\ 0 & 0 & \frac{1-\nu}{2} \end{bmatrix} \quad \text{For plane stress} \quad (20)$$

$$[\mathbf{E}] = \frac{E}{(1+\nu)(1-2\nu)} \begin{bmatrix} 1-\nu & \nu & 0 \\ \nu & 1-\nu & 0 \\ 0 & 0 & \frac{1-2\nu}{2} \end{bmatrix} \quad \text{For plane strain} \quad (21)$$

$$\frac{\partial\{\boldsymbol{\sigma}\}}{\partial\mathbf{u}} = \left[\frac{\partial\{\boldsymbol{\sigma}\}}{\partial u_1} \quad \frac{\partial\{\boldsymbol{\sigma}\}}{\partial v_1} \quad \frac{\partial\{\boldsymbol{\sigma}\}}{\partial u_2} \quad \frac{\partial\{\boldsymbol{\sigma}\}}{\partial v_2} \quad \frac{\partial\{\boldsymbol{\sigma}\}}{\partial u_3} \quad \frac{\partial\{\boldsymbol{\sigma}\}}{\partial v_3} \right] \quad (22)$$

so that

$$\frac{\partial\{\boldsymbol{\sigma}\}}{\partial u_i} = [\mathbf{E}] \frac{\partial\{\boldsymbol{\varepsilon}\}}{\partial u_i} \quad (23)$$

on the other hand

$$\{\boldsymbol{\varepsilon}\} = \begin{bmatrix} \frac{\partial}{\partial x} & 0 \\ 0 & \frac{\partial}{\partial y} \\ \frac{\partial}{\partial y} & \frac{\partial}{\partial x} \end{bmatrix} \begin{Bmatrix} u \\ v \end{Bmatrix} \quad (24)$$

$$u = \sum_i N_i u_i \quad \text{and} \quad v = \sum_i N_i v_i \quad (25)$$

so that

$$\frac{\partial\{\boldsymbol{\varepsilon}\}}{\partial u} = \left\{ \begin{array}{c} \frac{\partial}{\partial u} \sum_i \frac{\partial N_i}{\partial x} u_i \\ \frac{\partial}{\partial u} \sum_i \frac{\partial N_i}{\partial y} v_i \\ \frac{\partial}{\partial u} \sum_i \frac{\partial N_i}{\partial y} u_i + \frac{\partial}{\partial u} \sum_i \frac{\partial N_i}{\partial x} v_i \end{array} \right\} \quad (26)$$

and

$$\frac{\partial\{\boldsymbol{\sigma}\}}{\partial u_i} = [\mathbf{E}] \left\{ \begin{array}{c} \frac{\partial}{\partial u_i} \sum_i \frac{\partial N_i}{\partial x} u_i \\ \frac{\partial}{\partial u_i} \sum_i \frac{\partial N_i}{\partial y} v_i \\ \frac{\partial}{\partial u_i} \sum_i \frac{\partial N_i}{\partial y} u_i + \frac{\partial}{\partial u_i} \sum_i \frac{\partial N_i}{\partial x} v_i \end{array} \right\} \quad (27)$$

or more specifically, with l , m and n the indices of the node of the element under consideration (circular indices 1, 2, 3, 1 ...)

$$\frac{\partial \{\boldsymbol{\sigma}\}}{\partial u_i} = [\mathbf{E}] \left\{ \begin{array}{c} \frac{\partial}{\partial u_i} \sum_j (y_j - y_k) u_i \\ \frac{\partial}{\partial u_i} \sum_j (x_k - x_j) v_i \\ \frac{\partial}{\partial u_i} \sum_j (x_k - x_j) u_i + \frac{\partial}{\partial u_i} \sum_j (y_j - y_k) v_i \end{array} \right\} \quad (28)$$

$$= [\mathbf{E}] \left\{ \begin{array}{c} (y_m - y_n) \\ v_m - v_n \\ x_n - x_m + u_m - u_n \end{array} \right\} \quad (29)$$

Similarly

$$\frac{\partial \{\boldsymbol{\sigma}\}}{\partial v_i} = [\mathbf{E}] \left\{ \begin{array}{c} u_n - u_m \\ x_n - x_m \\ y_m - y_n + v_n - v_m \end{array} \right\} \quad (30)$$

If the x -axis is coincident with the direction defined by the flux density vector \mathbf{B} , we obtain the derivatives for the plane stress case as:

$$\frac{\partial \sigma_{\parallel}}{\partial u_i} = \frac{E}{1-\nu^2} (y_m - y_n); \quad \frac{\partial \sigma_{\parallel}}{\partial v_i} = 0 \quad (31)$$

$$\frac{\partial \sigma_{\perp}}{\partial v_i} = \frac{E}{1-\nu^2} (x_n - x_m); \quad \frac{\partial \sigma_{\perp}}{\partial u_i} = 0 \quad (32)$$

$$\frac{\partial \tau}{\partial u_i} = \frac{E}{1-\nu^2} (x_n - x_m); \quad \frac{\partial \tau}{\partial v_i} = \frac{E}{1-\nu^2} (y_m - y_n) \quad (33)$$

However, there are no data available for the effect of multidirectional mechanical stress on the magnetisation of iron. Furthermore, the effect of shear stress on the magnetic properties has never been studied. In some publications (Schneider 1982, Kashiwaya 1991, Sablik 1993, 1995), there has been an attempt to approach the effect of multidirectional stress in the same way as an equivalent unidirectional stress. These different approximations are not accurate enough and sometimes they are contradictory. The use of the developed formula for magnetostriction force is illustrated in a calculation example below (3.7.2).

3.5 The method of magnetostrictive stress

The method of virtual work developed above, although it gives good results for magnetic forces, requires accurate measurement of the magnetisation versus applied mechanical stress to enable the calculation of magnetostrictive forces.

From the measurement of magnetisation the derivative of the reluctivity with respect to unidirectional stress can, in principle, be specified by iterating calculations and measurements. Here, for simplicity, the derivative is specified from one cycle of measurements. Moreover, the effect of orthogonal and shear stresses on magnetisation is unknown and its measurement is complicated. For these reasons, the calculation of magnetostrictive forces is better carried out using measured magnetostrictive stress versus magnetic flux density and applied mechanical stress. This method, called the magnetostrictive stress method, is explained here.

First consider an element of iron in a magnetic field \mathbf{H} . Due to magnetostriction of iron, this element will shrink or stretch depending on the sign of its magnetostriction. This change in dimensions is described by a magnetostrictive strain tensor $\{\boldsymbol{\varepsilon}_{ms}\}$. Corresponding to this strain, a magnetostrictive stress tensor $\{\boldsymbol{\sigma}_{ms}\}$ can be calculated using Hook's law. The nodal magnetostrictive forces are calculated as the set of nodal forces due to this stress.

The measurement carried out and reported in Chapter 5 gives only the component of magnetostrictive stress or strain in a direction parallel to that of the magnetic field. The other component of magnetostrictive stress or strain orthogonal to the direction of the magnetic field \mathbf{H} can be calculated within two assumptions. First, there is no magnetostrictive shear stress or strain in the reference defined by the direction parallel to \mathbf{H} and the one orthogonal to it. Second, there is no volume magnetostriction, which is a good assumption in the range of flux density occurring in electrical machines. The latter assumption means that the magnetostriction strain in the direction orthogonal to that of the magnetic field is opposite and has half the amplitude compared to the strain parallel to the direction of the magnetic field.

The measurement described in Chapter 5 gives magnetostrictive stress $\sigma_{ms\parallel}$ in a direction parallel to that of the magnetic field as a two-dimensional cubic spline versus the magnetic flux density and the applied mechanical stress. If $\sigma_{ms\perp}$ is the magnetostrictive stress in a direction orthogonal to the magnetic field, we can write, using the first assumption,

$$\begin{bmatrix} \sigma_{ms\parallel} \\ \sigma_{ms\perp} \\ 0 \end{bmatrix} = \mathbf{E} \begin{bmatrix} \varepsilon_{ms\parallel} \\ \varepsilon_{ms\perp} \\ 0 \end{bmatrix} \quad (34)$$

The second assumption can be written as

$$\varepsilon_{ms\perp} = -\frac{1}{2}\varepsilon_{ms\parallel} \quad (35)$$

So that, in the case of plane stress, we get

$$\sigma_{ms\perp} = \frac{2\nu-1}{2-\nu}\sigma_{ms\parallel} \quad (36)$$

The magnetostrictive nodal forces are calculated for each element as follows. Let θ be the angle defined by the direction of the magnetic field and the x-axis. The projections of each edge of the element in the directions parallel and orthogonal to the magnetic field are respectively

$$s_{\parallel} = \cos(\theta)s_x + \sin(\theta)s_y \quad (37)$$

$$s_{\perp} = -\sin(\theta)s_x + \cos(\theta)s_y \quad (38)$$

where s_x and s_y are respectively the projection of the considered edge of the element on the x- and y-axis. The forces, per unit length, parallel and orthogonal to the direction of the magnetic field are respectively

$$F_{ms\parallel} = \sigma_{ms\parallel}s_{\parallel} \quad (39)$$

$$F_{ms\perp} = \sigma_{ms\perp}s_{\perp} \quad (40)$$

These forces are distributed equally between the two nodes of the given edge. The forces in the original Cartesian coordinate system are obtained as the projection of $F_{ms\parallel}$ and $F_{ms\perp}$ on the axis of that system

$$F_{msx} = \cos(\theta)F_{ms\parallel} - \sin(\theta)F_{ms\perp} \quad (41)$$

$$F_{msy} = \sin(\theta)F_{ms\parallel} + \cos(\theta)F_{ms\perp} \quad (42)$$

These forces are added to the magnetic nodal forces to get the nodal magnetic and magnetostrictive forces. They can also be used separately in calculations to emphasise the effect of magnetostriction only.

3.6 Maxwell stress tensor

In a cartesian coordiante system the Maxwell stress tensor can be given as

$$\boldsymbol{\tau} = \frac{1}{\mu_0} \begin{bmatrix} B_x^2 - \frac{1}{2}\mathbf{B}^2 & B_x B_y & B_x B_z \\ B_y B_x & B_y^2 - \frac{1}{2}\mathbf{B}^2 & B_y B_z \\ B_z B_x & B_z B_y & B_z^2 - \frac{1}{2}\mathbf{B}^2 \end{bmatrix} \quad (43)$$

The Maxwell stress tensor can be applied to calculate the magnetic force acting on any part of the machine e.g. the stator or rotor core of rotating electrical machines. If a closed surface Γ_j is chosen as a cylinder in the air gap, closed through the end region of the machine, and with another cylindrical surface outside the machine, the total force acting on the part considered can be deduced as

$$\begin{aligned} \mathbf{F} &= \oint_{\Gamma_j} \left(\frac{1}{\mu_0} B_n \mathbf{B} - \frac{1}{2\mu_0} \mathbf{B}^2 \mathbf{n} \right) d\Gamma \\ &= \oint_{\Gamma_j} \left(\frac{1}{2\mu_0} (B_n^2 - B_t^2) \mathbf{n} + \frac{1}{\mu_0} B_n B_t \mathbf{t} \right) d\Gamma \end{aligned} \quad (44)$$

where the volume integral $\int_V \nabla \cdot \boldsymbol{\tau} dV$ is reduced to the closed surface integral of Eq. (44); \mathbf{n} and \mathbf{t} stand respectively for the outward unit-vector normal to the differential surface $d\Gamma$ and the tangential one.

Since the integral on other surfaces than the one in the air gap is null, the integration in Eq. (44) reduces to an integration over the cylindrical surface inside the air gap. The quantity inside the integral of Eq. (44) is separated into the normal component (stress) and the circumferential component (shear), respectively

$$\sigma_r = \frac{1}{2\mu_0} (B_r^2 - B_\varphi^2) \quad (45)$$

and

$$\sigma_\varphi = \frac{1}{\mu_0} B_r B_\varphi \quad (46)$$

where the indices n and t have been replaced by r and φ , since the integration surface is now cylindrical.

From the point of view of vibrations and noise analysis, it is important to know the spatial distribution and the time dependence of the radial stress. For this purpose, the radial stress is developed into a two-dimensional Fourier series

$$\begin{aligned} \sigma_r = \sum_{m=0}^{\infty} \sum_{n=0}^{\infty} \lambda_{mn} \{ &a_{mn} \cos(mp\phi) \cos(n\omega t) + b_{mn} \cos(mp\phi) \sin(n\omega t) + \\ &c_{mn} \sin(mp\phi) \cos(n\omega t) + d_{mn} \sin(mp\phi) \sin(n\omega t) \} \end{aligned} \quad (47)$$

where m and n are respectively space- and time-harmonic numbers, p is the number of pole-pairs ω is the rotational speed of the magnetic field, t and ϕ are respectively the time and the angular position. The other constants are given by

$$a_{mn} = \frac{p\omega}{2\pi^2\mu_0r^2} \int_0^{\frac{2\pi}{p}} \int_0^{\frac{2\pi}{\omega}} \sigma_r \cos(mp\phi) \cos(n\omega t) d\phi dt \quad (48)$$

$$b_{mn} = \frac{p\omega}{2\pi^2\mu_0r^2} \int_0^{\frac{2\pi}{p}} \int_0^{\frac{2\pi}{\omega}} \sigma_r \cos(mp\phi) \sin(n\omega t) d\phi dt \quad (49)$$

$$c_{mn} = \frac{p\omega}{2\pi^2\mu_0r^2} \int_0^{\frac{2\pi}{p}} \int_0^{\frac{2\pi}{\omega}} \sigma_r \sin(mp\phi) \cos(n\omega t) d\phi dt \quad (50)$$

$$d_{mn} = \frac{p\omega}{2\pi^2\mu_0r^2} \int_0^{\frac{2\pi}{p}} \int_0^{\frac{2\pi}{\omega}} \sigma_r \sin(mp\phi) \sin(n\omega t) d\phi dt \quad (51)$$

$$\lambda_{mn} = \begin{cases} \frac{1}{4} & \text{for } m = n = 0 \\ \frac{1}{2} & \text{for } m = 0, n > 0 \text{ and } m > 0, n = 0 \\ 1 & \text{for } m > 0, n > 0 \end{cases} \quad (52)$$

Equation (47) can be written as a sum of waves circulating forward (+) and backward (-) with respect to the rotational direction of the rotor.

Hence, the radial stress can be written as

$$\sigma_r = \sum_{m=0}^{\infty} \sum_{n=0}^{\infty} \left\{ \frac{1}{2} \lambda_{mn} \left[(a_{mn} + d_{mn})^2 + (b_{mn} - c_{mn})^2 \right]^{\frac{1}{2}} \cos(-mp\phi + n\omega t + \gamma_+) + \frac{1}{2} \lambda_{mn} \left[(a_{mn} - d_{mn})^2 + (b_{mn} + c_{mn})^2 \right]^{\frac{1}{2}} \cos(mp\phi + n\omega t + \gamma_-} \right\} \quad (53)$$

In Eq. (53), the integer m defines the mode or the spatial frequency of the radial stress components, while n defines the time frequency of these components. In the time stepping method, the coefficients a_{mn} , b_{mn} , c_{mn} and d_{mn} are integrated at each step, and time-integrated from step to step so that no post-processing is needed.

3.7 Example of force calculation

3.7.1 Nodal forces

The nodal force method as described above and without magnetostriction has been used with a simple benchmark model (Takahashi 1994). The model consists of a centre pole between yokes with a small gap. The geometry of the device as presented by Takahashi et al. (1994) is shown in Fig. 6.

The geometry of the 2-D model and the FE mesh is shown in Fig. 7a. The calculated nodal forces for that mesh are shown in Fig. 7b. The simulation is performed with a conventional magneto-static FE program in Cartesian coordinates. The effect of saturation is taken into account in the form of a nonlinear BH-magnetisation curve for the yoke and the pole.

The magnetisation curve used here is not the same as the one used in the reported benchmark of Takahashi (1994). This missing information as well as the 2-D approach suggested that the comparison of the forces should be made with known methods (Maxwell stress tensor and Lorentz force) and not with measured results.

The mesh of Fig. 7a was adaptively refined. The total force acting on the iron pole and that on the current carrying conductor are calculated. The nodal force method and either the Maxwell stress tensor for the iron pole or the Lorentz formula for the conductor are used. The integration path for the Maxwell stress tensor is kept the same regardless of the changed FE meshes. Fig. 8 shows the z-components of the total force (calculated with the nodal forces method.) vs. the excitation current in ampere-turns (AT)

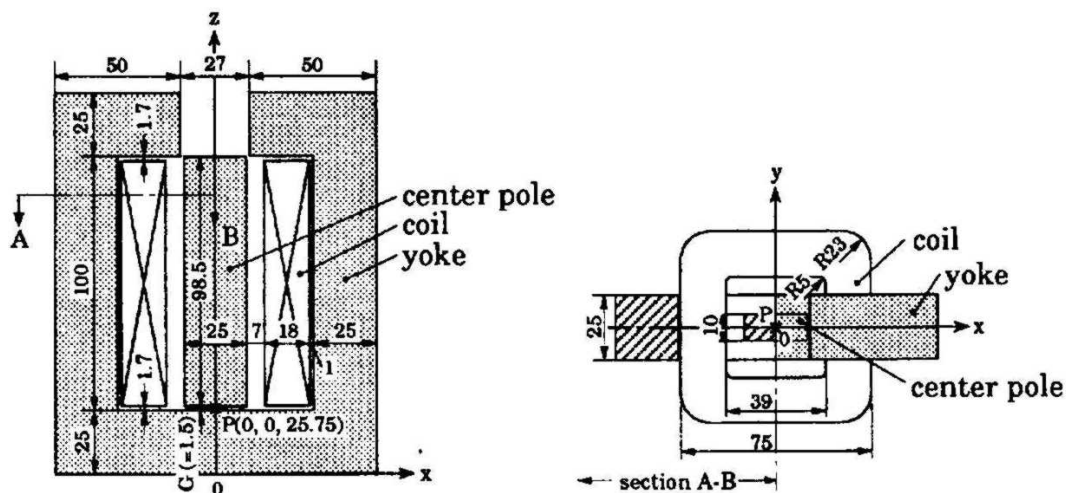


Fig. 6: Geometry of the benchmark device (Takahashi 1994).

Fig. 9 shows the z -components of the total forces vs. the number of nodes in the FE mesh at 1000 AT. The calculated forces agree with the results of the measured benchmark (Takahashi 1994) for excitation currents of 5000 AT. At lower currents, the forces are much smaller. This can be caused by the differences between the material magnetisation curves (not reported by Takahashi (1994)) and also by the 2-D approach. Moreover, the magnetisation curves used for the calculation of the magnetic forces are linearised at low values of the magnetic field strength. This last procedure, explained later in Chapter 6, makes the magnetic forces smaller at low values of the magnetic field strength.

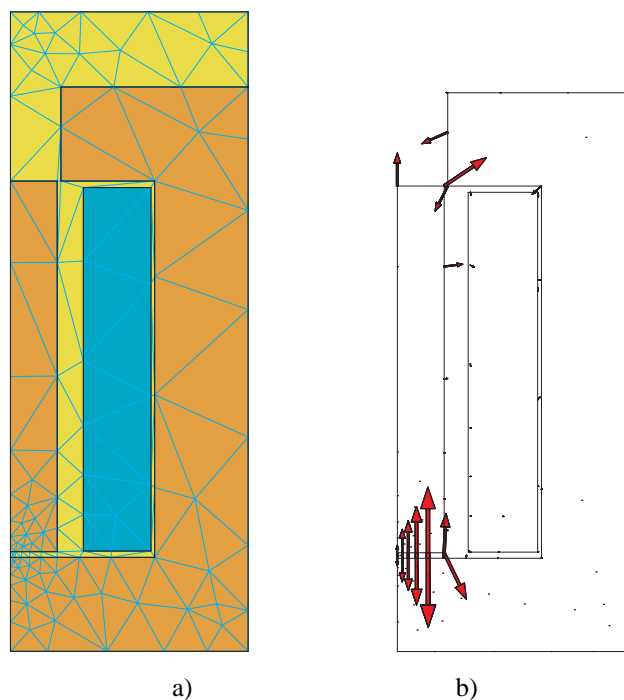


Fig. 7: Model and FE mesh (a) nodal forces (b).

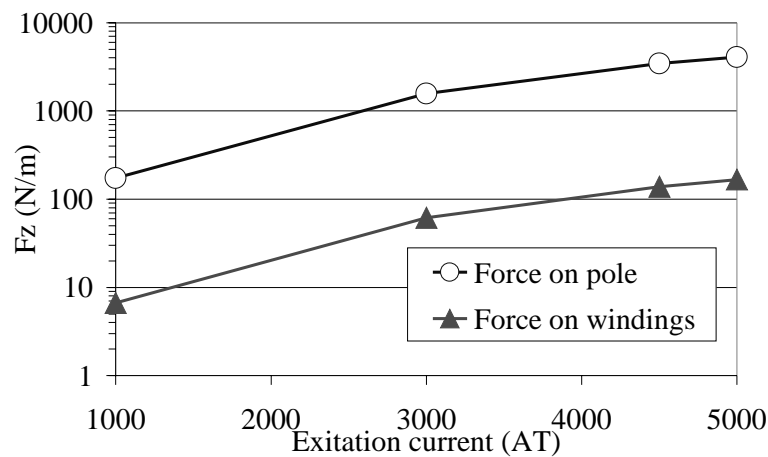


Fig. 8: Forces vs. excitation current.

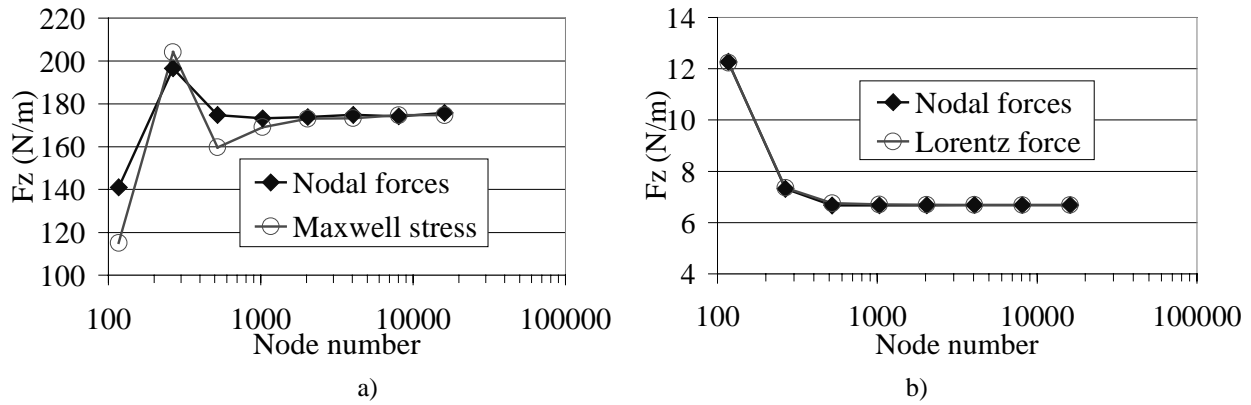


Fig. 9: Force on the iron pole (a) and the winding (b).

The results of this section are shown for the purpose of confirming the best accuracy of the method of virtual work as compared to the Maxwell stress tensor for the calculation of total magnetic forces. Although the two methods give the same result at high FE mesh density, the method of virtual work (nodal forces) gives better results already at low FE mesh density. This result is in accordance with the method used for the magnetic field calculation, which is based on the minimisation of the energy. It is clear that the calculation of the forces from the energy is more accurate than their calculation from field quantities which are calculated as derivatives of the magnetic vector potential and include inaccuracies.

3.7.2 Magnetostriction forces

The calculation of magnetostrictive forces is carried out for a simple geometry with two different methods to show the validity and accuracy of these methods.

The first method is the magnetostrictive stress method presented above where the magnetostrictive forces are calculated directly from the measured magnetostrictive stress. The second method is the energy derivative method presented above, which takes into account the dependency of magnetisation on stress. The geometry is an iron core of width $w_x = 0.2$ m, thickness $w_y = 0.02$ m and infinitely long. The cross-section of the iron core is discretised into a 2-D FE mesh as shown in Fig. 10. The flux density is set to be constant and have a uniform value of 1 T in x-direction of the Cartesian coordinate frame. The external mechanical stress is set to zero.

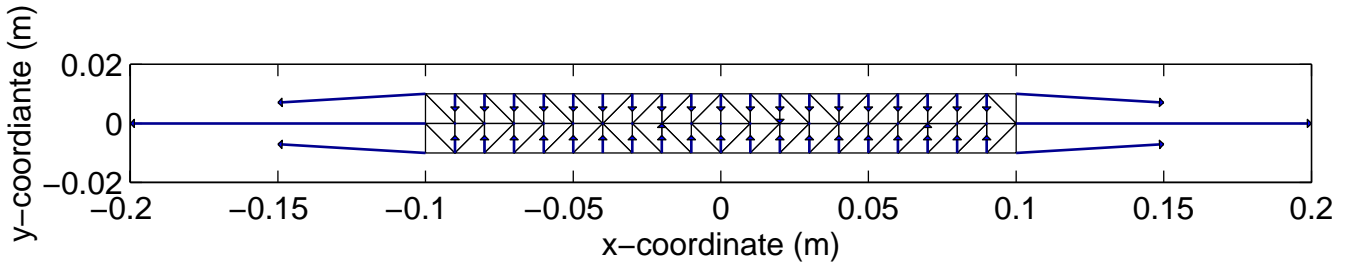


Fig. 10: FE mesh and scaled magnetostrictive forces.

Magnetostrictive stress method

At the chosen flux density and external mechanical stress, the measured magnetostrictive stress is 0.154 MPa. The corresponding magnetostrictive forces calculated with the magnetostrictive stress method are plotted in Fig. 10. The non-zero absolute values of the x-components of the forces are equal to 769.9 N/m at the corner nodes and 1539.7 N/m at the middle node. The corresponding values of the y-component are respectively equal to 181.1 N/m and 362.3 N/m. Zero values of the force occur at inside nodes as well as for the x-component for nodes on the horizontal edges and the y-component for vertical edges (except for the corner nodes).

Corresponding to the magnetostrictive forces of Fig. 10, the stresses

$$\sigma_x = 2 \frac{F_x}{w_y}; \quad \sigma_y = 20 \frac{F_y}{w_x} \quad (54)$$

are respectively 0.154 MPa and -0.036 MPa, which correspond to the magnetostrictive stress measured in the direction of the magnetic field and the stress in the orthogonal direction calculated from the stress in the parallel direction. These stresses correspond respectively to a parallel and orthogonal magnetostriction of $0.9 \mu\text{m/m}$ and $-0.45 \mu\text{m/m}$. These values are calculated with a Poisson ratio of 0.3 and a Young modulus of 183.6 GPa.

Energy method

The same model as above has been solved using the energy derivative method for magnetostrictive force calculation. Because of the lack of data on the dependence of magnetisation upon the multidirectional mechanical stress, the measured data with unidirectional stress has been used and the effect of orthogonal stress is modelled making the same assumptions as above. Namely, the transverse magnetostriction is half the parallel and in the opposite direction, and no volume

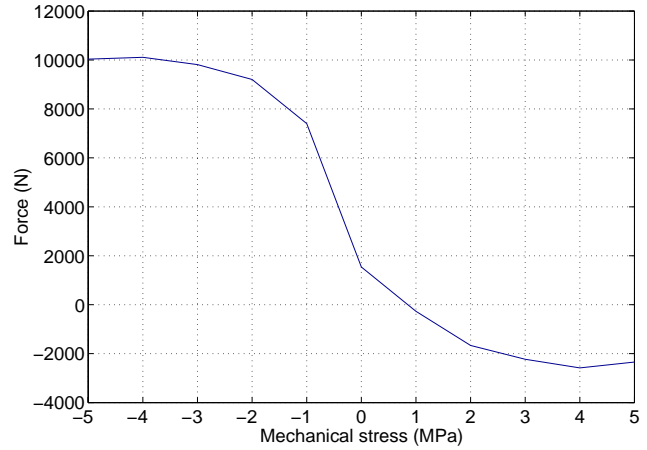
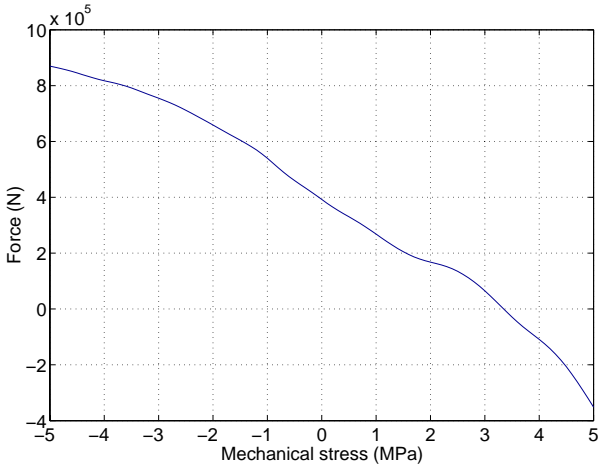
magnetostriction occurs. The first assumption is taken into account only for the calculation of the forces in the orthogonal direction; it is not the real effect of multidirectional stress on the magnetisation.

The calculated forces are of the same form as in the magnetostrictive stress method; they can be seen from Fig. 10. However, the corresponding values of the forces are the non-zero absolute values of the x -components equal to $3.32e+5$ N/m at the corner nodes and $6.64e+5$ N/m at the middle node. The y -components are respectively equal to $0.78e+5$ N/m and $1.56e+5$ N/m. Zero values of the force occur at inside nodes as well as for the x -component for nodes on the horizontal edges and the y -component for vertical edges (except for the corner nodes).

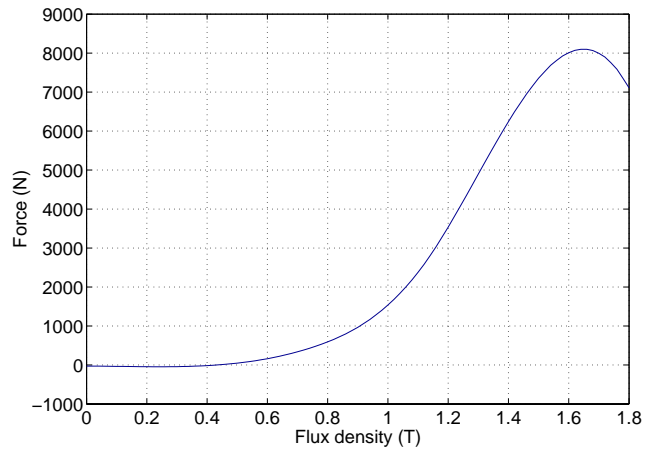
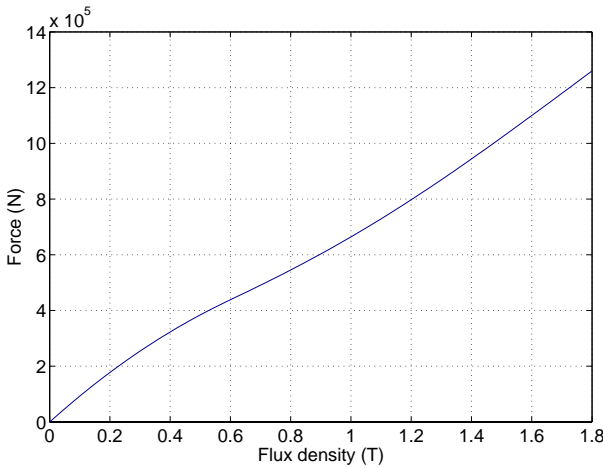
While the shape of the forces, their distribution and ratio are the same as in the magnetostrictive stress method, their absolute values are more than 400 times larger than those calculated with this method. These last ones agree well with the measurements. It is obvious that this difference is due to the lack of information on the effect of multidirectional stress on the magnetisation. Indeed, in the calculation of these forces, the effect of orthogonal stress on the magnetisation acts in the opposite way to the stress in the parallel direction. This would result in a decrease of the forces as a result of a decrease in the derivative of reluctivity, as can be seen from Eq. (10). Another cause of the difference is the inaccuracy in the measurement of magnetisation. In this last measurement, only the averaged single valued curves are taken. This is a good approximation for the magnetic field computation, but it does not approximate well for the magnetostrictive force calculation.

The effect of mechanical stress on the magnetostrictive forces is shown using the example model above. The force in the x -direction of the node in the middle of the right edge has been calculated at various applied mechanical stresses. Fig. 11 shows the result of these calculations with both the magnetostrictive stress method and the energy method; the flux density was 1 T.

The magnetostrictive forces show the same trend with respect to mechanical stress as reported by Ruuskanen (1987). However, the forces calculated with the energy derivative method do not show the saturation effect due to the mechanical stress. The forces calculated with the magnetostrictive stress method show some fluctuations. This is not a real phenomenon; it is due only to the representation of magnetostrictive stress with two-dimensional cubic splines and to measurement inaccuracy.



(a) energy method (b) magnetostrictive stress method
 Fig. 11: Dependence of the magnetostrictive force on mechanical stress.



(a) energy method (b) magnetostrictive stress method
 Fig. 12: Dependence of magnetostriction forces on the flux density.

The change in magnetostrictive forces as a function of the flux density has also been checked by setting the mechanical stress to 0 Pa and varying the flux density from 0 to 1.8 T. These results are reported in Fig. 12. Here the trend is also almost the same for the two methods, but the absolute values are different. Moreover, the decreases of magnetostriction at high flux densities are not seen in the energy derivative method, neither is its correct behaviour seen at very low values of the magnetic flux density.

3.7.3 Maxwell stress method

Here, the method mentioned above that consists of developing the normal component of the Maxwell stress tensor into a two-dimensional Fourier series is applied to a synchronous generator.

The synchronous machine is simulated at its rated operation point using time stepping FE software. In this calculation, because of its symmetry, only half of the machine needs to be modelled. The geometry of the machine and the FE mesh used in the computation are shown in Fig. 13 (because of its symmetry, only half of the machine is shown).

The total of eleven (11) spatial modes ($m = 0, 2, 4, \dots, 20$ in Eq. (53)) and up to the hundredth (100th) frequency component of each mode has been calculated. These frequencies are all multiples of the fundamental frequency (60 Hz).

The results of this calculation are presented in Fig. 14, where the highest peaks are labelled with the corresponding mode number and frequency, as well as the direction of rotation. The frequencies on the x -axis are linearly distributed, while the amplitudes of the stress components on the y -axis are in logarithmic scale. There is one curve for each mode and each direction of rotation.

To show the correlation between the frequencies of the stress and those of the noise from the machine, measurements have been undertaken for the vibration of the stator core, as well as for the noise. The results of those measurements are set out in Fig. 15 for the vibrations and Fig. 16 for the noise. Most of the peaks measured either for the vibration of the stator core or for the noise are also present in the spectra of the stress and vice-versa. This shows that there is a strong correlation between the spectra of the stress and those of the vibrations and noise.

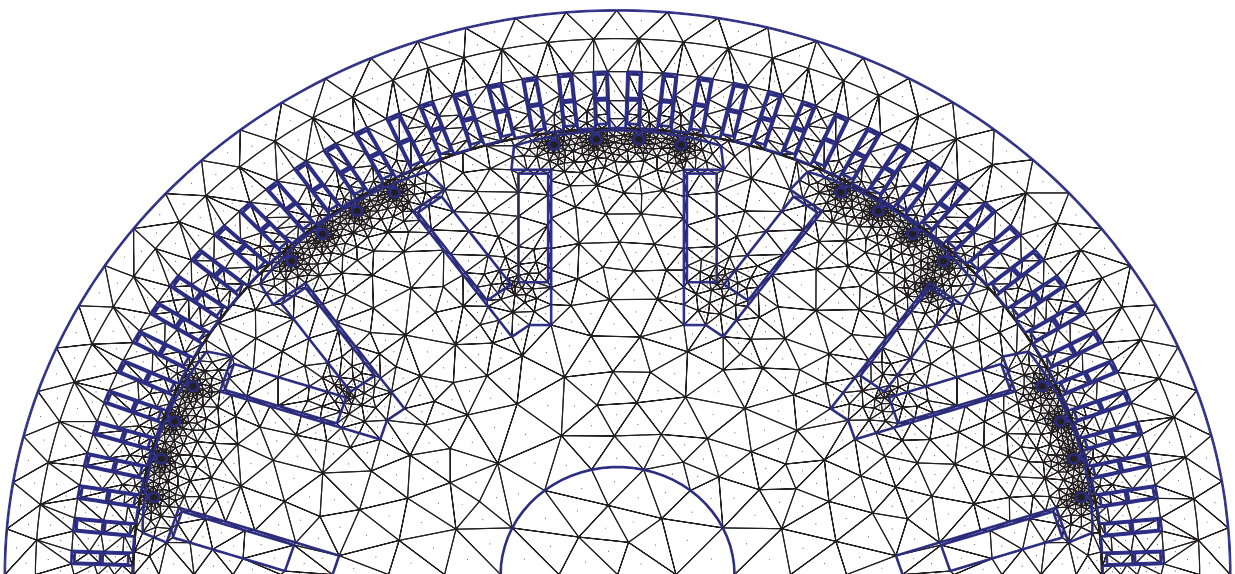


Fig. 13: Geometry and FE mesh of the synchronous generator.

The spectral decomposition of the stress (Fig. 14) shows that, at high frequencies, the sixth ($m = 6$) mode shape and the sixteenth ($m = 16$) mode shape have the largest amplitudes at the respective frequencies of 1080 Hz and 960 Hz. The tenth ($m = 10$) and twentieth ($m = 20$) components have very large amplitudes at the respective frequency of 120 Hz and 240 Hz. These are, however, not the only peaks in the spectra.

The origin of the two last components ($m = 10$ and $m = 20$) is evident. The machine having ten poles, and the force distribution having its maximums at the pole shoe, means that the waves with the numbers of pole pairs equal to ten and twenty are oscillating respectively at twice (120 Hz) and four times (240 Hz) the line frequency. However, the origin of the other modes is more complicated. They can be explained by the effect of slot harmonics combined with the effect of the fractional number of slots per pole and phase. The saturation of iron also causes some harmonics in the flux density and subsequently in the radial component of the stress.

3.8 Conclusions

The calculation of magnetic reluctance forces is best performed using the method of energy derivative, which gives the nodal forces directly. The method of Maxwell stress tensor can be used for the total magnetic force calculation but it does not take the magnetostriction effect into account. Furthermore, the use of the normal component of the Maxwell stress tensor as surface force distribution is shown to have a weak theoretical background. Its possible use for the analysis of noise and vibrations of rotating electrical machines is demonstrated with an example and its advantage is shown.

As to the magnetostriction, it is demonstrated that the magnetostriction forces are best calculated with the method of magnetostrictive stress. Theoretically, they can also be calculated with the method of energy derivative, but this approach still requires some development and accurate measurements, which have to be iterated with calculations to define the constitutive equations of the material.

4 Magnetoelastic coupling

In this chapter, the main equations for the magnetic and elastic field problems are introduced. The different kinds of coupling between these two problems are explained and the coupling method used in this work is developed. The aim of this chapter is to develop and present the equations needed for the implementation of magnetoelastic software for the simulation of rotating electrical machines.

4.1 Magnetic field

In this study, the magnetic field is calculated using the finite element method in two dimensions, together with the time stepping scheme. The finite element method used here is based on the $A-\Phi$ formulation of the magnetic field, while the Crank-Nicholson method is used for time integration.

The electrical machines are treated as quasi-static magnetic systems (Arkkio 1987). In this case, the Maxwell field equations reduce to

$$\nabla \times \mathbf{E} = -\frac{\partial \mathbf{B}}{\partial t} \quad (55)$$

$$\nabla \times \mathbf{H} = \mathbf{J} \quad (56)$$

and the constitutive equations to

$$\mathbf{H} = \nu \mathbf{B} \quad (57)$$

$$\mathbf{J} = \sigma \mathbf{E} \quad (58)$$

Using the vector potential \mathbf{A} and the reduced scalar potential Φ defined by

$$\mathbf{B} = \nabla \times \mathbf{A} \quad (59)$$

and

$$\mathbf{E} = -\frac{\partial \mathbf{A}}{\partial t} - \nabla \Phi \quad (60)$$

we get the equations for the vector and scalar potentials

$$\nabla \times (\nu \nabla \times \mathbf{A}) + \sigma \frac{\partial \mathbf{A}}{\partial t} + \sigma \nabla \Phi = 0 \quad (61)$$

and

$$\nabla \cdot \left(\sigma \frac{\partial \mathbf{A}}{\partial t} \right) + \nabla \cdot (\sigma \nabla \Phi) = 0 \quad (62)$$

For the sake of solution uniqueness, the "Coulomb gauge" is commonly used, i.e.

$$\nabla \cdot \mathbf{A} = 0 \quad (63)$$

In the 2 dimensional case, the Coulomb gauge is satisfied implicitly.

The electrical machine is connected to the network and is usually voltage driven. In the two-dimensional formulation, the voltage equation of conductors (with area S)

$$U = RI + R \int_S \sigma \frac{\partial \mathcal{A}}{\partial t} \cdot dS \quad (64)$$

has to be solved simultaneously with the field equations (61) and (62) (Arkkio 1987). The source of the field being a known potential difference, the equation for the vector potential is

$$\nabla \times (\nu \nabla \times \mathcal{A}) + \sigma \frac{\partial \mathcal{A}}{\partial t} = \frac{\sigma}{l} U e_z \quad (65)$$

where the potential difference between the ends of the conductors U and the conductivity σ are constant at every point on the cross section area of the conductor. l is the length of the conductor. A complete derivation of the above equations is given in Arkkio (1987).

The cross-section of the electrical machine is subdivided into triangular elements. The magnetic vector potential is then approximated within each element in a standard fashion, and the potential distribution in the various elements is constrained to be continuous across inter-element boundaries. The system is discretised, and the set of equations obtained is solved using a computer program.

The nonlinearity of the iron requires an iterative solution process, in order to find the correct solution of the vector potential, which also satisfies the material equations. This is achieved with the Newton-Raphson iteration method (Zienkiewicz 1977).

In electrical machines, there is a rotor movement. Hence, the equations of movement, as well as the changes in the geometry of the cross-section of the machine, have to be taken into account. The equations of movement are solved with the FEM system of equation, while the change in the geometry is brought about with the time-stepping method (Arkkio 1987).

In the time-stepping method, the time interval is also discretised into time steps of equal length. The FE mesh of the region, between the static and moving parts of the machine, is regenerated after each step. The system is solved at each step, taking into account the induced voltages due to the rotor's movement. A full description of the finite element method for electrical machines, as well as that of the time stepping method, is given by Arkkio (1987).

In matrix form, the magnetic problem at each time step reduces to the following equations

$$\begin{bmatrix} \mathbf{S}(A_{k+1}) & [\mathbf{D}^r]^{-T} & [\mathbf{KD}^s]^{-T} \\ \mathbf{D}^r & \mathbf{C}^r & \mathbf{0} \\ \mathbf{KD}^s & \mathbf{0} & \mathbf{G}^s \end{bmatrix} \begin{bmatrix} A_{k+1} \\ \mathbf{u}_{k+1}^r \\ \mathbf{i}_{k+1}^s \end{bmatrix} = \begin{bmatrix} \mathbf{S}(A_k)A_k + [\mathbf{D}^r]^{-T} \mathbf{u}_k^r + [\mathbf{D}^s]^{-T} \mathbf{K}^T \mathbf{i}_k^s \\ \mathbf{D}^r A_k - \mathbf{C}^r \mathbf{u}_k^r - \mathbf{G}^r \mathbf{i}_k^r \\ \mathbf{KD}^s A_k - \mathbf{H}^s \mathbf{i}_k^s - \mathbf{C}^s (V_{k+1}^s + V_k^s) \end{bmatrix} \quad (66)$$

where \mathbf{C}^r , \mathbf{D}^r , \mathbf{D}^s and \mathbf{G}^s are matrices that couple the magnetic vector potential, the voltages and currents in the windings of the machines. The superscripts r and s refer respectively to the rotor and stator windings. \mathbf{K} is a matrix that describes the type of connection of the stator windings. A full description of these matrices and their derivation is given in Arkkio (1987). \mathbf{S} is the magnetic stiffness matrix, the elements of which are given by

$$\begin{aligned} S_{ij} &= \int_{\Omega} \nu \nabla N_i \cdot \nabla N_j d\Omega \\ &= \int_{\hat{\Omega}} \nu \nabla N_i \cdot \nabla N_j \det(\mathbf{J}) d\hat{\Omega} \end{aligned} \quad (67)$$

N_i is the shape function related to the node i , ν the reluctivity of material in the element under consideration, Ω the area of the element, $\hat{\Omega}$ the area of the reference element and \mathbf{J} the Jacobian matrix for the transformation from the reference frame to the global one. The elements of the magnetic stiffness matrix depend on the reluctivity, which in turn depends on the solution of the vector potential. This is a nonlinear problem, the solution of which will be explained when dealing with magnetoelastic coupling. If there is a strong magnetoelastic coupling, the reluctivity depends also on the mechanical stress. These aspects of the problem will be handled later in this chapter when dealing with magnetoelastic coupling.

4.2 Elastic field

The elastic field problem is solved in this work using the displacement approach (Bathe 1982) and the three-point recurrence scheme for second-order equations in the dynamic case (Zienkiewicz 1977).

4.2.1 Equilibrium equations

There are at least three different ways to derive the elastic equilibrium equations (Bathe 1982). In this work, the principle of virtual displacements is chosen because of its simplicity. This method leads to a mechanism for generating the finite element equations that govern the response of a structure or continuum.

The domain under consideration is the stator core of the electrical machine. This domain can be under the effect of surface tractions \mathbf{f}^S , body forces \mathbf{f}^B or concentrated forces \mathbf{F}^i . These forces include all externally applied forces and reactions and have in general three components corresponding to the three coordinate axes

$$\mathbf{f}^S = \begin{bmatrix} f_x^S \\ f_y^S \\ f_z^S \end{bmatrix}; \quad \mathbf{f}^B = \begin{bmatrix} f_x^B \\ f_y^B \\ f_z^B \end{bmatrix}; \quad \mathbf{F}^i = \begin{bmatrix} F_x^i \\ F_y^i \\ F_z^i \end{bmatrix} \quad (68)$$

The displacements of the domain from the unloaded configuration are denoted by \mathbf{u} , where

$$\mathbf{u}^T = [u \quad v \quad w] \quad (69)$$

The strains corresponding to these displacements are

$$\boldsymbol{\varepsilon}^T = [\varepsilon_{xx} \quad \varepsilon_{yy} \quad \varepsilon_{zz} \quad \gamma_{xy} \quad \gamma_{yz} \quad \gamma_{zx}] \quad (70)$$

and the stresses corresponding to $\boldsymbol{\varepsilon}$ are

$$\boldsymbol{\sigma}^T = [\sigma_{xx} \quad \sigma_{yy} \quad \sigma_{zz} \quad \tau_{xy} \quad \tau_{yz} \quad \tau_{zx}] \quad (71)$$

The principle of virtual displacements states that the equilibrium of the domain requires that, for any compatible, small virtual displacements (which satisfy the essential boundary conditions imposed on the domain), the total internal virtual work is equal to the total external work:

$$\int_V \bar{\boldsymbol{\varepsilon}}^T \boldsymbol{\sigma} dV = \int_V \bar{\mathbf{u}}^T \mathbf{f}^B dV + \int_S \bar{\mathbf{u}}^T \mathbf{f}^S dS + \sum_i \bar{\mathbf{u}}^T \mathbf{F}^i \quad (72)$$

The internal virtual work is given on the left side of (72) and the external virtual work of the forces is on the right side. The bar on the top of variables means they are virtual.

After FE discretisation, the displacements measured in a local coordinate system x, y, z within each element m are approximated by

$$\mathbf{u}^{(m)}(x, y, z) = \mathbf{N}^{(m)}(x, y, z) \hat{\mathbf{u}} \quad (73)$$

where $\mathbf{N}^{(m)}$ is the displacement interpolation matrix, also called matrix of shape functions, and $\hat{\mathbf{u}}$ is the vector of the three global displacement components at all nodal points

$$\hat{\mathbf{u}}^T = [u_1 \quad v_1 \quad w_1 \quad \dots \quad w_n] \quad (74)$$

Although $\hat{\mathbf{u}}$ includes the displacements of all the nodal points, only the displacements at the nodes of a given element affect the displacement and strain distributions in that element.

The strains in element m are

$$\boldsymbol{\varepsilon}^{(m)}(x, y, z) = \mathbf{B}^{(m)}(x, y, z) \hat{\mathbf{u}} \quad (75)$$

where $\mathbf{B}^{(m)}$ is the strain-displacement matrix, the rows of which are obtained from the rows of $\mathbf{N}^{(m)}$ by appropriate differentiation and combinations.

The stresses are evaluated from the element strains and initial stresses $\boldsymbol{\sigma}^{\text{I}(m)}$, if any, using

$$\boldsymbol{\sigma}^{(m)} = \mathbf{E}^{(m)} \boldsymbol{\varepsilon}^{(m)} + \boldsymbol{\sigma}^{\text{I}(m)} \quad (76)$$

where $\mathbf{E}^{(m)}$ is the elasticity matrix of element m .

Equation (72) is written as a sum of integrations over the volume and areas of all finite elements.

$$\sum_m \int_{V^{(m)}} \bar{\boldsymbol{\varepsilon}}^{(m)\text{T}} \boldsymbol{\sigma}^{(m)} dV^{(m)} = \sum_m \int_{V^{(m)}} \bar{\mathbf{u}}^{(m)\text{T}} \mathbf{f}^{\text{B}(m)} dV^{(m)} + \sum_m \int_{S^{(m)}} \bar{\mathbf{u}}^{\text{S}(m)\text{T}} \mathbf{f}^{\text{S}(m)} dS^{(m)} + \sum_i \bar{\mathbf{U}}^i\text{T} \mathbf{F}^i \quad (77)$$

Using the approximation in Eq. (73) and the relation of Eq. (76), Eq. (77) can be written in the compact format

$$\mathbf{K}\mathbf{u} = \mathbf{R} \quad (78)$$

where \mathbf{u} now contains the nodal displacements,

$$\mathbf{K} = \sum_m \underbrace{\int_{V^{(m)}} \mathbf{B}^{(m)\text{T}} \mathbf{E}^{(m)} \mathbf{B}^{(m)} dV^{(m)}}_{\mathbf{K}^{(m)}} \quad (79)$$

and

$$\mathbf{R} = \mathbf{R}_\text{B} + \mathbf{R}_\text{C} + \mathbf{R}_\text{I} + \mathbf{R}_\text{S} \quad (80)$$

$$\mathbf{R}_\text{C} = \mathbf{F} \quad (81)$$

$$\mathbf{R}_\text{I} = \sum_m \underbrace{\int_{V^{(m)}} \mathbf{B}^{(m)\text{T}} \boldsymbol{\sigma}^{\text{I}(m)} dV^{(m)}}_{\mathbf{R}_\text{I}^{(m)}} \quad (82)$$

$$\mathbf{R}_\text{S} = \sum_m \underbrace{\int_{S^{(m)}} \mathbf{N}^{\text{S}(m)\text{T}} \mathbf{f}^{\text{S}(m)} \mathbf{B}^{(m)} dS^{(m)}}_{\mathbf{R}^{\text{S}(m)}} \quad (83)$$

The matrix $\mathbf{N}^{\text{S}(m)}$ that appears in Eq.(83) is obtained from $\mathbf{N}^{(m)}$ by substituting the element surface coordinates.

Since this work deals with time-dependent fields, the effects of inertia and damping have to be taken into account. This is done using d'Alembert's principle, which includes the inertia forces as part of the body forces. The damping forces are also included as velocity-dependent terms in the body forces. So that

$$\mathbf{R}_B = \sum_m \int_{V^{(m)}} \mathbf{N}^{(m)T} \left[\mathbf{f}^{B(m)} - \rho^{(m)} \mathbf{N}^{(m)} \ddot{\mathbf{u}} - \kappa^{(m)} \mathbf{N}^{(m)} \dot{\mathbf{u}} \right] dV^{(m)} \quad (84)$$

Introducing Eq. (84) into Eq. (78) and rearranging gives the final second-order matrix-equation of the elastic system

$$\mathbf{M}\ddot{\mathbf{u}} + \mathbf{C}\dot{\mathbf{u}} + \mathbf{K}\mathbf{u} = \mathbf{R} \quad (85)$$

where $\dot{\mathbf{u}} = \frac{\partial \mathbf{u}}{\partial t}$ and $\ddot{\mathbf{u}} = \frac{\partial^2 \mathbf{u}}{\partial t^2}$ are the first- and second-order derivatives of the nodal displacements with respect to time and

$$\mathbf{M} = \sum_m \underbrace{\int_{V^{(m)}} \rho^{(m)} \mathbf{N}^{(m)T} \mathbf{N}^{(m)} dV^{(m)}}_{\mathbf{M}^{(m)}} \quad (86)$$

$$\mathbf{C} = \sum_m \underbrace{\int_{V^{(m)}} \kappa^{(m)} \mathbf{N}^{(m)T} \mathbf{N}^{(m)} dV^{(m)}}_{\mathbf{C}^{(m)}} \quad (87)$$

where $\rho^{(m)}$ and $\kappa^{(m)}$ are respectively the mass density and damping property parameter of element m . The matrices \mathbf{M} , \mathbf{C} , and \mathbf{K} are respectively the mass, damping and stiffness matrices of the system. These matrices are assembled in a standard fashion from element matrices $\mathbf{M}^{(m)}$, $\mathbf{C}^{(m)}$ and $\mathbf{K}^{(m)}$. The knowledge of the parameter $\kappa^{(m)}$ is in general lacking. The damping matrix is then evaluated using the so-called Rayleigh damping

$$\mathbf{C} = \alpha \mathbf{M} + \beta \mathbf{K} \quad (88)$$

with α and β appropriately chosen. These parameters can be calculated from two values of modal damping at given frequencies. Reciprocally, the modal damping at any given frequency can be estimated from the values of α and β . The choice of these parameters is explained in Chapter 7.

4.2.2 Boundary conditions

In the analysis of the elastic field of structures or continua, there are two kinds of boundary conditions. The essential boundary conditions, also called *displacement* or *geometrical boundary conditions*, and the natural boundary conditions, also called *force boundary conditions*. The first ones are the prescribed displacements or rotations, while the second ones are the applied external forces. The latter are taken into account while evaluating the externally applied nodal-point force vector. The displacement boundary conditions are handled in standard fashion (Bathe 1982).

Equation (85) is rewritten as

$$\begin{bmatrix} \mathbf{M}_{aa} & \mathbf{M}_{ab} \\ \mathbf{M}_{ba} & \mathbf{M}_{bb} \end{bmatrix} \begin{bmatrix} \ddot{\mathbf{u}}_a \\ \ddot{\mathbf{u}}_b \end{bmatrix} + \begin{bmatrix} \mathbf{C}_{aa} & \mathbf{C}_{ab} \\ \mathbf{C}_{ba} & \mathbf{C}_{bb} \end{bmatrix} \begin{bmatrix} \dot{\mathbf{u}}_a \\ \dot{\mathbf{u}}_b \end{bmatrix} + \begin{bmatrix} \mathbf{K}_{aa} & \mathbf{K}_{ab} \\ \mathbf{K}_{ba} & \mathbf{K}_{bb} \end{bmatrix} \begin{bmatrix} \mathbf{u}_a \\ \mathbf{u}_b \end{bmatrix} = \begin{bmatrix} \mathbf{R}_a \\ \mathbf{R}_b \end{bmatrix} \quad (89)$$

where the displacements with subscript a are unknown and those with subscript b are prescribed.

Taking only the first line of the matrix equation in Eq. (89), we get

$$\mathbf{M}_{aa}\ddot{\mathbf{u}}_a + \mathbf{C}_{aa}\dot{\mathbf{u}}_a + \mathbf{K}_{aa}\mathbf{u}_a = \mathbf{R}_a - \mathbf{M}_{ab}\ddot{\mathbf{u}}_b - \mathbf{C}_{ab}\dot{\mathbf{u}}_b - \mathbf{K}_{ab}\mathbf{u}_b \quad (90)$$

so that we need to form the system matrices only for the unknown displacements or degrees of freedom. The load vector needs to be modified to include the effect of known nonzero displacements.

When studying the stator core of electrical machines, the problem of imposing boundary conditions is critical. Some studies on the effect of different boundary conditions on the vibrational behaviour of the stator core of such a machine have been undertaken for small size induction machines. The mounting of the machine seems to have an important role in determining the vibration frequencies of different vibration modes. However, for large machines, there are no studies relating to this problem. Moreover, some studies used different kind of symmetries to set the boundary conditions. One of these symmetries is illustrated in Fig. 17. This kind of symmetry is not accurate, since it forces the nodes on the symmetry boundaries to have zero displacement in at least one direction, which is not in accordance with the physical behaviour of the machine. We know that the teeth of the stator are displaced in all directions.

In this work, I choose to impose boundary conditions that are the most consistent with the goal of this research. Namely, the outer edge of the stator core is allowed to move in the radial direction but is prohibited from rotating around the centre of the machine. For nodes on this outer surface, this corresponds to a free radial displacement and zero tangential displacement.

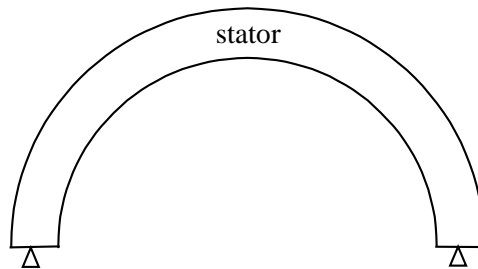


Fig. 17: Symmetric boundary conditions.

Since the degrees of freedom, on which the boundary conditions are imposed (i.e. radial and tangential displacements), are not aligned with the global or local Cartesian coordinate system, we need to express them in terms of the corresponding degrees of freedom of the defined assemblage (i.e. displacements in the Cartesian coordinate system). Thus, we write

$$\mathbf{u} = \mathbf{T}\bar{\mathbf{u}} \quad (91)$$

with $\bar{\mathbf{u}}$ the vector of nodal displacements in the required direction. \mathbf{T} is an identity matrix that has been altered by the direction cosines of the components in $\bar{\mathbf{u}}$ measured on the original displacement direction. Equation (85) becomes

$$\bar{\mathbf{M}}\ddot{\bar{\mathbf{u}}} + \bar{\mathbf{C}}\dot{\bar{\mathbf{u}}} + \bar{\mathbf{K}}\bar{\mathbf{u}} = \bar{\mathbf{R}} \quad (92)$$

with

$$\bar{\mathbf{M}} = \mathbf{T}^T \mathbf{M} \mathbf{T}; \quad \bar{\mathbf{C}} = \mathbf{T}^T \mathbf{C} \mathbf{T}; \quad \bar{\mathbf{K}} = \mathbf{T}^T \mathbf{K} \mathbf{T}; \quad \bar{\mathbf{R}} = \mathbf{T}^T \mathbf{R} \quad (93)$$

In the two-dimensional approximation, two different approaches can be adopted. They are the plane stress and plane strain.

The plane stress means that the only non-zero components of stress are in-plane. The other components are zero. For the plane strain, the in-plane components of strain are non-zero and the others are zero. Subsequently, the off-plane components of strain and stress respectively in plane stress and plane strain are different from zero. However, their contributions to the internal work vanish, since their counterparts, components of stress and strain, respectively, are zero.

The implementation of the plane stress or plane strain is the same; the only difference is in the expression for the elasticity matrix $[\mathbf{E}]$. In this work, the plane stress approach was adopted, but the computation routines are such that calculations with the plane strain approach are also possible. The choice of one or other is more or less subjective. The main criterion behind this choice is the fact that, in rotating electrical machines, both ends of the machine are allowed to move freely. This situation corresponds better to the plane stress approach.

4.2.3 Time discretisation

From the previous section, we obtained a second-order time-differential equation for the elastic field problem. The solution of such an equation can be achieved using one of the recurrence schemes summarised by Zienkiewicz (1977).

The recurrence formula corresponding to Eq. (85) is

$$\begin{aligned}
& \left[\mathbf{M} + \gamma \Delta t \mathbf{C} + \beta \Delta t^2 \mathbf{K} \right] \mathbf{u}_{k+1} \\
& + \left[-2\mathbf{M} + (1-2\gamma) \Delta t \mathbf{C} + \left(\frac{1}{2} - 2\beta + \gamma \right) \Delta t^2 \mathbf{K} \right] \mathbf{u}_k \\
& + \left[\mathbf{M} - (1-\gamma) \Delta t \mathbf{C} + \left(\frac{1}{2} + \beta - \gamma \right) \Delta t^2 \mathbf{K} \right] \mathbf{u}_{k-1} = \\
& \Delta t^2 \left(\beta \mathbf{R}_{k+1} + \left(\frac{1}{2} - 2\beta + \gamma \right) \mathbf{R}_k + \left(\frac{1}{2} + \beta - \gamma \right) \mathbf{R}_{k-1} \right)
\end{aligned} \tag{94}$$

where Δt is the length of the time step, γ and β are constants defining the type of recurrence scheme used; the indices $k+1$, k and $k-1$ refer respectively to the present and the two previous time steps. As expected, the solution of equation (85) or (94) requires the knowledge of two prior solutions as initial ones. These initial solutions can be calculated with a static approach. If the system is sufficiently damped, the zero solution will be enough to reach a stable solution after some transient calculation time.

4.3 Magnetoelastic coupling

When speaking about coupling, we need to clarify the terminology related to this subject. Inside the material itself, there are some physical phenomena that govern the behaviour of the material under external constraints such as mechanical stress, magnetic field, temperature field and so on. The response of the material to different constraints can be measured separately and constitutive laws can be derived. The effect of the interactions between different phenomena can be also measured to a certain extent.

From the point of view of modelling, the different physical phenomena defining the behaviour of the material or a structure can be modelled as uncoupled, or as coupled at different levels, depending on the objectives and goals of the models. The coupling can be local or global. On one hand, the local coupling consists of coupled constitutive equations of the material, while on the other hand, the global coupling consists of coupled field solutions, either with or without coupled constitutive equations. Furthermore, the coupling can be direct or indirect. The meaning of these terms is explained in the following sections and illustrated in Fig. 18.

4.3.1 Indirect coupling

Indirect coupling means that the magnetic, mechanical, thermal and other properties of the material are not directly related to each other, either because we do not know the exact relation between these properties, or because the dependence of one on the other is so small that we can ignore it. If we ignore the coupling between materials' properties we can still have a coupling between different fields. Indirect coupling can be either weak (unidirectional) or strong.

Weak coupling

The weak coupling is one possibility allowed by indirect coupling. It means that the effect of the solution of one field on the other is only unidirectional. At a material-properties level, it also means that the effect of the solution of one field on the properties related to the other field is ignored.

In magnetoelastic coupling, the weak coupling corresponds to the effect of the magnetic field on the elastic field through magnetic forces, without any effect on the properties of the material. The magnetic forces are then used as a load in the elastic field analysis. In this case, there is no back effect of the elastic field on the magnetic field or on the magnetic properties of the material. This approach is commonly used in the conventional design of electrical machines and apparatus that use conventional materials such as iron, steel and copper and are not subject to very strict requirements as to acoustic noise and vibrations.

Neither the effect of magnetostriction, nor the effect of geometrical changes due to elastic displacement, can be taken into account accurately in such an analysis. The magnetostriction of iron is stress sensitive within the range of stress occurring in electrical machines; the new geometry requires new magnetic analysis either with FE, or analytically if we suppose linear behaviour.

The weak coupling is usually implemented so that the magnetic field is first solved with a computer program or one of its components. Then, from the solution of the magnetic field, the magnetic forces are calculated using one of the force calculation methods presented in Chapter 3. The magnetic forces are then fed to another computer program that performs the elastic or mechanical analysis to solve the displacement field from which different mechanical quantities can be calculated (see). In this approach, the magnetic analysis is concerned with the electrical design of the machine.

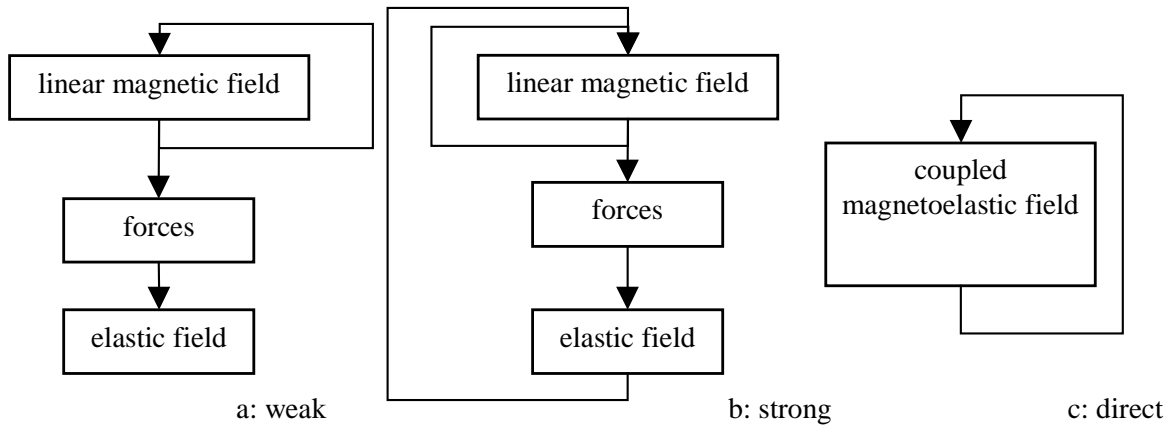


Fig. 18: Flow charts of different kinds of coupling.

It is meant to calculate the voltage, current, torque, power and other operational quantities. The mechanical analysis on the other hand is meant to determine whether the mechanical parts of the machine can stand the magnetic forces. The analysis checks the validity of the mounting, the vibrational behaviour and possibly the noise of the machine.

Weak coupling is also used in magneto-thermal analysis, where the calculated electrical and magnetic losses are used as load in the thermal problem. Only the approximate effect of temperature on the resistance of conductors is taken into account. Usually, the solution of the thermal analysis is not used to calculate the exact resistance corresponding to the calculated temperature.

Strong coupling

The indirect coupling can be implemented also as strong coupling. In this case, not only the effect of the magnetic field on the elastic one is taken into account, but also the effect of the elastic field on the magnetic one is accounted for. This kind of analysis is necessary if the mechanical stress in the machine is so high that it changes the magnetic properties of the material. The elastic displacement field can also change the geometry of the machine and affect the solution of the magnetic field. The strong coupling requires an iterative procedure using either the same computer program or different programs to solve the magnetic and elastic field.

In FE analysis, the indirect coupling, either weak or strong, is implemented by assembling different system matrices for the magnetic and elastic field. Moreover, the elastic and magnetic properties of the material are separated. The Poisson ratio and Young modulus do not depend on the magnetic field, while the magnetic permeability is either not dependent on mechanical stress (weak coupling)

or is represented by a set of stress parameterised magnetisation curves (strong coupling). This approach makes it possible to account for both geometrical changes and magnetostriction.

4.3.2 Direct coupling

In general, the direct coupling requires the knowledge of the interaction between different phenomena governing the behaviour of the material. It also requires the knowledge of the interaction between the analysed fields.

In magnetoelastic models, the strong coupling requires constitutive equations that couple the magnetic and the elastic properties of the material. These equations define the relations between the magnetic field \mathbf{H} , the magnetic flux density \mathbf{B} , the elastic stress σ and the elastic strain ε . Such relations have been presented by Besbes et al. (2001). The presented relations require complicated measurements for the determination of the parameters that are material dependent. The relation between the nodal magnetic vector potential and elastic nodal displacement is also needed to achieve such an analysis. These relations can be either explicit or implicit. The explicit case is possible only in very simple geometry. Thus, only the implicit case can be of interest. The implicit case is to some extent similar to the indirect coupling. Flow charts of Fig. 18 illustrate the different kinds of coupling and the differences between them.

4.3.3 Hybrid method

The transient dynamic analysis of a magnetoelastically coupled system brings more possibilities to the types of coupling mentioned above. In this work, a hybrid method from strong and direct coupling is used with the time stepping scheme to analyse the vibrations of the stator of electrical machines under the effect of magnetic and magnetostriction forces. This method is developed here. The flow chart of the method is illustrated in Fig. 19.

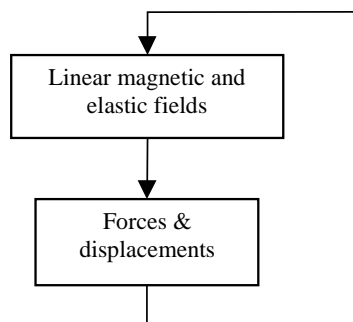


Fig. 19: Flow chart of the hybrid method of coupling.

The FE time stepping system of equations for the magnetic field (Eq. (66)) and elastic field (Eq. (94)) are gathered to form one matrix equation

$$\begin{bmatrix} S(A_{k+1}, \mathbf{u}_{k+1}) & [\mathbf{D}^r]^T & [K\mathbf{D}^s]^T & \mathbf{0} \\ \mathbf{D}^r & \mathbf{C}^r & \mathbf{0} & \mathbf{0} \\ K\mathbf{D}^s & \mathbf{0} & \mathbf{G}^s & \mathbf{0} \\ \mathbf{0} & \mathbf{0} & \mathbf{0} & \tilde{\mathbf{K}} \end{bmatrix} \begin{bmatrix} A_{k+1} \\ \mathbf{u}_{k+1}^r \\ \mathbf{i}_{k+1}^s \\ \mathbf{u}_{k+1} \end{bmatrix} = \begin{bmatrix} S'(A_k, \mathbf{u}_k)A_k + [\mathbf{D}^r]^T \mathbf{u}_k^r + [\mathbf{D}^s]^T \mathbf{K}^T \mathbf{i}_k^s \\ \mathbf{D}^r A_k - \mathbf{C}^r \mathbf{u}_k^r - \mathbf{G}^r \mathbf{i}_k^r \\ K\mathbf{D}^s A_k - \mathbf{H}^s \mathbf{i}_k^s - \mathbf{C}^s (\mathbf{V}_{k+1}^s + \mathbf{V}_k^s) \\ \tilde{\mathbf{F}}_{k+1}(A_{k+1}) \end{bmatrix} \quad (95)$$

where

$$\tilde{\mathbf{K}} = [\mathbf{M} + \gamma \Delta t \mathbf{C} + \beta \Delta t^2 \mathbf{K}] \quad (96)$$

$$\tilde{\mathbf{F}}_{k+1} = \Delta t^2 \left(\beta \mathbf{F}_{k+1} + \left(\frac{1}{2} - 2\beta + \gamma \right) \mathbf{F}_k + \left(\frac{1}{2} + \beta - \gamma \right) \mathbf{F}_{k-1} \right)$$

and

$$\begin{aligned} & - \left[-2\mathbf{M} + (1-2\gamma) \Delta t \mathbf{C} + \left(\frac{1}{2} - 2\beta + \gamma \right) \Delta t^2 \mathbf{K} \right] \mathbf{u}_k \\ & - \left[\mathbf{M} - (1-\gamma) \Delta t \mathbf{C} + \left(\frac{1}{2} + \beta - \gamma \right) \Delta t^2 \mathbf{K} \right] \mathbf{u}_{k-1} \end{aligned} \quad (97)$$

Equation (95) is nonlinear and contains quantities that depend on the solution itself. On one hand, the nonlinearity is due to the magnetic properties of the material, while, on the other, the force vector needs the solution of the magnetic field and the magnetic stiffness matrix depends on the solution of the elastic field. This is what we call implicit coupling between the magnetic and elastic fields. The magnetic permeability of the material depends not only on the magnetic field strength, but also on the mechanical stress, thus, on the solution of the elastic field. The knowledge of this constitutive relation would allow us to have a direct coupling, but this is not possible without accurate and complicated measurements. Thus the idea of a hybrid model that calls for iterations inside the same time step for the two reasons mentioned above, namely nonlinearity and implicit coupling.

The solution of Eq. (95) is performed using Newton-Raphson iteration scheme. The residual of the equation is

$$[\mathbf{r}] = \begin{bmatrix} S(A_{k+1}, \mathbf{u}_{k+1}) & [\mathbf{D}^r]^T & [K\mathbf{D}^s]^T & \mathbf{0} \\ \mathbf{D}^r & \mathbf{C}^r & \mathbf{0} & \mathbf{0} \\ K\mathbf{D}^s & \mathbf{0} & \mathbf{G}^s & \mathbf{0} \\ \mathbf{0} & \mathbf{0} & \mathbf{0} & \tilde{\mathbf{K}} \end{bmatrix} \begin{bmatrix} A_{k+1} \\ \mathbf{u}_{k+1}^r \\ \mathbf{i}_{k+1}^s \\ \mathbf{u}_{k+1} \end{bmatrix} - \begin{bmatrix} S'(A_k, \mathbf{u}_k)A_k + [\mathbf{D}^r]^T \mathbf{u}_k^r + [\mathbf{D}^s]^T \mathbf{K}^T \mathbf{i}_k^s \\ \mathbf{D}^r A_k - \mathbf{C}^r \mathbf{u}_k^r - \mathbf{G}^r \mathbf{i}_k^r \\ K\mathbf{D}^s A_k - \mathbf{H}^s \mathbf{i}_k^s - \mathbf{C}^s (\mathbf{V}_{k+1}^s + \mathbf{V}_k^s) \\ \tilde{\mathbf{F}}_{k+1}(A_{k+1}) \end{bmatrix} \quad (98)$$

The Jacobian matrix is defined as

$$[P_{ij}] = \begin{bmatrix} \frac{\partial \mathbf{r}}{\partial \mathcal{A}} & \frac{\partial \mathbf{r}}{\partial \mathbf{u}^r} & \frac{\partial \mathbf{r}}{\partial \mathbf{i}^s} & \frac{\partial \mathbf{r}}{\partial \mathbf{u}} \end{bmatrix} \quad (99)$$

For a linear elastic problem, we have $\frac{\partial \tilde{\mathbf{K}}}{\partial \mathbf{u}} = [\mathbf{0}]$, and because the elastic stiffness matrix does not depend on the magnetic field, we also have $\frac{\partial \tilde{\mathbf{K}}}{\partial \mathcal{A}} = [\mathbf{0}]$. The matrices \mathbf{C} , \mathbf{D} , \mathbf{G} and \mathbf{K} do not depend on any of the unknown variables, neither does the system matrix depend on the current and voltage variables. The Jacobian matrix for the system of equations is then

$$[\mathbf{P}] = \begin{bmatrix} \mathbf{S}(A_{k+1}, \mathbf{u}_{k+1}) + \frac{\partial \mathbf{S}(A_{k+1}, \mathbf{u}_{k+1})}{\partial \mathcal{A}} A_{k+1} & [\mathbf{D}^r]^\top & [\mathbf{KD}^s]^\top & \frac{\partial \mathbf{S}(A_{k+1}, \mathbf{u}_{k+1})}{\partial \mathbf{U}} A_{k+1} \\ \mathbf{D}^r & \mathbf{C}^r & \mathbf{0} & \mathbf{0} \\ \mathbf{KD}^s & \mathbf{0} & \mathbf{G}^s & \mathbf{0} \\ -\frac{\partial \tilde{\mathbf{F}}_{k+1}}{\partial \mathcal{A}} & \mathbf{0} & \mathbf{0} & \tilde{\mathbf{K}} - \frac{\partial \tilde{\mathbf{F}}_{k+1}}{\partial \mathbf{u}} \end{bmatrix} \quad (100)$$

At each iteration-step n we have to solve the linear system of equations

$$[\mathbf{P}] \begin{bmatrix} \Delta A_{k+1}^n \\ \Delta \mathbf{u}_{k+1}^{r,n} \\ \Delta \mathbf{i}_{k+1}^{s,n} \\ \Delta \mathbf{u}_{k+1}^n \end{bmatrix} = \begin{bmatrix} \mathbf{S}'(A_k) A_k + [\mathbf{D}^r]^\top \mathbf{u}_k^r + [\mathbf{D}^s]^\top \mathbf{K}^\top \mathbf{i}_k^s - \left(\mathbf{S}(A_{k+1}^n) A_{k+1}^n + [\mathbf{D}^r]^\top \mathbf{u}_{k+1}^{r,n} + [\mathbf{D}^s]^\top \mathbf{K}^\top \mathbf{i}_{k+1}^{s,n} \right) \\ \mathbf{KD}^s A_k - \mathbf{H}^s \mathbf{i}_k^s - \mathbf{C}^s (\mathbf{V}_{k+1}^s + \mathbf{V}_k^s) - \left(\mathbf{KD}^s A_{k+1}^n - \mathbf{H}^s \mathbf{i}_{k+1}^{s,n} - \mathbf{C}^s (\mathbf{V}_{k+1}^s + \mathbf{V}_k^s) \right) \\ \mathbf{D}^r A_k - \mathbf{C}^r \mathbf{u}_k^r - \mathbf{G}^r \mathbf{i}_k^r - \left(\mathbf{D}^r A_{k+1}^n - \mathbf{C}^r \mathbf{u}_{k+1}^{r,n} - \mathbf{G}^r \mathbf{i}_{k+1}^{r,n} \right) \\ \tilde{\mathbf{F}}_{k+1}^n - \tilde{\mathbf{K}} \mathbf{u}_{k+1}^n \end{bmatrix} \quad (101)$$

and evaluate the variables for the next iteration-step $n+1$ as

$$\begin{aligned} A_{k+1}^{n+1} &= A_{k+1}^n + \Delta A_{k+1}^n \\ \mathbf{u}_{k+1}^{r,n+1} &= \mathbf{u}_{k+1}^{r,n} + \Delta \mathbf{u}_{k+1}^{r,n} \\ \mathbf{i}_{k+1}^{s,n+1} &= \mathbf{i}_{k+1}^{s,n} + \Delta \mathbf{i}_{k+1}^{s,n} \\ \mathbf{u}_{k+1}^{n+1} &= \mathbf{u}_{k+1}^n + \Delta \mathbf{u}_{k+1}^n \end{aligned} \quad (102)$$

The matrix \mathbf{P} contains terms that need some development. First, the term with $\frac{\partial \tilde{\mathbf{F}}_{k+1}}{\partial \mathbf{u}}$ is ignored as being a second-order derivative of magnetic energy with respect to displacement. Second, the term with $\frac{\partial \tilde{\mathbf{F}}}{\partial \mathcal{A}}$, which can be calculated as

$$\frac{\partial \tilde{\mathbf{F}}}{\partial \mathcal{A}} = \left[-\frac{\partial \mathbf{S}}{\partial \mathbf{u}} \mathbf{A} \right]^\top \quad (103)$$

This can be demonstrated in case of $\beta = 1$ for which $\frac{\partial \tilde{\mathbf{F}}}{\partial \mathcal{A}} = \frac{\partial \mathbf{F}}{\partial \mathcal{A}}$.

$$\begin{aligned}
\frac{\partial \mathbf{F}}{\partial \mathbf{A}} &= -\frac{\partial}{\partial \mathbf{A}} \frac{\partial W}{\partial \mathbf{u}} \\
&= -\frac{\partial}{\partial \mathbf{A}} \frac{\partial}{\partial \mathbf{u}} \int_0^A \mathbf{A}^T \mathbf{S} dA \\
&= \left[-\frac{\partial \mathbf{S}}{\partial \mathbf{u}} \mathbf{A} \right]^T
\end{aligned} \tag{104}$$

In Eq. (104), the symmetry $\mathbf{S}^T = \mathbf{S}$ has been used as well as the alternative expression for magnetic energy in terms of FE variables. The equality in Eq. (103) renders the system matrix symmetric. The term with $\frac{\partial \mathbf{S}}{\partial \mathbf{u}}$ can be assembled from the same term calculated at element level

$$\frac{\partial \mathbf{S}^e}{\partial \mathbf{u}} = \begin{bmatrix} \frac{\partial \mathbf{S}^e}{\partial u_1} & \frac{\partial \mathbf{S}^e}{\partial v_1} & \frac{\partial \mathbf{S}^e}{\partial u_2} & \frac{\partial \mathbf{S}^e}{\partial v_2} & \frac{\partial \mathbf{S}^e}{\partial u_3} & \frac{\partial \mathbf{S}^e}{\partial v_3} \end{bmatrix} \tag{105}$$

the elements of which are given by

$$\begin{aligned}
\frac{\partial S_{ij}}{\partial u_l} &= \int_{\hat{\Omega}} \frac{\partial}{\partial u_l} [\mathbf{v} \nabla N_i \cdot \nabla N_j \det(\mathbf{J})] d\hat{\Omega} \\
&= \overbrace{\int_{\hat{\Omega}} \frac{\partial \mathbf{v}}{\partial u_l} [\nabla N_i \cdot \nabla N_j \det(\mathbf{J})] d\hat{\Omega}}^{(1)} + \\
&\quad \overbrace{\int_{\hat{\Omega}} \mathbf{v} \frac{\partial}{\partial u_l} ([\nabla N_i \cdot \nabla N_j \det(\mathbf{J})]) d\hat{\Omega}}^{(2)}
\end{aligned} \tag{106}$$

with

$$\text{term1} = \int_{\hat{\Omega}} \frac{\partial \mathbf{v}(\mathbf{B}^2, \sigma)}{\partial u_l} [\nabla N_i \cdot \nabla N_j \det(\mathbf{J})] d\hat{\Omega} \tag{107}$$

and

$$\text{term2} = \int_{\hat{\Omega}} \mathbf{v} \frac{\partial \det(\mathbf{J})}{\partial u_l} ([\nabla N_i \cdot \nabla N_j]) d\hat{\Omega} + \int_{\hat{\Omega}} \mathbf{v} \frac{\partial ([\nabla N_i \cdot \nabla N_j])}{\partial u_l} \det(\mathbf{J}) d\hat{\Omega} \tag{108}$$

In Eq. (107), we have

$$\frac{\partial \mathbf{v}(\mathbf{B}^2, \sigma)}{\partial u_l} = \frac{\partial \mathbf{v}}{\partial \mathbf{B}^2} \frac{\partial \mathbf{B}^2}{\partial u_l} + \frac{\partial \mathbf{v}}{\partial \sigma_{\parallel}} \frac{\partial \sigma_{\parallel}}{\partial u_l} + \frac{\partial \mathbf{v}}{\partial \sigma_{\perp}} \frac{\partial \sigma_{\perp}}{\partial u_l} + \frac{\partial \mathbf{v}}{\partial \tau} \frac{\partial \tau}{\partial u_l} \tag{109}$$

If we consider only the effect of unidirectional mechanical stress in the direction of the flux density \mathbf{B} , we get

$$\frac{\partial S_{ij}}{\partial u_l} = \int_{\hat{\Omega}} \left\{ \left(\left(\frac{\partial v}{\partial \mathbf{B}^2} \frac{\partial \mathbf{B}^2}{\partial u_l} + \frac{\partial v}{\partial \sigma} \frac{\partial \sigma}{\partial u_l} \right) \det(\mathbf{J}) + v \frac{\partial \det(\mathbf{J})}{\partial u_l} \right) [\nabla N_i \cdot \nabla N_j] + v \frac{\partial ([\nabla N_i \cdot \nabla N_j])}{\partial u_l} \det(\mathbf{J}) \right\} d\hat{\Omega} \quad (110)$$

where the terms with $\frac{\partial v}{\partial \mathbf{B}^2}$, $\frac{\partial \mathbf{B}^2}{\partial u_l}$, $\frac{\partial v}{\partial \sigma}$, $\frac{\partial \sigma}{\partial u_l}$ and $\frac{\partial \det(\mathbf{J})}{\partial u_l}$ have been developed in the force calculation and the terms with $\nabla N_i \cdot \nabla N_j$ and $\det(\mathbf{J})$ are calculated in a standard fashion.

We also have the following terms needed for the calculation of Eq. (110)

$$\frac{\partial \nabla N_i \cdot \nabla N_j}{\partial u_l} = \left(-\frac{\frac{\partial \det(\mathbf{J})}{\partial u_l}}{\det(\mathbf{J})} \right) \nabla N_i \cdot \nabla N_j + \frac{1}{\det(\mathbf{J})^2} \left[\left(\left(2 \frac{\partial N_l}{\partial \eta} J_{21} \right) \frac{\partial N_i}{\partial \xi} - \left(\frac{\partial N_l}{\partial \xi} J_{21} + J_{11} \frac{\partial N_l}{\partial \eta} \right) \frac{\partial N_i}{\partial \eta} \right) \frac{\partial N_j}{\partial \xi} + \left(\left(2 \frac{\partial N_l}{\partial \xi} J_{11} \right) \frac{\partial N_i}{\partial \eta} - \left(\frac{\partial N_l}{\partial \xi} J_{21} + J_{11} \frac{\partial N_l}{\partial \eta} \right) \frac{\partial N_i}{\partial \xi} \right) \frac{\partial N_j}{\partial \eta} \right] \quad (111)$$

and

$$\frac{\partial \nabla N_i \cdot \nabla N_j}{\partial v_l} = \left(-\frac{\frac{\partial \det(\mathbf{J})}{\partial v_l}}{\det(\mathbf{J})} \right) \nabla N_i \cdot \nabla N_j + \frac{1}{\det(\mathbf{J})^2} \left[\left(\left(2 \frac{\partial N_l}{\partial \eta} J_{22} \right) \frac{\partial N_i}{\partial \xi} - \left(\frac{\partial N_l}{\partial \xi} J_{22} + J_{12} \frac{\partial N_l}{\partial \eta} \right) \frac{\partial N_i}{\partial \eta} \right) \frac{\partial N_j}{\partial \xi} + \left(\left(2 \frac{\partial N_l}{\partial \xi} J_{12} \right) \frac{\partial N_i}{\partial \eta} - \left(\frac{\partial N_l}{\partial \xi} J_{22} + J_{12} \frac{\partial N_l}{\partial \eta} \right) \frac{\partial N_i}{\partial \xi} \right) \frac{\partial N_j}{\partial \eta} \right] \quad (112)$$

In the calculations of Chapter 7, the coupling terms between the magnetic and elastic problems in the system matrix are small compared to the other terms. This results in an ill-conditioned matrix that would require extra conditioning for the coupled problem. However, this procedure was not needed, since the iteration process converged without these coupling terms, but with an extra iteration at each step. On one hand, this makes the calculation time longer; on the other, it saves time, since no conditioning is needed.

In systems with large displacements or a strong dependency of the force on the magnetic vector potential (i.e. on the magnetic field distribution), the solution process would require either a

conditioning of the matrix or many more iterations. In that case, an estimation of the calculation time for both processes is needed to make a choice that minimises the global calculation time. This situation will be experienced when both the magnetoelastic coupling and the stress-dependency of the magnetostrictive forces are taken into account in Chapter 7. Indeed, in that case, the iteration process does not converge.

4.4 Conclusions

Different kinds of magnetoelastic coupling have been presented and discussed. A hybrid method of magnetoelastic coupling has been introduced and the equations related to this method have been derived from the magnetic and elastic field equations.

It is shown that the effect of mechanical stress on the magnetostriction of magnetic materials can be taken into account only in a strong coupling approach either directly or indirectly. The introduced hybrid method of coupling is able to account for both the geometrical changes and the magnetostriction with its stress dependency.

The Hybrid method for magnetoelastic coupling is used in the coupled calculations of Chapter 7. The stress-dependency of the magnetic properties (only the magnetostriction) is taken into account in separate cases to show their effect on the vibrations.

5 Measurements

The aim of this chapter is to introduce a device for measuring the magnetic properties of electrical steel sheets, and to describe the set-up of the device. The measured properties are the magnetic flux density versus the magnetic field strength, together with the externally applied mechanical stress, and the magnetostrictive stress versus the magnetic flux density, together with the externally applied mechanical stress. The measurements demonstrate the dependency of the measured quantities on the applied mechanical stress. The results of these measurements are developed in a form adequate for further use in the computations of Chapters 6 and 7.

5.1 Measurement of magnetisation

The FE computation of magnetic fields in electrical machines requires knowledge of the magnetic properties of materials used in the machine. Among these properties, the specific total loss and the magnetisation data of magnetic materials are needed. The manufacturers of electrical steel sheets usually provide these properties.

There are several standard methods for the measurement of magnetic properties of magnetic materials. One of the most widely used methods is the 25 cm Epstein frame method (IEC 60404-2 1996). These methods give the magnetisation data as a function of magnetic field strength; the specific total loss is given as a function of magnetic flux density.

However, the calculation of magnetic and magnetostriction forces as described in Chapter 3, as well as the magnetoelastic coupling as described in Chapter 4, requires more complex material properties. These are the magnetisation and the magnetostriction data, not only as a function of the magnetic field strength or magnetic flux density, but also as a function of the externally applied mechanical stress. This kind of data is not standard, neither is it provided by the manufacturers of electrical steel sheets. In this work, the measurement of such data was conducted using a slightly modified version of the 25 cm Epstein frame. The modifications mainly involve the dimensions of the test specimen and the use of extra insulation between strips. These modifications are necessary to allow for the application of externally applied mechanical stress. This particular modification was applied and measured by a system of screws and load cells as shown in Fig. 20. A photo of the Epstein frame is shown in Fig. 21.

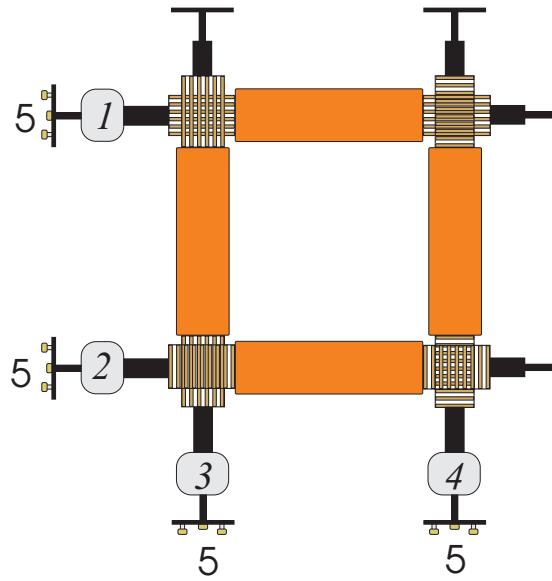


Fig. 20: Schematic of the modified Epstein frame (1,2,3 and 4 are load cells, 5 screw system to apply mechanical stress).

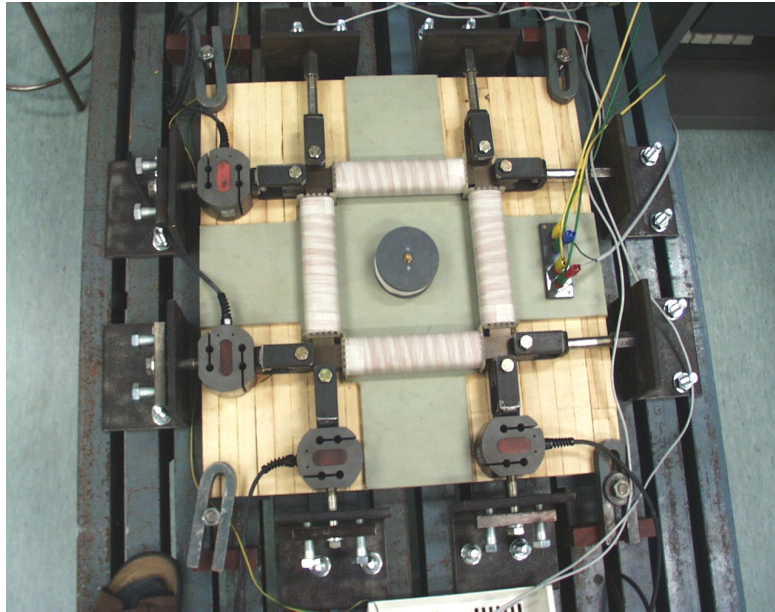


Fig. 21: Photo of the modified Epstein frame (load cells and screw systems are visible).

The screw system allowed for the application of both tensile (positive) and compressive (negative) mechanical stresses. The use of plastic strips in between the iron strips prevented them bending when compressive stress was applied.

The measurement set-up for the stress-dependent magnetisation data is shown in Fig. 22. The dc-measurement method was used. The mechanical stress was varied from a value of -5.23 MPa to 5.23 MPa by steps of 0.436 MPa. At each step, the dc-measurement of the magnetisation was carried out by changing the primary current from a minimum value to a maximum one and back to the first value in very small steps, very slowly.

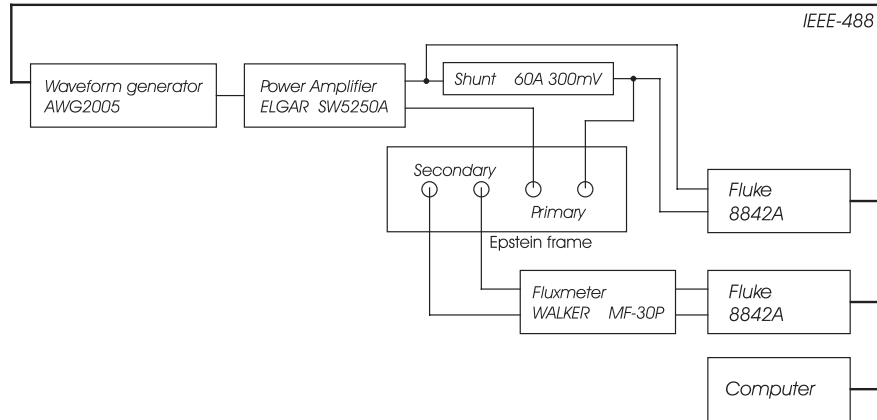


Fig. 22: Measurement set-up for stress-dependent magnetisation.

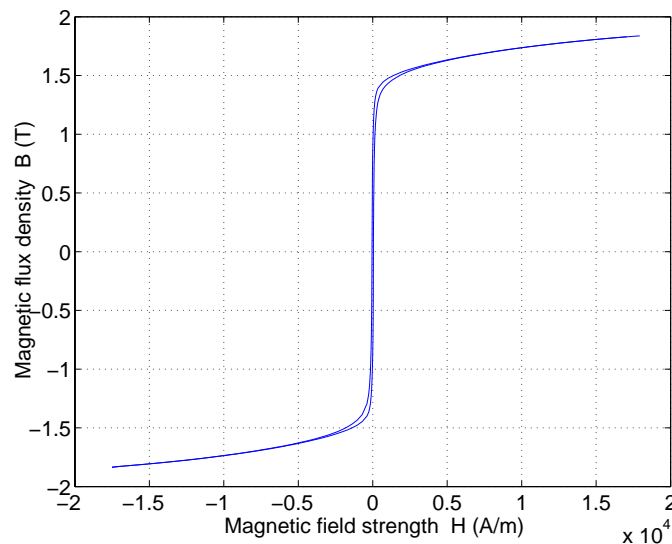


Fig. 23: Measured hysteresis loop at no externally applied mechanical stress.

The corresponding maximum and minimum values of the average magnetic field strength in iron were calculated from the measured current as, respectively, -18 kA/m and 18 kA/m and those of the magnetic flux density were calculated from the induced voltage as, respectively, -1.8 T and 1.8 T .

The measured hysteresis loop at no mechanical stress ($\sigma = 0$) is shown in Fig. 23. Single-valued magnetisation curves were calculated from the hysteresis loops at each value of the applied mechanical stress. The calculation procedure for single-valued magnetisation and magnetostriction curves is explained later in this chapter. The positive parts of the single-valued curves (first quadrant) were taken as magnetisation data for the electrical steel sheet. These magnetisation curves are shown in Fig. 24 as functions of applied mechanical stress. Further, the parameterised magnetisation curves have been developed into two-dimensional cubic spline form to make their use easy within the FE computation and to enable the calculation of the magnetoelastic coupling terms developed in Chapter 4.

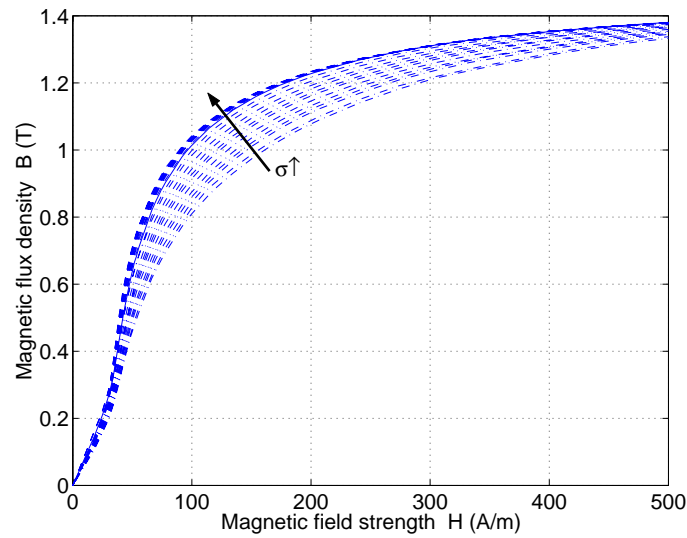


Fig. 24: Magnetisation curves as functions of externally applied mechanical stress.

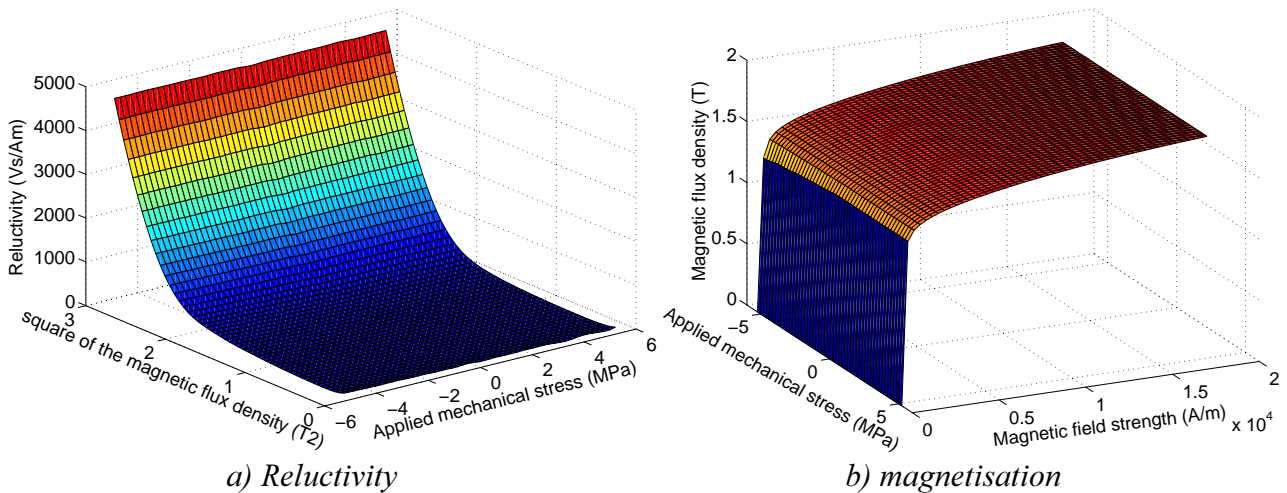


Fig. 25: Plot of the cubic spline data.

A plot of the two-dimensional cubic spline approximation of the reluctivity is shown in Fig. 25a. The corresponding plot of the magnetisation data is shown in Fig. 25b. The development of the measured data into two-dimensional cubic spline was performed using standard and own routines in a commercial software package (Matlab[®] university version 6.01).

The results of Fig. 25 were used in the calculation of magnetostrictive forces in the example of Section 3.7.2 in conjunction with the method of energy derivative presented in Chapter 3.

5.2 Measurement of magnetostriction

The measurement of magnetostriction was conducted using the same set-up as for the measurement of magnetisation. The only difference is the piezo-electric force transducer introduced between the

load cell and the specimen holder. The transducer was used for the measurement of the force due to magnetostriction in the direction parallel to the magnetic field. The magnetic field density measured by the integrator, as well as the magnetic field strength calculated from the current of the primary winding and the magnetostrictive forces measured by the piezo-electric transducer, were collected in the measurement computer as functions of time. The measurement frequency was 5 Hz.

The mechanical stress was varied as in the measurement of magnetisation from -5.23 MPa to 5.23 MPa by steps of 0.436 MPa. At each step, the magnetic field was varied from -18 kA/m to 18 kA/m by varying the current of the primary winding of the Epstein frame. The corresponding maximum and minimum values of the magnetic field density were -1.8 T and 1.8 T. Each step of measurement produced a magnetostrictive hysteresis loop that consisted of magnetostrictive stress as a function of magnetic field density. The procedure of calculating those loops from measured forces is explained later in this chapter. One such hysteresis loop measured at a mechanical stress of 0.0 Pa is shown in Fig. 26a. The corresponding magnetostriction loop is shown in Fig. 26b. The magnetostrictive hysteresis loops were averaged to obtain single-valued magnetostrictive curves at different values of the applied mechanical stress. Some of these curves are shown in Fig. 27a. The corresponding magnetostriction is shown in Fig. 27b.

For a better use of the magnetostrictive data in computations, these data were presented in the so-called two-dimensional cubic spline form as a function of the magnetic field density and the applied mechanical stress. Such a representation is shown in Fig. 28. The data presented in Fig. 28 are used in the simulations of Chapter 7, as well as in the example in 3.7.2, in conjunction with the method of magnetostrictive stress.

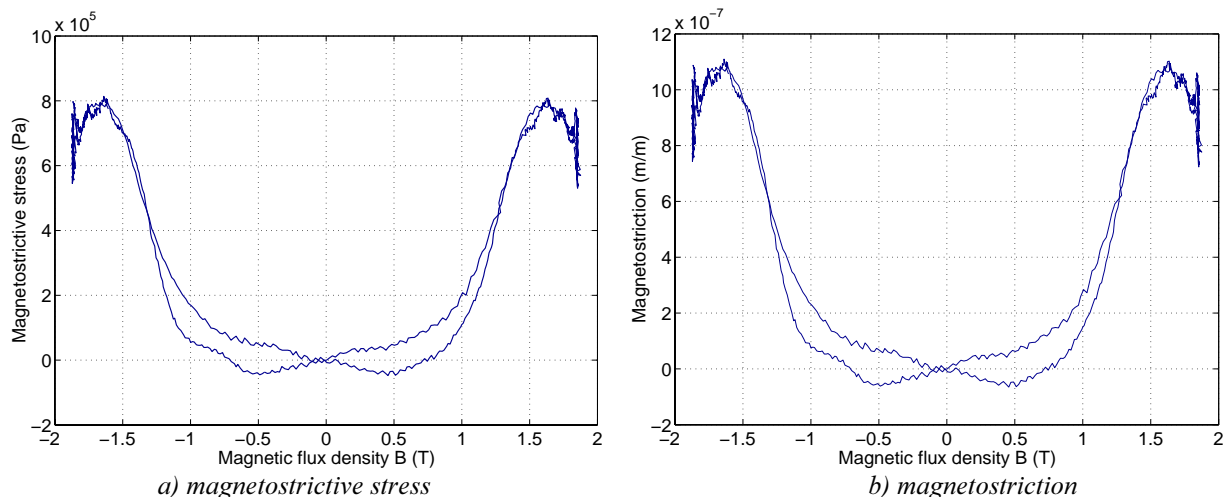


Fig. 26: Magnetostrictive hysteresis loop at 0.0 Pa.

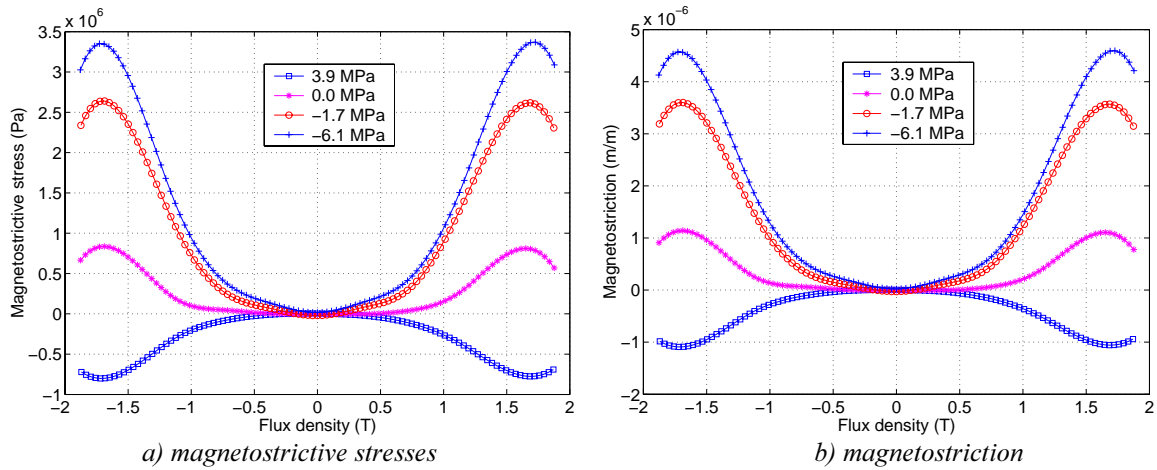


Fig. 27: Magnetostriction curves at different values of the applied mechanical stress.

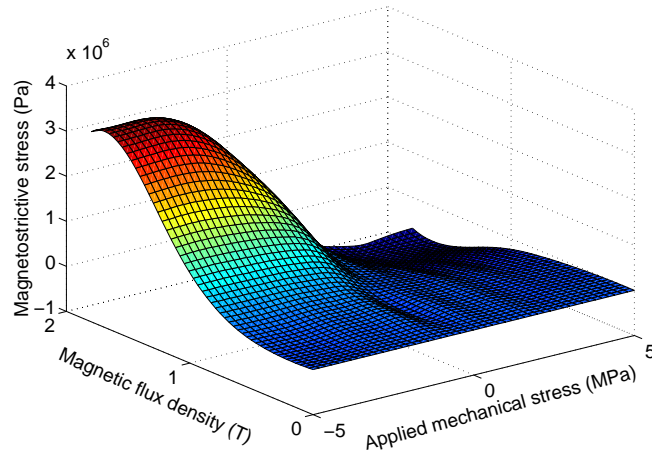


Fig. 28: Plot of the two-dimensional cubic spline magnetostrictive stress.

5.3 Calculation of single-valued curves

The measured hysteresis curves, both of magnetisation and magnetostriction, contain measurement noise and need to be filtered. Furthermore, the data needed for computation have to be single-valued. For these reasons, the measurement results have been handled as follows.

The data points are reordered to obtain smooth curves. The descending hysteresis branch is resampled at the same abscisses as the ascending one and the average ordinates are taken as single values (see Fig. 29). This procedure corresponds to the interpolation of the flux density of the descending branch of the magnetisation curve at a given measured value of the magnetic field strength on the ascending branch. The single value of the magnetic flux density corresponding to the measured magnetic field strength on the ascending branch is the average value of the measured flux density on the ascending branch and the interpolated one on the descending branch.

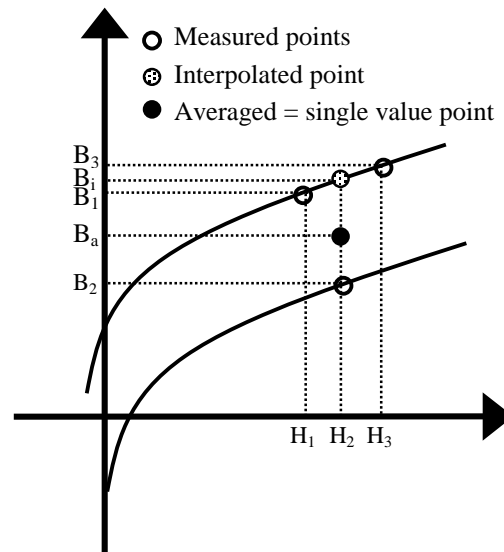


Fig. 29: Illustration of the averaging procedure.

The same procedure is applied to the magnetostrictive stress, where the abscisse is now the magnetic flux density and the ordinate is the magnetostrictive stress. Fig. 29 illustrates the averaging procedure.

5.4 Calculation of magnetostriction from measurements

The presented device for measuring magnetostriction gives a force from which the magnetostriction and the magnetostrictive stress need to be calculated. The procedure for calculating these quantities is presented here.

One strip of the measurement device with its supports and holders, can be schematised as shown in Fig. 30a. This part is mechanically equivalent to the system of springs shown in Fig. 30b. The force measured by the piezo-electric force transducer is the force in the system of springs at equilibrium after the magnetostriction takes place. Since the measurement is made at a frequency of 5 Hz, the mass effect can be ignored. The spring constants of the iron strip, the force transducer, the load cell and the support are respectively $k_{\text{iron}}=1.7\text{E}+8$ N/m, $k_{\text{FT}}=1\text{E}+8$ N/m, $k_{\text{LC}}=5\text{E}+8$ N/m, and $k_{\text{support}}=5\text{E}+6$ N/m. The elongation of each spring at equilibrium can be calculated from the measured force and the spring constants in a conventional way as $|\Delta x| = \frac{F}{k}$. The elongation of the iron due to the magnetostriction is then the sum of the elongations of each spring.

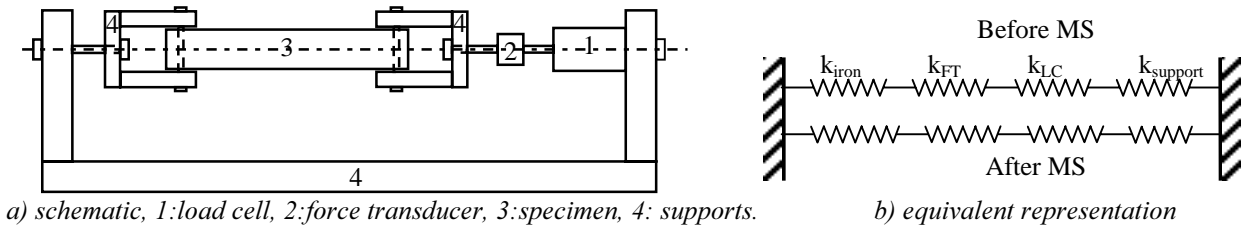


Fig. 30: Schematic of the measurement device and its equivalent representation.

To produce the same magnetostrictive elongation λ in the iron, a force $F_{ms} = -k_{iron}\lambda$ is needed. The magnetostrictive stress is calculated as the stress due to this magnetostrictive force i.e. $\sigma_{ms} = \frac{F_{ms}}{S}$, S being the cross section of the iron strip.

5.5 Conclusions

A simple but sufficiently accurate measurement device is presented. The measurement set-up enables measurements of both magnetisation and magnetostriction as functions of the externally applied stress.

The measurement results show a strong dependency of the magnetostriction on the externally applied mechanical stress, while the dependency of the magnetisation on the mechanical stress is strong only at low values of the magnetic field strength and at the knee of the magnetisation curve.

The measured data have been developed into a format adequate for further use in FE computations of electrical machines.

6 Validation

The method developed in this work to calculate magnetic and magnetostrictive forces and magnetoelastic coupling is first validated with a validation device. It is then applied to the analysis of synchronous and induction machines. The results of measurements using the validation device, and of computations made on it, are presented below.

The validation device was constructed to verify the calculation of magnetic and elastic fields and magnetostriction forces. The goal was to design a motor-like device in which the reluctance or Maxwell forces were minimal, causing it to vibrate under the effect of magnetostrictive forces only. A comparison of the calculation results with those from measurements would confirm the validity of the calculation method. The results of the measurements would verify the nature of the vibrations of rotating electrical machines under the effect of magnetostriction.

6.1 Structure and construction of the device

The validation device consists of an induction machine in which the rotor has not been cut from the stator. The device is, then, just like a induction machine, short in axial length and without an air gap. The rotor part (if it can be called such) of the machine is different from a normal machine in the sense that it has no windings. This device was designed, construct and measured within this research work (the design and construction were done as a master's thesis (Cester 2002) in the Laboratory of Electromechanics at Helsinki University of Technology). Its geometrical and electrical parameters are given in Appendix A. Fig. 31 shows a photo of this device.

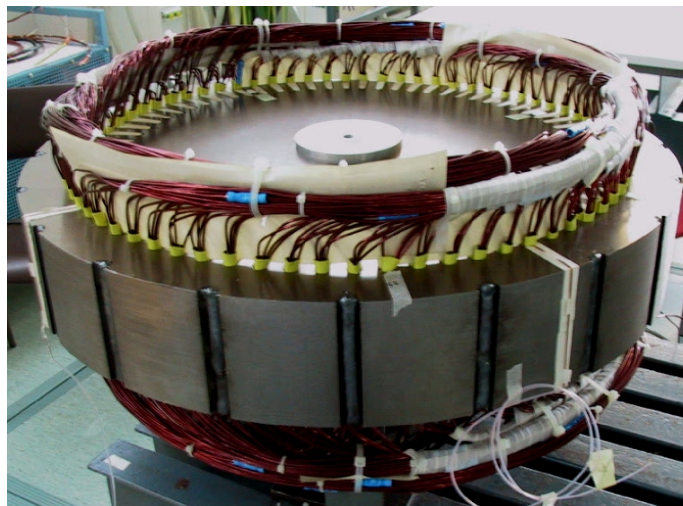


Fig. 31: Validation device (Cester 2002).

The validation device is chosen and designed to simulate the flux path of an induction machine, while minimizing forces other than magnetostrictive. In a normal machine, the main forces are those at the interface between the stator or the rotor and the air gap. These forces are known as Maxwell forces (or reluctance forces). The absence of the air gap in the validation device means that there are no such forces. The Lorentz forces, on the other hand, cannot be avoided. However, their effect on the vibrations of the validation device can be ignored for two reasons. First, the currents in the windings of the device are much lower than these of a real machine (less than 4 A here vs. more than 50 A in a normal machine). This makes these forces very slight. Second, the windings of the validation device are confined in a soft plastic tube that is supported by wooden parts inside the slots, as shown in Fig. 32. As the soft plastic and the wood both have good mechanical damping properties, and, as the winding mass is very small compared to the mass of the core, the vibrations of the windings at the relevant frequencies (50 ... 200 Hz) are not transmitted to the core of the device.

Usually, the windings of the stator of an induction machine are first formed separately, and then introduced into the slots. In the constructed validation device, this procedure is not possible because the slots are closed. The windings have to be assembled by the manual procedure of inserting the conductor into the top of the device and pushed through to the bottom, from where it is taken into the next slot, and so on (Cester 2002).

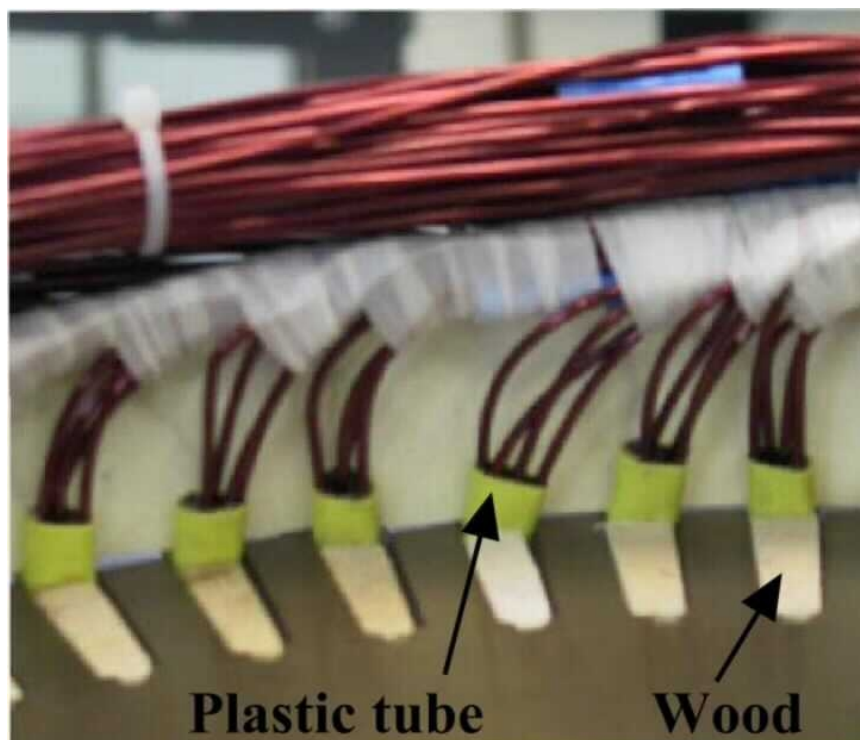


Fig. 32: Fixing of windings (Cester 2002).

6.2 Measurements and simulations

Measurements

The measurement of the validation device was achieved using conventional measurement devices, namely, a Wide Band Power Analyser Norma D6100 and a search coil (5 turns, 4100 mm²) around the yoke of the stator core, for electric and magnetic quantities. A Polytech OFV-302 Single Point Interferometer laser vibrometer with a standard head was used for the measurement of the velocity of the outer surface of the device. The measurement set-up is shown in Fig. 33 (Cester 2002).

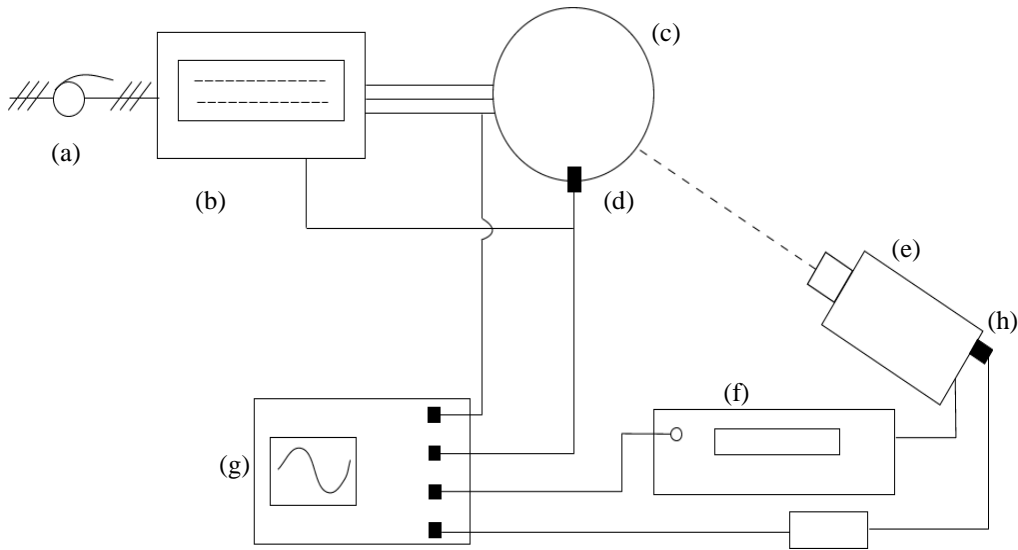
The velocity measurement was made at different points on the surface of the validation device. The voltages induced in the search coils, as well as the current and the voltage of the first phase of the winding, were recorded in real-time. The validation device was supplied with different voltages at the frequency of 50 Hz; the recording time was 500 ms, which corresponds to 25 periods of the line voltage. The sampling frequency was 50 kHz, so that a total of 25 000 data points were recorded for each measured quantity.

The measurement of the validation device began with the measurement of the natural frequencies of the device and its support. For this purpose, a hammer-test type measurement was made. In this measurement, the device was excited with a hammer hit and the velocity signal was analysed. The velocity of the surface of the device is reported in Fig. 34a.

The velocity signal was analysed by DFT in order to determine the natural frequencies of the supported device. The frequency content of the velocity signal is reported in Fig. 34b. These results state that, in the measurement of the velocity due to magnetostriction, the frequency components at about 10 Hz have to be filtered for the signal to be meaningful.

Simulations

The validation device was also simulated with the developed software. The simulations were made under the same conditions as the measurements. The same voltages were used in the simulations and the same measured quantities were calculated from the computations results.



(a) auto-transformer; (b) Norma multi-meter; (c) machine; (d) search coil; (e) laser head; (f) laser controller; (g) PC transient recorder; (h) accelerometer.

Fig. 33: Measurement set-up for the validation device.

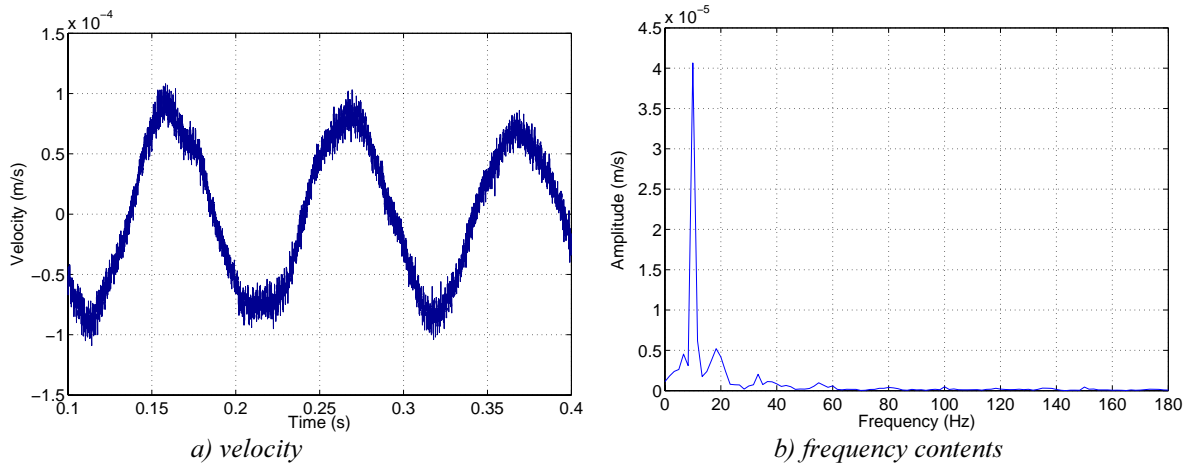


Fig. 34: Velocity signal in the hammer test and its frequency contents.

The results of the measurements were compared to the results of the simulations. These results for a terminal voltage of 400 V at the frequency of 50 Hz, which correspond to a maximum flux density in the yoke of the device of about 1.24 T, are presented below. The rest of these results, with voltages of 300 V and 500 V and a frequency of 50 Hz, are given in Appendix B.

Fig. 35 shows the simulated flux lines in the cross section of the validation device with a line voltage of 400 V at a frequency of 50 Hz. Fig. 36 shows the calculated magnetostrictive forces at the last time step. The forces were normalised; the maximum force was 3 580 N/m. The calculated deformation at the end of the simulation (600 000 times magnified) is shown in Fig. 37. The results presented in Fig. 35, Fig. 36 and Fig. 37 correspond to the same time step.

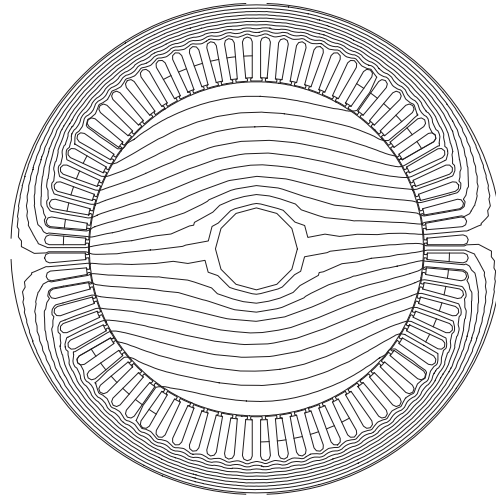


Fig. 35: Flux lines in the cross-section of the validation device (simulated).

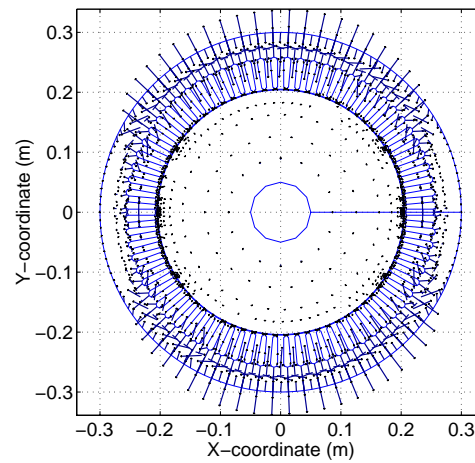


Fig. 36: Magnetostrictive forces (simulated, normalised to 32 450 N/m).

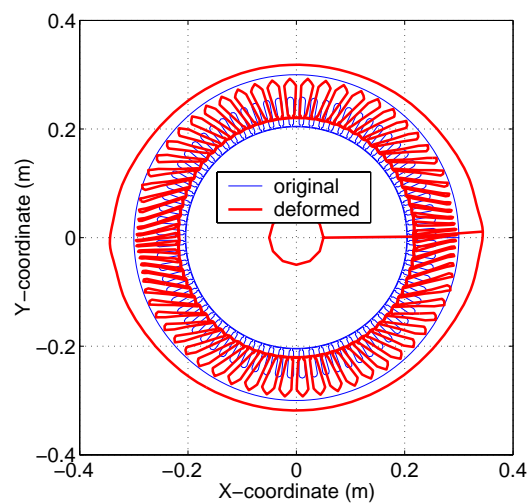


Fig. 37: Deformation of the validation device (simulated, 600 000 times magnified).

The vibration velocities were measured at different points on the outer surface of the validation device. The quantities corresponding to the configuration of Fig. 38 are presented here.

Fig. 39 shows the velocity measured at point A shown in Fig. 38, i.e. situated on the outer surface and with an angle of 50 deg. from the position of the search-coil. The line voltage was 400 V and the frequency 50 Hz.

The velocity indicated in Fig. 39 has been integrated in time to get the displacement of the measured point on the surface. Fig. 40 shows the displacement of point A calculated from the measured velocity (a), as well as the displacement from the simulation (b). The displacements of point B are also presented in Fig. 41.

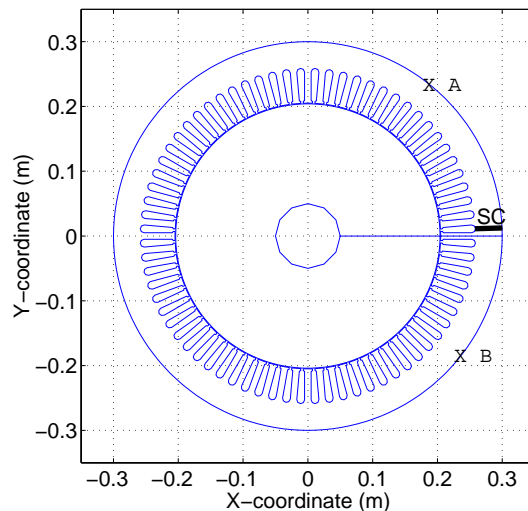


Fig. 38: Position of the search-coil (SC) and the points A and B at which the velocity was measured.

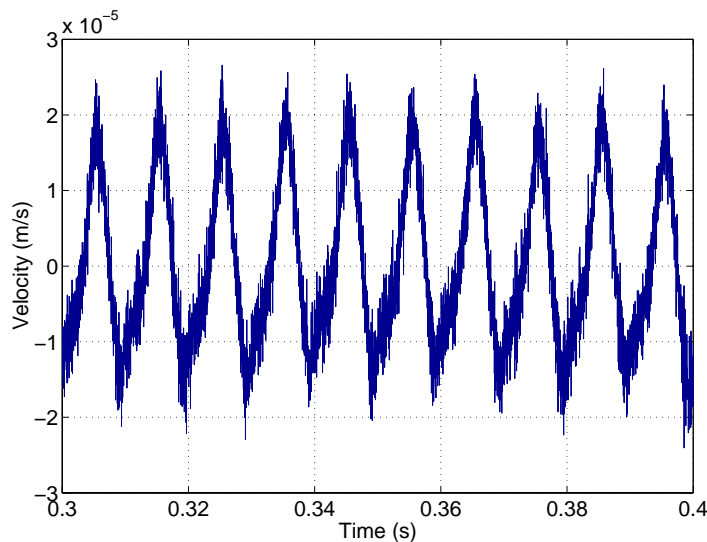
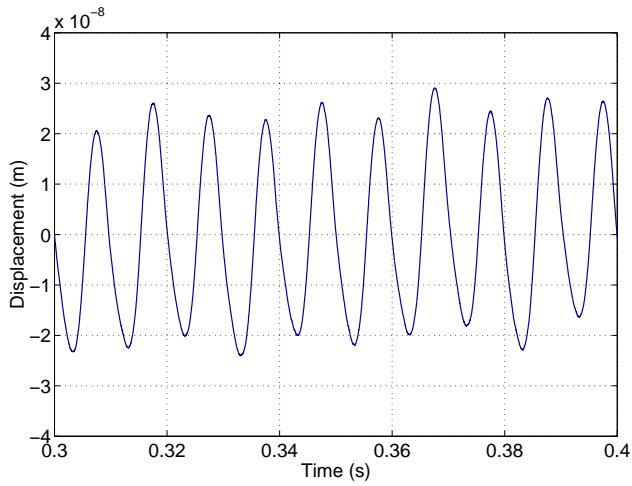
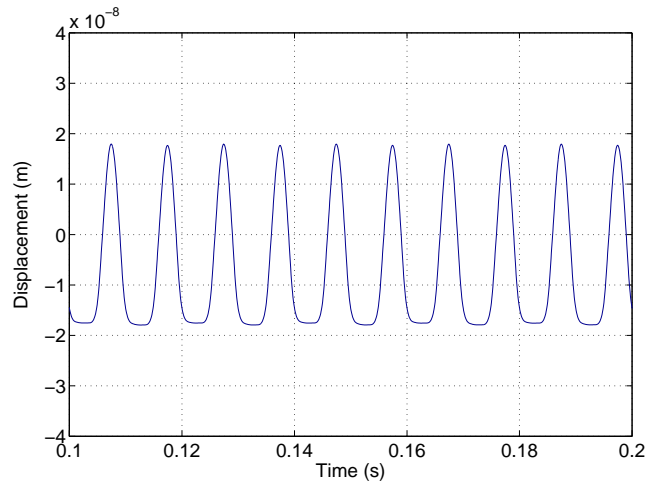


Fig. 39: Measured velocity at point A.

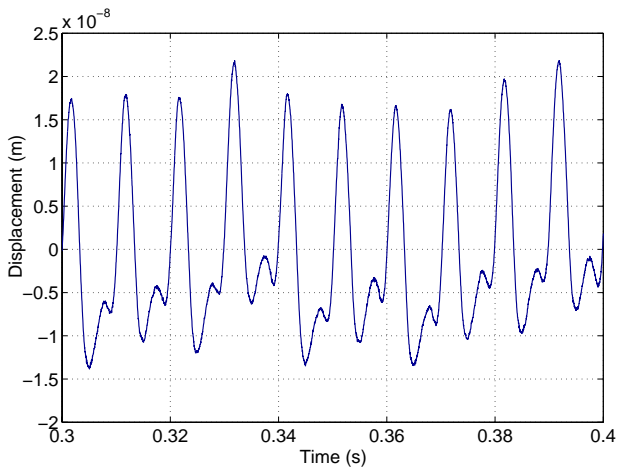


a) measured

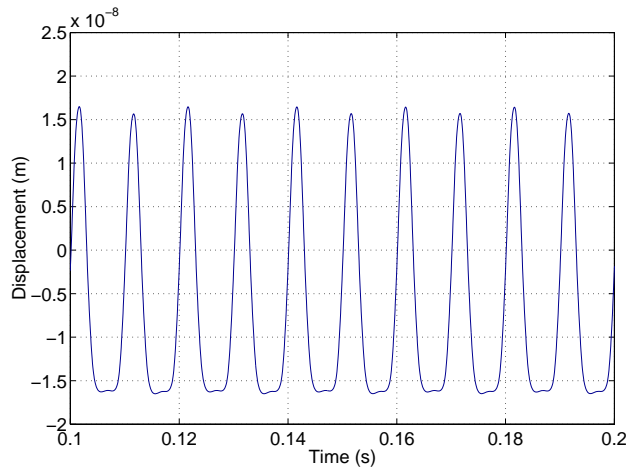


b) simulated

Fig. 40: Displacement of point A.

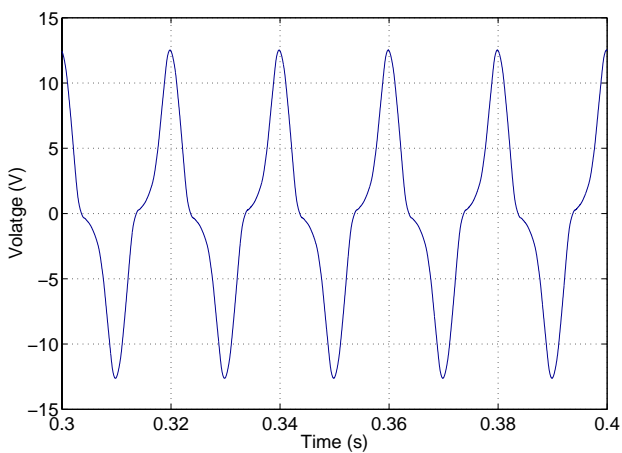


a) measured

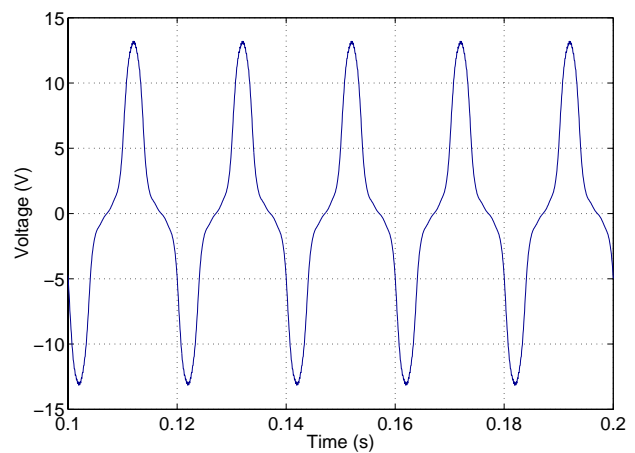


b) simulated

Fig. 41: Displacement of point B.



a) measured



b) simulated

Fig. 42: Voltage of the search coil.

The measured voltage induced in the search coil was compared with the same voltage calculated from the magnetic field from simulations. These results are shown in Fig. 42.

Some differences between the measured and simulated displacements have to be explained. They are due to differences between the measured and simulated magnetic quantities. One of the differences is due to the data on the magnetisation of the iron core. Indeed, the magnetisation curve used in the simulations is not exactly the measured one, but is linearised at low values of the magnetic field strength. In this way, the Newton-Raphson iteration is sure to converge and the software rendered robust. This difference causes higher harmonics to occur in the flux density and the measured search-coil voltage. The difference between the measured magnetisation data and those used in simulations can be seen from Fig. 43. For the validation device, this difference is crucial, since there is no air gap and the device is highly non-linear. However, in normal rotating electrical machines, the air gap linearises the machine at low values of the magnetic field strength, so the difference between the measured magnetisation and the used one is not very important.

Moreover, the slope at the origin of the magnetisation curve, measured with an Epstein frame, is different from the one measured from the constructed validation device. This difference can also be seen from Fig. 43. The latter magnetisation curve was measured in the following manner. The windings of the validation device are opened, a current is fed through the shaft of the device and the induced voltage in the search-coil is measured. From the current and the induced voltage, the magnetisation curve is plotted. The differences may be due to differences in the material itself; the one used for the validation device is not necessarily the same as that measured with an Epstein frame (they are from different lots) or due to mechanical handling in the manufacturing process of the validation device. The Epstein frame is a standard that does not necessarily reproduce the actual magnetisation curve of the material.

The differences in the wave form of the displacements at point A and B are explained by the anisotropy of the material. Indeed, the validation device has been constructed so that all the electrical sheets are in the same direction with regards to materials rolling direction. Although the material is supposed to be isotropic, a certain amount of anisotropy occurs. The different phases of the winding are not symmetric and the flux density is different from the calculated one. The magnetostriction also presents anisotropy, which is not accounted for in the calculations. In normal electrical machines, this anisotropy is avoided by transposing the electrical sheets.

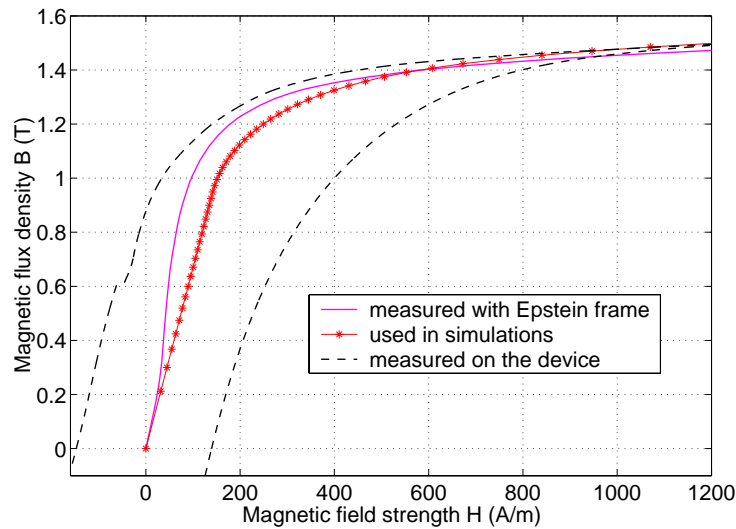


Fig. 43: The magnetisation curves measured and the one used in simulations.

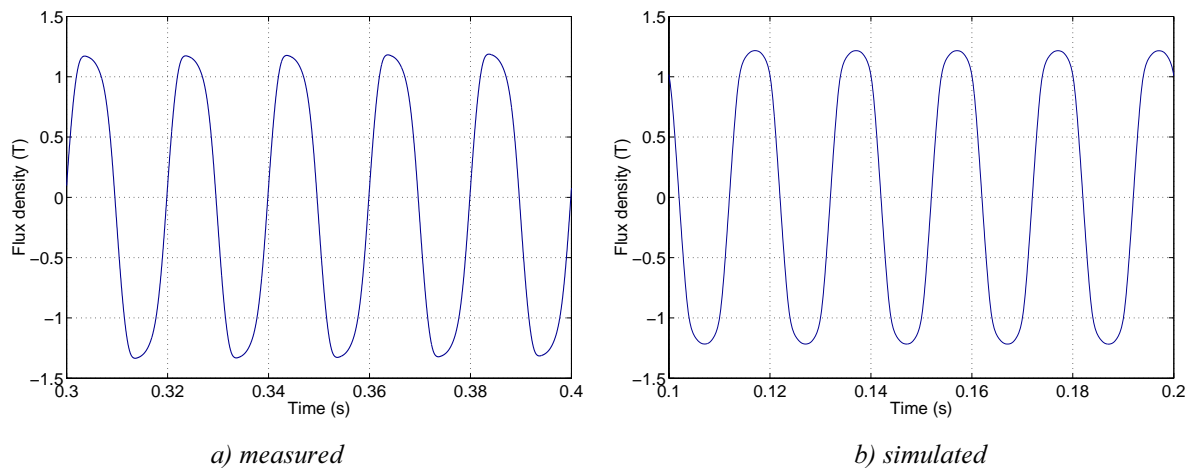


Fig. 44: Flux density across the search-coil.

The measured and simulated voltages of the search-coil presented in Fig. 42 were integrated to obtain the magnetic flux density across the surface of the coil. The measured and simulated flux densities are shown in Fig. 44. Here also the differences in the wave form of the calculated and simulated flux density are due to both linearisation and anisotropy.

Finally, the measured and calculated phase currents are presented in Fig. 45. It is clear that, due to the magnetisation curve used, the measured and simulated phase currents are different. The maximum value of the measured phase current is larger than the simulated one. This difference does not affect very much the magnetostriction since the measured and simulated flux densities are almost the same.

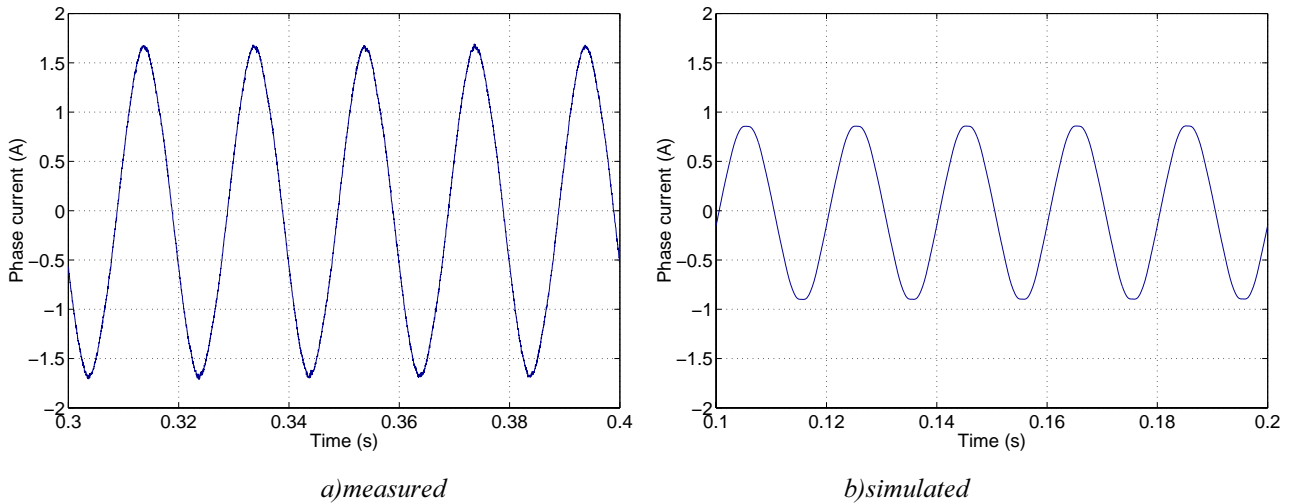


Fig. 45: Phase current.

6.3 Conclusions

A validation device that simulates the flux path of a rotating electrical machine and minimises all forces other than magnetostrictive was constructed. The measurements made on this device show that magnetostriction has a considerable effect on the amplitude of vibrations of rotating electrical machines.

The differences between the measurements and the simulations are explained. They are caused by the high non-linearity of the test device and the anisotropy of the iron. In a normal machine, these differences are expected to be lower due to the linearising effect of the air gap and the skewing of the iron sheets.

Comparison of the calculated and measured electromagnetic and elastic behaviour of the validation device shows acceptable agreement and proves the validity of the model presented in this work. Within the assumptions made on the anisotropy, the correctness of the computation procedures based on this model is also proved.

7 Simulations and results

In this chapter, results of computations with different approaches are presented and compared with each other. Two types of machines are studied; the first one is a relatively large synchronous generator and the second one is a small-size induction motor. The aim of this chapter is twofold: to show the computational differences between different approaches and to establish the effect of magnetostriction and magnetoelastic coupling on the vibrations of rotating electrical machines.

The different approaches used in the following computations are referred to in this work as *quasi-static*, *dynamic*, *coupled*, *uncoupled*, *damped*, *undamped*, *with magnetostriction* and *without magnetostriction*.

In the quasi-static approach, the effects of mass and damping are ignored in the elastic equations, while, in the dynamic approach, at least the effect of mass is taken into account. If the damping is non-zero in the dynamic approach, it is called a damped approach, while a dynamic approach with zero damping is called an undamped approach. If the geometrical changes are also taken into account in the solution of the magnetic field, the approach is called coupled, otherwise it is called uncoupled. Magnetostriction may be taken into account or not in all these approaches.

Magnetostriction can be taken into account in a stress-dependent or stress-independent manner. The stress-dependent case means that the effect of mechanical stress on the magnetostriction is accounted for.

All the above-mentioned approaches are computed with the time-stepping method (including the so-called quasi-static approach). In the coupled quasi-static approach, the geometrical changes are accounted for only after each step, not during the iteration. In the coupled dynamic approach, these geometrical changes are accounted for in the iteration process, so that the coordinates of the nodes can be changed after each iteration.

Discrete Fourier Transform (DFT) was used to analyse the frequency content of the velocity signal calculated in the simulations. The parameters used with DFT are summarised in Table 1 for each simulated machine.

Table 1: Parameters used with DFT.

	Frequency	Time-steps	Time step Per period	Sampling frequency	Resolution	Maximum Frequency
Synchronous machine	60 Hz	3 000	300	18 kHz	6 Hz	9 000 Hz
Induction machine and test device	50 Hz	3 000	300	15 kHz	5 Hz	7 500 Hz

7.1 Synchronous machine

The analysed synchronous machine is a 3.025 MVA generator. This generator is driven by a diesel motor in a large ship power-plant. The electrical and geometrical parameters of the machine are given in Appendix C.

Different kinds of magnetoelastic computations were undertaken to check the effect of calculation methods on the results and the effect of different phenomena on the vibrational behaviour of the machine. Among the calculated cases, the quasi-static approach, and the dynamic one with different damping factors, either coupled or not, were applied. The results of these calculations are presented below.

The calculated deformation of the stator core, at any given time step, and with whichever method, has the same form, as have the calculated magnetic and magnetostrictive forces; only the absolute values change. The stator deformation and the radial displacement of a node on the outer surface of the stator core (point P in Fig. 46a), calculated with the quasi-static approach, are shown in Fig. 46. The magnetic and magnetostrictive forces are shown in Fig. 47, where the forces have been normalised. The maximum value of the magnetic forces is 3 023 N/m and that of the magnetostrictive forces is 8 900 N/m.

The major part of the deformation of the stator core corresponds to a static shrink at spatial mode zero, on top of which deformations corresponding to different spatial modes are superposed. This result is in accordance with that obtained from the calculations of the forces with the Maxwell stress tensor, where the fundamental and the dc components of the radial stress were hundreds of times bigger than the other ones.

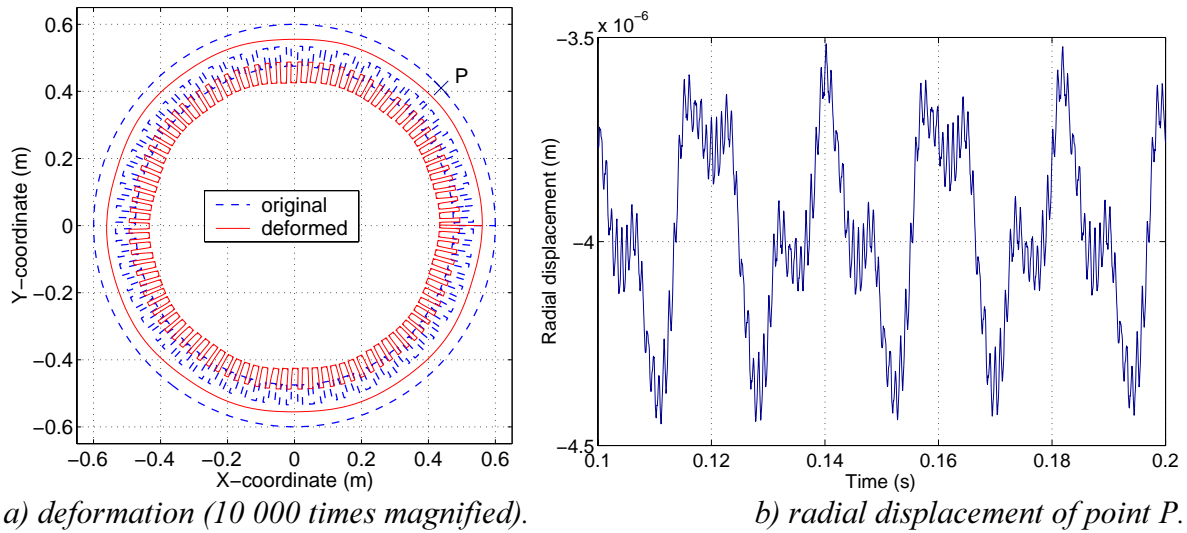


Fig. 46: Stator deformation and radial displacement (quasi-static).

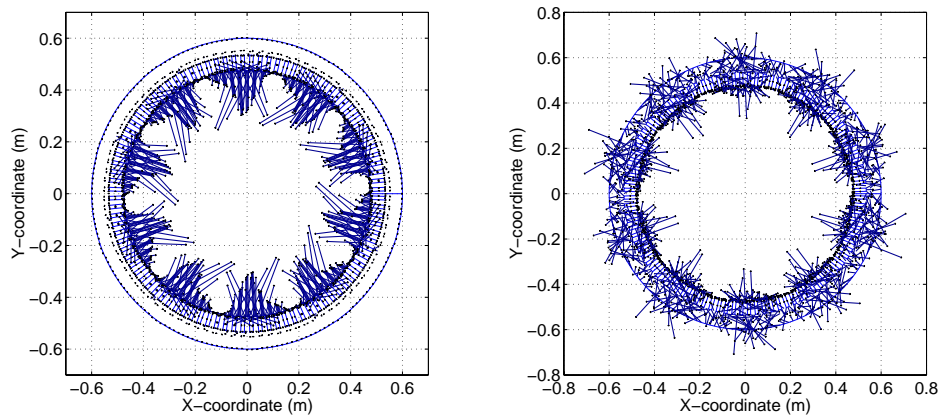


Fig. 47: Magnetic and magnetostrictive forces (quasi-static).

The magnetic forces are distributed along the nodes at the interface between iron and air or iron and copper. This phenomenon is due to two facts. On one hand, the major part of the magnetic energy is stored in the air, while only a small part of it is stored in the iron. On the other hand, the change of the magnetic energy of one element due to the virtual displacement of nodes inside the iron is compensated by a change in neighbour elements due to the close values of reluctivity in these elements. This results in a net nodal force close to zero. Only the great difference between the reluctivity of iron and that of air (or copper) causes large changes in magnetic energy and large forces.

The magnetostrictive forces are also distributed on the surface of the stator core, but there are still some considerable forces inside the iron core. This can be understood by looking at the magnetic flux path. Due to the magnetostriction, the iron stretches along the flux lines and shrinks in the orthogonal direction. The flux lines are mostly parallel to the outer surface of the stator core in the

yoke and to the surface of the slots in the teeth. Only at the extremities of the electrical poles are there curvatures of the flux lines. Hence, at these curvatures, the contributions to nodal magnetostrictive forces from neighbour elements do not compensate each other and a net nodal force occurs.

The Discrete Fourier Transform was applied to the velocity of the node on the outer surface of the stator. The frequency content of the velocity is shown in Fig. 48. These results are calculated with the quasi-static approach and without taking into account the effect of magnetostriction. The results of calculations with the other approaches and with magnetostriction forces are presented later in this chapter and compared to the first ones. The frequency content of the velocity calculated without magnetostriction shows a sharp, high, peak at 1 080 Hz. This result is in accordance with the measured result, and also with those calculated with the Maxwell stress tensor method. The other peaks mentioned in the measurements (Chapter 3) are also visible in the frequency contents of the velocity.

7.1.1 Quasi-static case

Calculations with time stepping and the quasi-static elastic approach were undertaken where the magnetostriction is either taken into account or not. The effect of the displacement field on the FE magnetic mesh has also been checked within the quasi-static elastic approach. In this last case, the nodal coordinates are updated after each step, but not within the iterations. The difference in magnitude of radial displacement of the same node is shown in Fig. 49. A positive difference means that the amplitude of the first case is bigger than that of the second case.

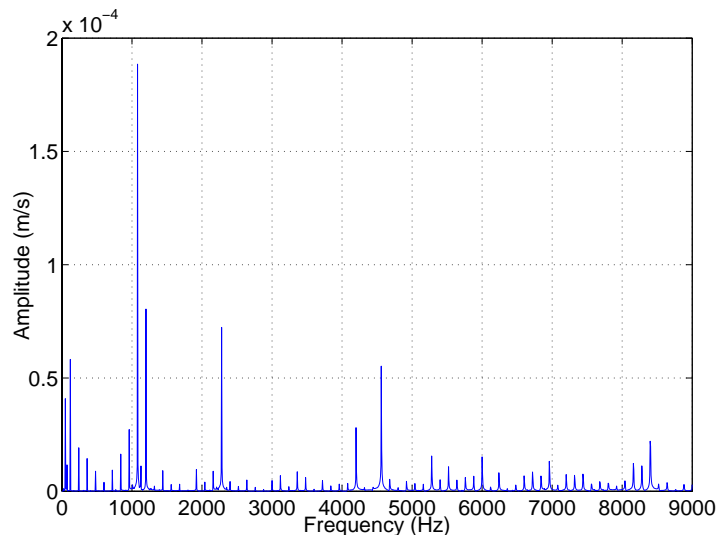


Fig. 48: Frequency contents of the velocity at point P in Fig. 46a.

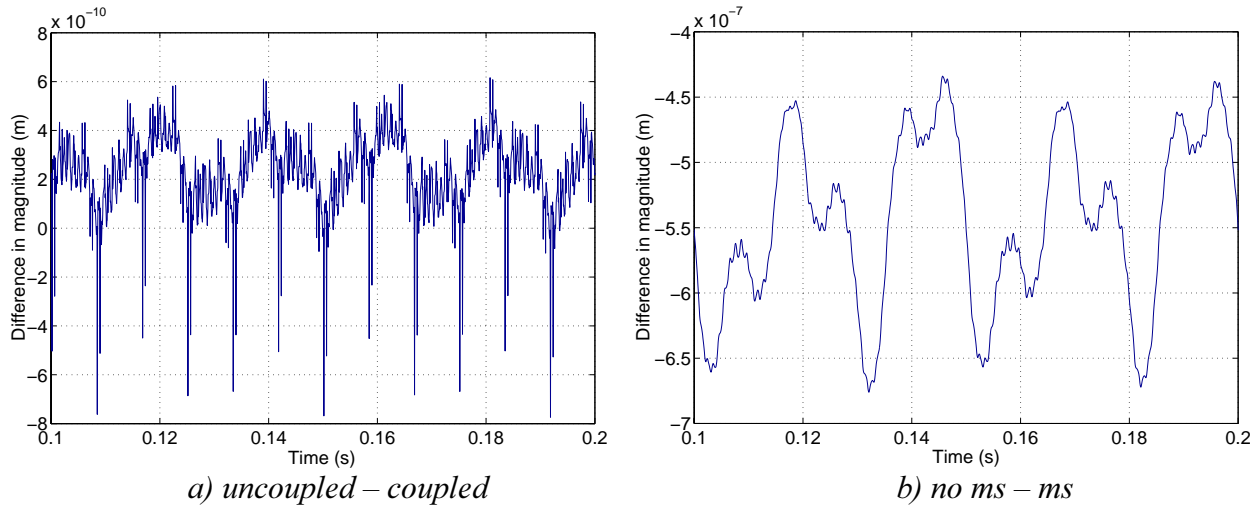


Fig. 49: Difference in magnitude of radial displacements of point P in Fig. 46a.

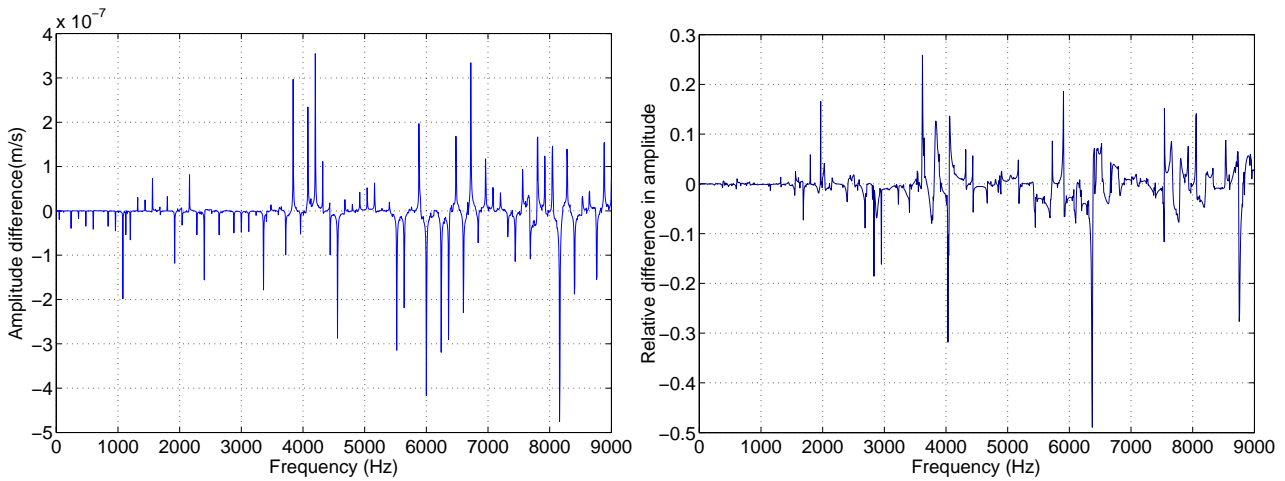


Fig. 50: Difference in frequency contents uncoupled – coupled.

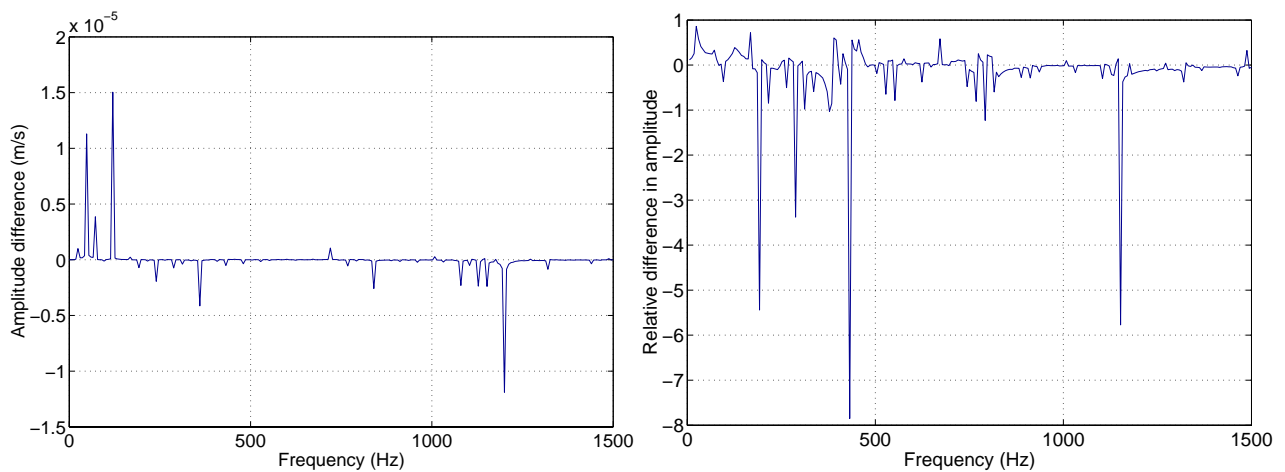


Fig. 51: Difference in frequency contents no magnetostriction – magnetostriction.

The magnetostriction causes the amplitude of the dc-component of the mode zero of the radial displacements to be smaller than those calculated without magnetostriction. Moreover, the difference is composed of different frequencies. The coupling also changes the vibrations of the

stator core in a very complicated manner. These results will be commented on later in this chapter at the frequency analysis level.

The frequency contents of the velocity as shown in Fig. 48 have also been calculated for both the above-mentioned cases. The difference between frequency contents calculated with the quasi-static uncoupled approach and the coupled one, both without magnetostriction, are shown in Fig. 50. The difference between the uncoupled cases, one without magnetostriction and the other with are shown in Fig. 51.

The relative differences in the amplitude of velocities between the uncoupled and coupled cases range from -50% up to 30% , depending on the frequency. The most affected frequencies are those

higher than $1\,000\text{ Hz}$. The relative difference is calculated as $\frac{|v_1| - |v_2|}{|v_1|}$. A negative relative

difference means that the amplitudes of vibration are highest in the second case, while a positive relative difference means that the amplitudes of vibrations are highest in the first case. Both negative and positive relative differences occur, as can be seen from Fig. 50. Due to the change in magnetic field distribution in the core of the machine due to the vibrations of the stator core, there is an electromagnetoelastic coupling phenomenon that changes the amplitude of vibrations when compared to the uncoupled case. This phenomenon has been noticed by Arkkio (2001) in a different approach.

Arkkio (2001) forced the stator of an induction machine to vibrate at given frequencies and modes and calculated the power that the electromagnetic system absorbs from the vibrating stator core. He used a relatively large amplitude of vibrations ($45\ \mu\text{m}$, representing 10% of the radial air gap) in order to distinguish the damping forces from the radial magnetic forces. The method to compute the forces was validated by measurements. Both positive and negative damping was found to occur, depending on the frequency of vibration. The damping in this case was associated with the eddy-current losses in the windings. The results of the computations presented in this chapter show the same behaviour, except that here the coupling is bi-directional and the vibrations are not artificially forced but the effect of the magnetic and/or magnetostrictive forces.

In the text below, the changes in the amplitude of velocities will be referred to as *damping* when the relative changes are positive and *amplification* when they are negative. This is just an analogy

because, in reality, the phenomena occur at the same time. Strictly speaking, these phenomena are computational damping and amplification, respectively.

The magnetostriction causes the same phenomenon as the coupling, but the relative difference in the velocity amplitude now ranges from -800% up to 100% , depending on the frequency (see Fig. 51). Some frequencies are damped due to the magnetostriction, including the component at 120 Hz (25%). The most damped frequencies are 24 Hz 85% , 168 Hz 70% , 390 Hz 60% , 440 Hz and 456 Hz 55% . Other frequencies are amplified (e.g. 192 Hz 540% , 288 Hz 330% , 432 Hz 785% and 1152 Hz 585%). According to Låftman (1995), magnetostriction can damp vibrations due to magnetic forces; this can be explained by reference to the damping of some frequencies including the one at twice the fundamental harmonic. However, this is not the whole truth, since other frequency components are largely increased.

7.1.2 Dynamic case

The dynamic case, which is the main concern of this thesis, has been calculated with different approaches. First, the undamped dynamic case has been compared with the quasi-static case. The differences in amplitude of radial displacements of a node on the outer surface of the stator core are shown in Fig. 52. The differences in frequency contents of the velocities of the same node are shown in Fig. 53. The effect of inertia (more than 1500% in some frequency components of the velocity) is clearly too important to be ignored in time stepping elastic calculations. Moreover, the components of velocity at high frequency are damped, except at certain values. This damping is partly due to the calculation method, which includes artificial damping of high frequencies and makes the method stable (Zienkiewicz 1977).

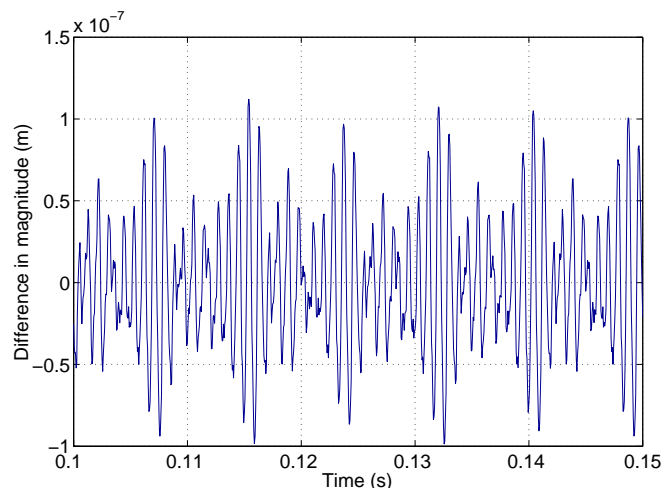


Fig. 52: Difference in radial displacement quasi-static – dynamic.

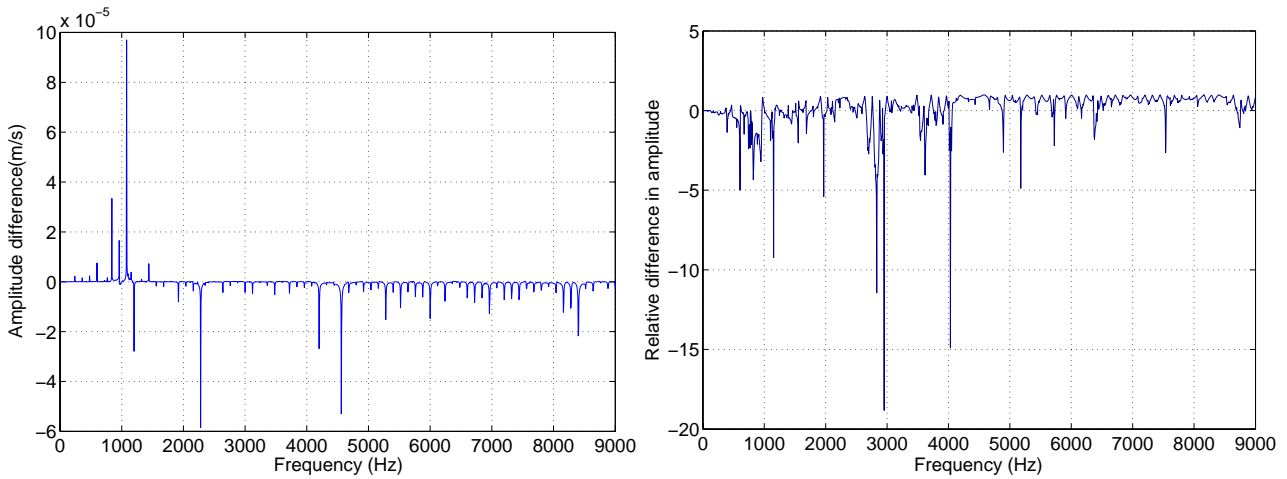


Fig. 53: Difference in frequency contents quasi-static – dynamic.

One problem encountered in the dynamic computation was the effect of structural damping and its extent in the core of electrical machines. Several computations have been undertaken to check the effect of damping. In these calculations, the uncoupled approach was used and the magnetostriction was ignored. The calculated cases with different values of the Rayleigh damping factors α , β and the corresponding modal damping at 60 and 1 000 Hz are listed in Table 2.

Table 2: Calculated cases and corresponding modal damping.

α	β	Modal damping at 60 Hz	Modal damping at 1000 Hz
0.00E+00	0.00E+00	0 %	0 %
0.00E+00	1.11E-09	0 %	0.0003 %
0.00E+00	1.11E-08	0.0002 %	0.0035 %
0.00E+00	1.11E-05	0.21 %	3.48 %
0.00E+00	1.11E-04	2.1 %	34.8 %
0.00E+00	1.11E-03	21 %	348 %
0.00E+00	1.11E-02	209 %	3480 %
0.00E+00	1.11E-01	2090 %	34800 %
5.00E+00	1.11E-09	0.66 %	0.04 %
7.00E+00	1.11E-06	0.92 %	0.40 %
4.00E+01	0.00E+00	5.31 %	0.32 %

The modal damping is usually of the order of 0.1 % ... 2 %, so that the calculated cases are largely beyond these limits. The differences in the frequency contents of the nodal velocity between the undamped case and a damped one with $\alpha = 0$ and $\beta = 1.11E - 5$ are shown in Fig. 54.

For all realistic values of α and β (including null values), the shape and amplitude of the displacements are almost the same. Only for high values of α and β , which correspond to strong damping, do the displacements decrease strongly and no vibrations are seen. For those reasons, the undamped case was chosen for the further analysis of other phenomena such as magnetostriction and coupling.

The effect of damping can be seen from Fig. 54, where the low-frequency components of up to 1000 Hz are strongly damped (from 50 % to 60 %). Some high-frequency components are amplified, but almost all the peaks are damped.

The effects of coupling and magnetostriction within the dynamic approach have been checked using the undamped model. The difference between the radial displacements of a node on the outer surface of the stator core for both the coupled and uncoupled without magnetostriction case, and for the uncoupled case with magnetostriction and without, are shown in Fig. 55. Here again, the same magnetic damping phenomenon occurs. However, the relative differences of the amplitudes of vibrations are small (from -17 % up to 6 %), as can be seen from Fig. 56. The coupling causes a high-frequency component at 8 160 Hz. The effect of this component on the noise is very small due to its high frequency and low amplitude (at high frequencies, the power content of a unit-amplitude velocity component is lower than that at low frequencies).

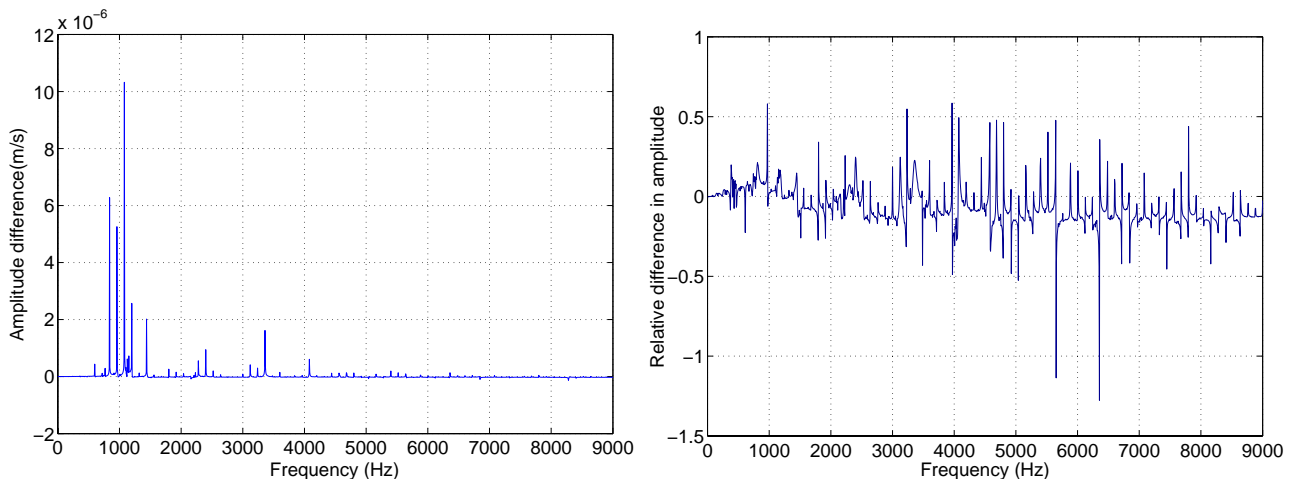


Fig. 54: Difference in frequency contents of the velocity undamped–damped.

The effect of coupling and magnetostriction on the frequency contents of the velocity of the same node can be seen from Fig. 56 as the difference between the coupled and uncoupled cases, both without magnetostriction, and from Fig. 57 as the difference between the uncoupled cases, either with or without magnetostriction.

The effect of magnetostriction is very considerable compared with that of coupling (from -800% up to 100%). The magnetostriction damps some frequency components including the one at 120 Hz , which is usually attributed to magnetostriction, (25%) while it increases others. The effect of magnetostriction can be ignored for frequencies higher than $1\,500\text{ Hz}$.

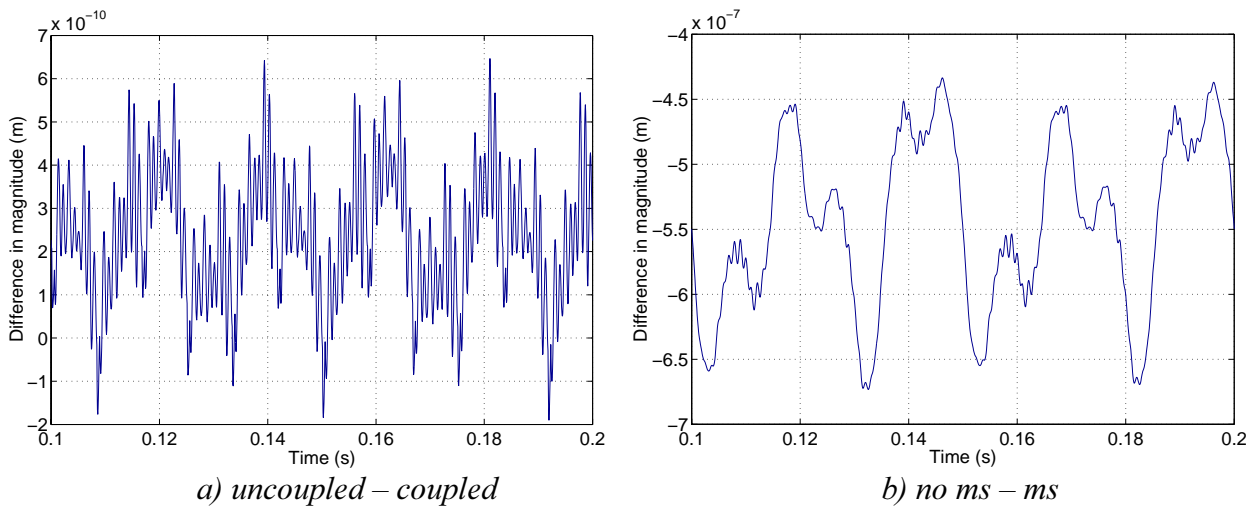


Fig. 55: Differences in radial displacement.

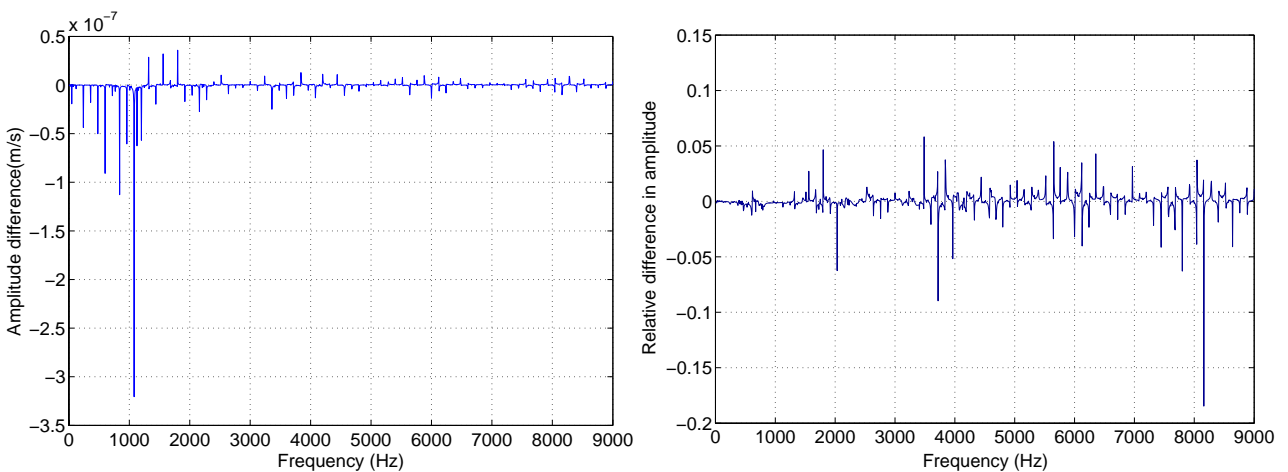


Fig. 56: Difference in frequency contents uncoupled - coupled.

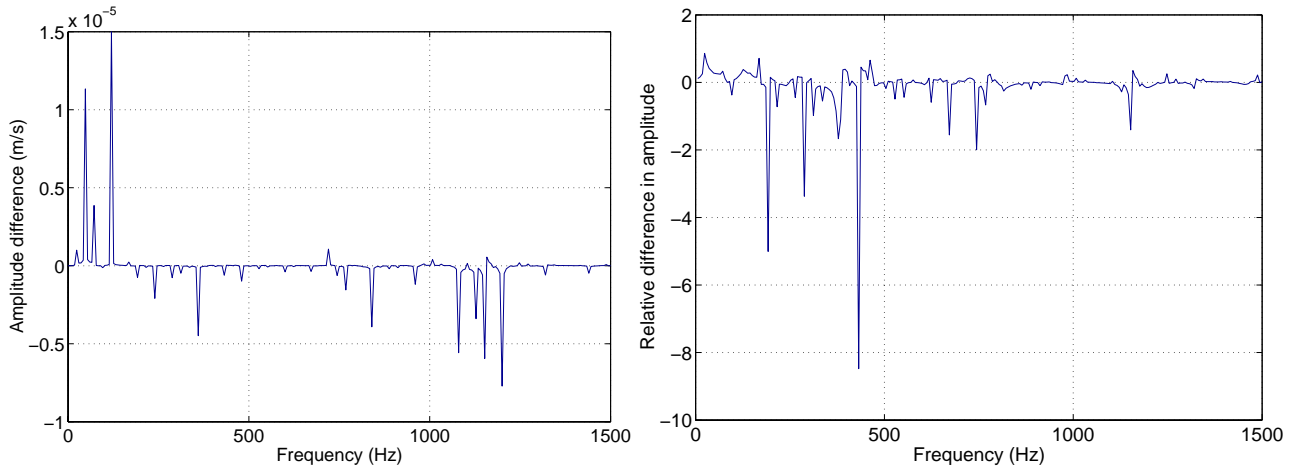


Fig. 57: Difference in frequency contents no magnetostriction – magnetostriction.

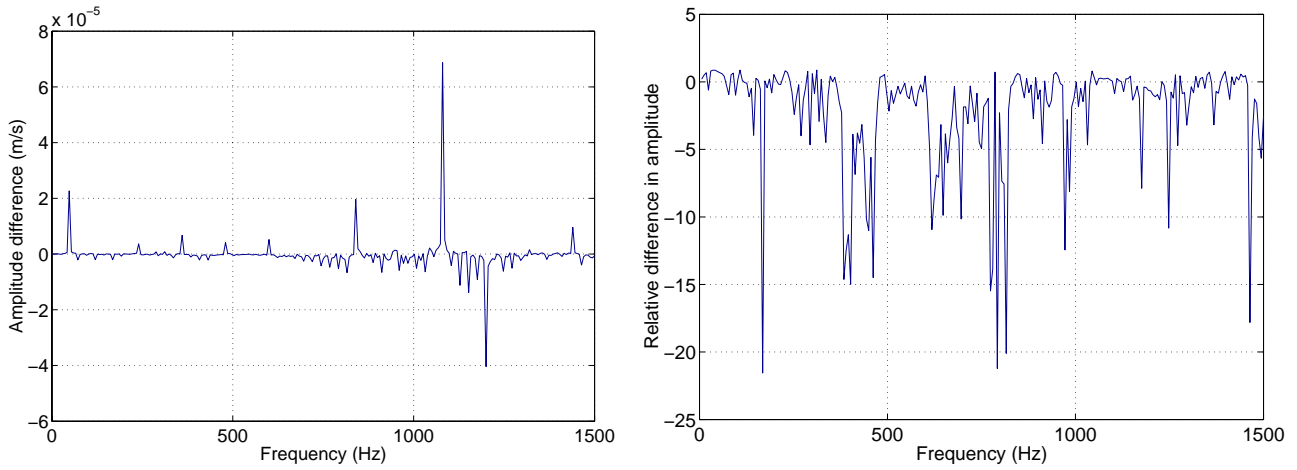


Fig. 58: Difference in frequency contents stress-independent vs. stress-dependent.

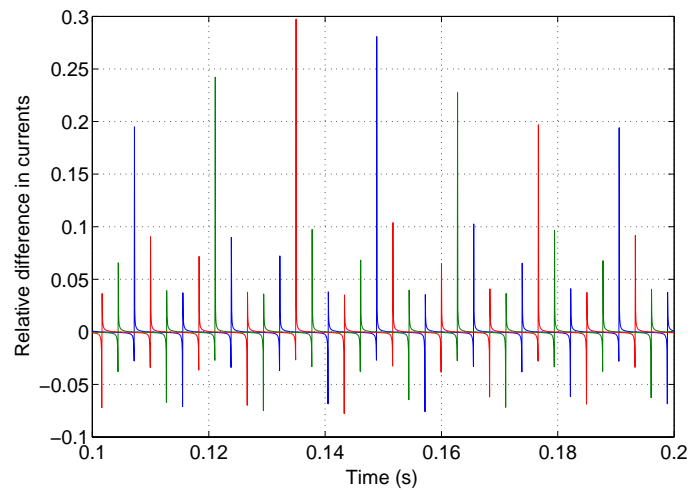


Fig. 59: Relative difference in terminal currents uncoupled-coupled.

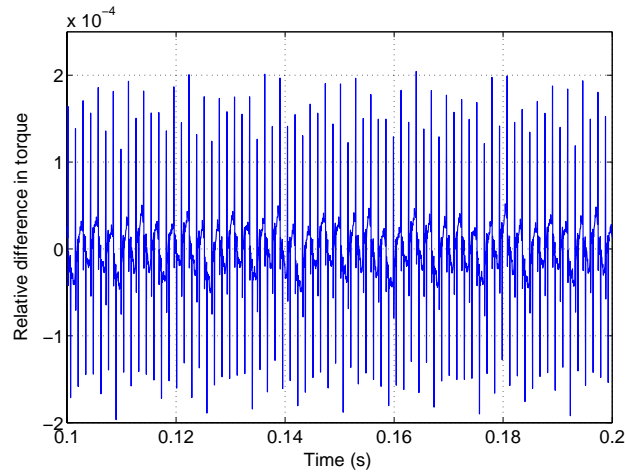


Fig. 60: Relative difference in torque uncoupled-coupled.

The effect of stress on magnetostriction has also been checked. The differences in the frequency contents of the velocity of the same node on the outer surface of the stator core are presented in Fig. 58. Here the stress-dependency of the magnetostriction increases almost all the frequency components. Some of them are increased by up to 2 000 %. However, the high frequencies are increased much more (not shown in Fig. 58). This increase is not correct, being due to the inaccuracy of the linear triangular elastic elements combined with large values of the magnetic forces. It is also partly due to the effect of magnetostrictive stress on the calculated mechanical stress. Indeed, modelling the magnetostriction with equivalent forces causes mechanical stresses to occur in the material although the structure modelled is free to stretch or shrink. This phenomenon has been explained in Chapter 2.

Fig. 59 shows the relative difference in terminal currents between the cases uncoupled and coupled

$\left(\frac{|I_{uncoupled}| - |I_{coupled}|}{|I_{uncoupled}|} \right)$. Sharp peaks of up to 25 % of the terminal current are calculated when the

coupling is taken into account. This difference in current is not necessary visible in the Real Mean Square values of the current since it can be a result of a phase shift only. The magnetoelastic coupling does not have a major effect on the calculated torque, as can be seen from Fig. 60, where

the relative difference in electromagnetic torque $\left(\frac{|T_{uncoupled}| - |T_{coupled}|}{|T_{uncoupled}|} \right)$ is shown (less than 2E-4 %).

7.2 Induction machine

The analysed induction machine is a small-size 37 kW motor, the parameters of which are given in appendix D.

The same set of computations carried out for the synchronous generator has been carried out for this motor. Results of these computations are presented below.

First, the quasi-static case without coupling is presented as a reference. The deformation of the stator core, as well as the radial displacements of a node on the outer surface of the core, is shown in Fig. 61. The deformation shows a clear fourth spatial mode. This fact is attributed to the form of the magnetic forces, which show a fourth mode also, as the machine has four poles.

The normalised magnetic and magnetostrictive forces are shown in Fig. 62. The maximum value of the magnetic forces was 920 N/m, while that of the magnetostrictive forces was 4 580 N/m. The maximum magnetostriction forces are about five times larger than the magnetic forces. The frequency contents of the velocity of the same node on the outer surface of the stator core have been calculated from the radial displacements by differentiating and using DFT. The result is shown in Fig. 63.

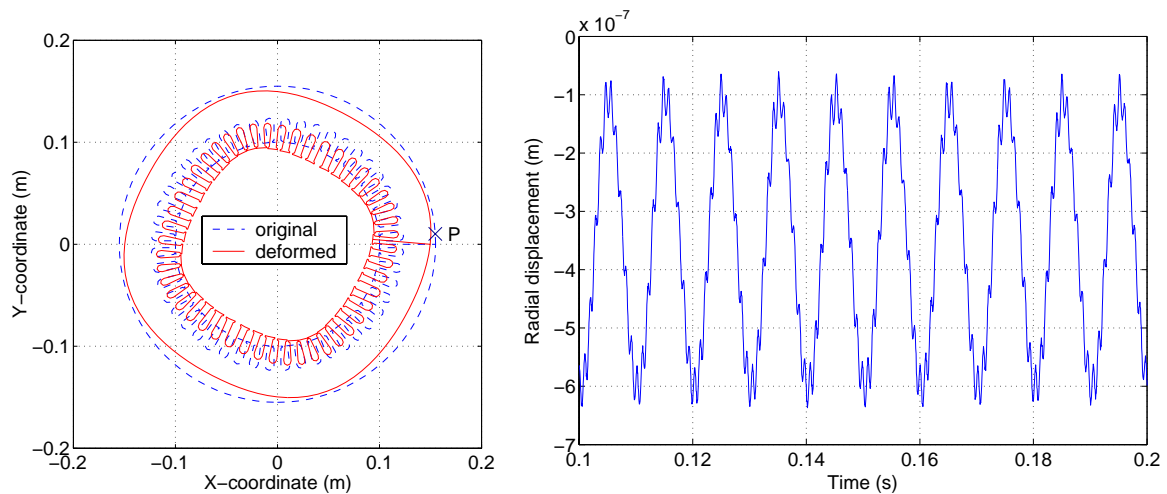
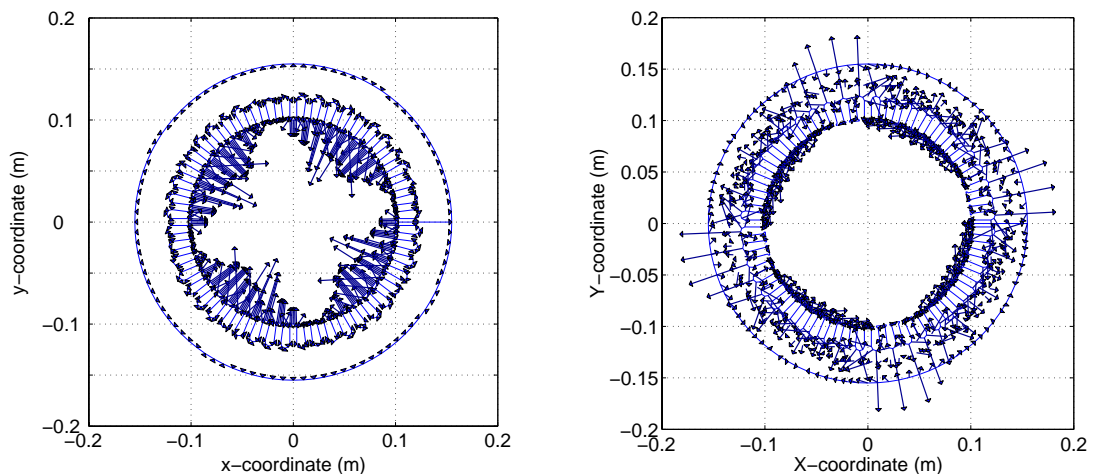


Fig. 61: Deformation (20 000 x magnified) and radial displacement point P.



a) magnetic (normalised to 10 180 N/m)

b) magnetostrictive (normalised to 76 300 N/m)

Fig. 62: Magnetic and magnetostrictive forces.

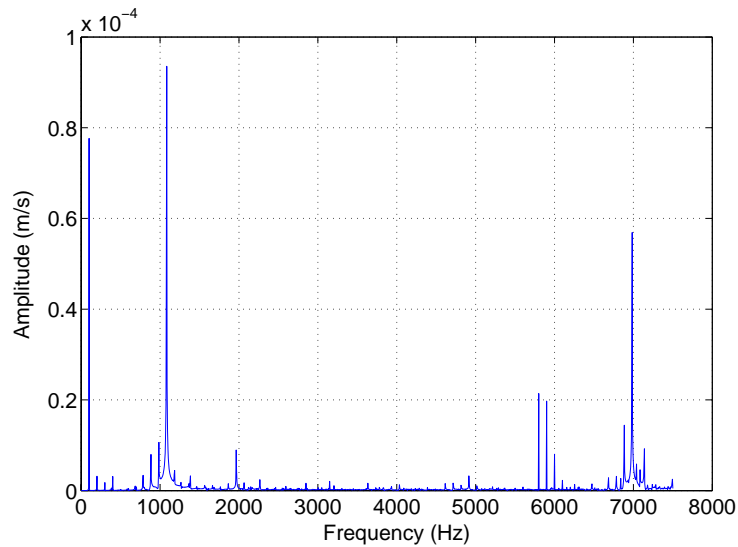


Fig. 63: Frequency contents of the velocity of a node on the outer surface of the stator core.

The velocity shows sharp peaks at the frequencies of 100, 1 085, 5 800, 5 900 and 6 985 Hz (see Fig. 63). The first corresponds to twice the frequency of the main, the second is equivalent to that of 1 080 Hz in the synchronous generator and the others can be attributed to slot- and winding-harmonics or other phenomena like saturation.

7.2.1 Dynamic and coupled cases

The dynamic case has been calculated as undamped, whether coupled or not. The effect of magnetostriction has been studied by comparing calculations with magnetostrictive forces included and calculations without magnetostrictive forces. The differences between the radial displacements of a node on the outer surface of the stator core, calculated first with the uncoupled model, and then with the coupled, are presented in Fig. 64a. The effect of magnetostriction can be seen from Fig. 64b.

The qualitative, behaviour of the large stator (synchronous machine) and small stator (induction machine) with respect to the coupling and magnetostriction is the same. However, The effect of coupling is more important in large stator than in the smaller one. Quantitatively, the coupling and magnetostriction affect the different stator in a very different manner. This will be seen later in this chapter when the analysis is performed at frequency level.

The velocity of the same node on the outer surface of the stator core has been studied by both differentiation and using DFT (DFT parameters are reported in Table 1 above).

The differences in the frequency contents for the quasi-static – dynamic, uncoupled – coupled (without magnetostriction) and no magnetostriction – magnetostriction (uncoupled) cases are shown respectively in Fig. 65, Fig. 66 and Fig. 67.

It is clear here again that the dynamic nature of the stator vibrations has to be taken into account for more accurate evaluations of these vibrations. The relative difference in the amplitudes of velocities calculated with the quasi-static elastic approach and the dynamic one is from -500% up to 100% ; almost all the frequencies are affected (see Fig. 65). Due to the higher mechanical stiffness of the small stator, the high frequencies are much affect than the low one. This was not the case for the large stator of the synchronous machine. This latter one is mechanically less stiff, which explains its behaviour in the calculations with coupled approach.

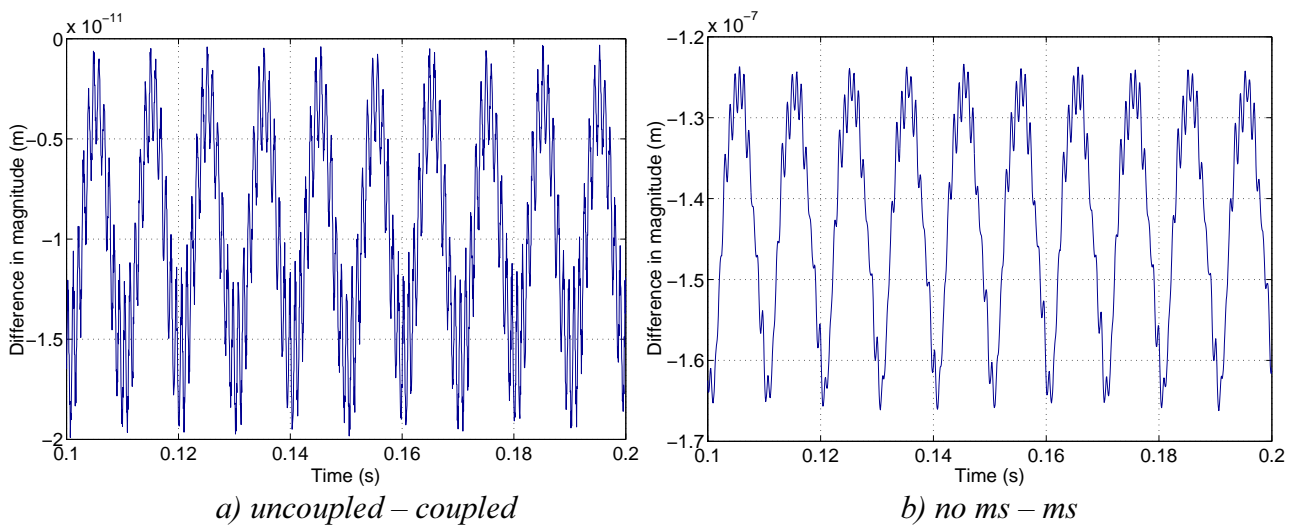


Fig. 64: Difference in radial displacement.

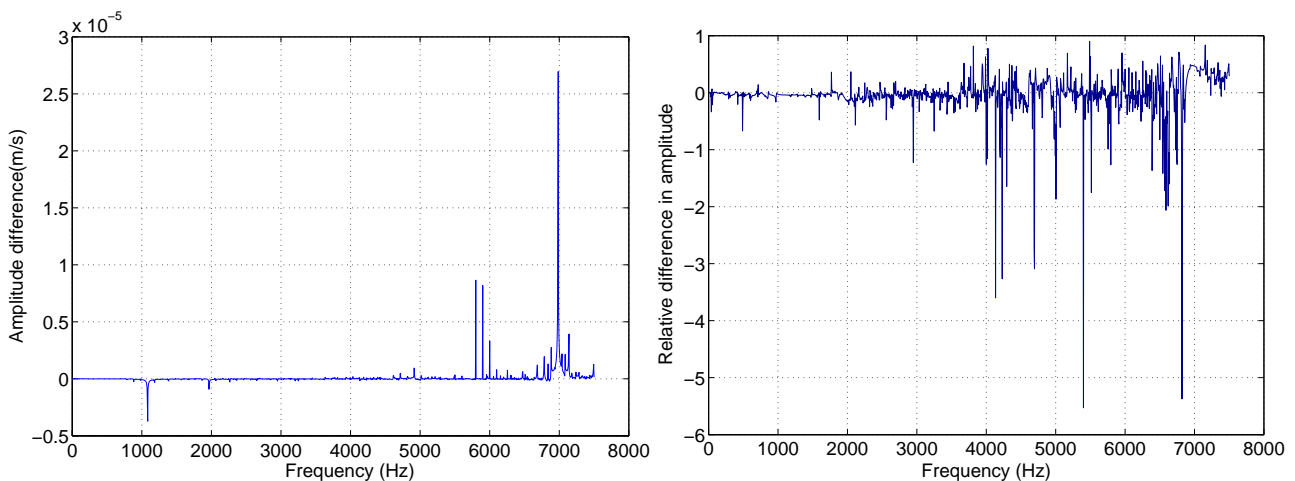


Fig. 65: Difference in frequency contents quasi-static – dynamic.

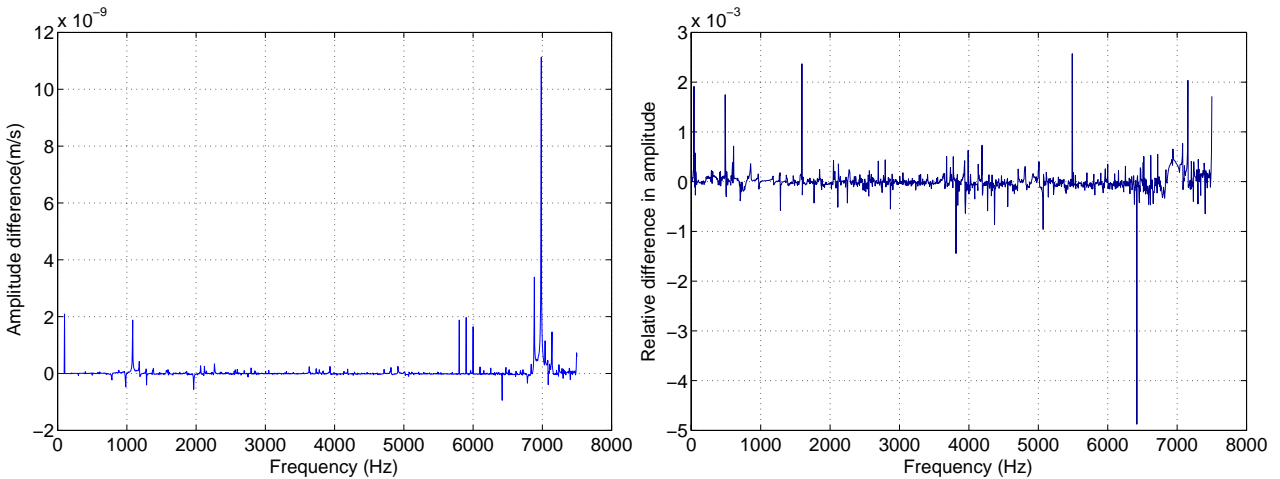


Fig. 66: Difference in frequency contents uncoupled – coupled.

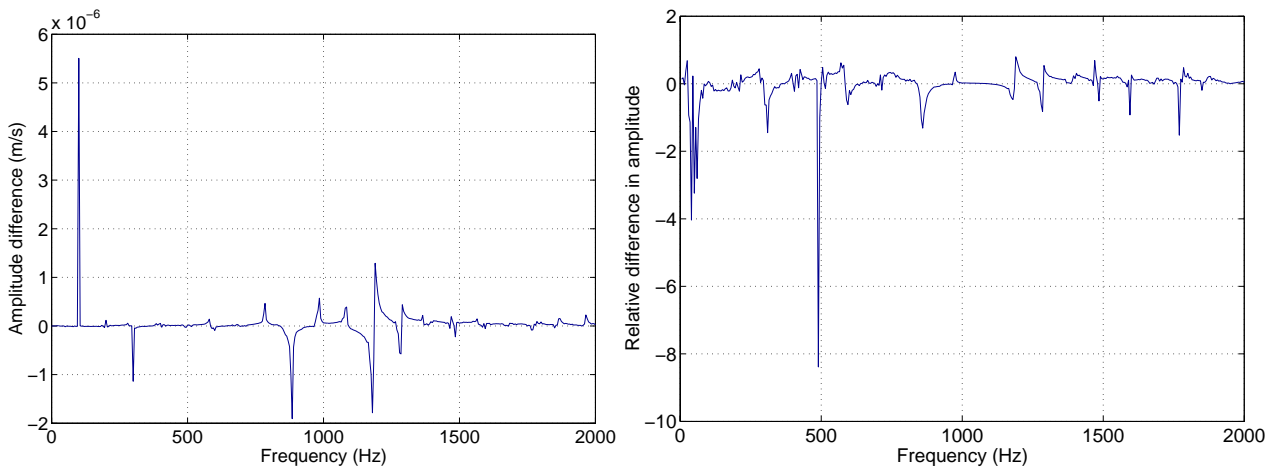


Fig. 67: Difference in frequency contents no ms – ms.

The effect of coupling on the stator vibration of the small induction machine is almost non-existent (0.5 % at its maximum see Fig. 66). This is because the small stator is mechanically stiffer than the large one. The displacements are very small and their effect on the magnetic calculation is negligible.

On one hand, the magnetostriction in the case of the small stator damps some frequency components of the velocity, e.g., those at 25 Hz (70 %), 100 Hz (7 %), 280 Hz (45 %) and 1190 Hz (80 %). On the other hand, some frequency components are much more increased, like the ones at 40, 50 and 60 Hz (respectively 400, 320 and 280 %) also the one at 490 Hz (840 %) among others (see Fig. 67). The argument in Låftman (1995), according to which the magnetostriction might damp the vibrations due to magnetic forces, can only be partly validated with these results. Furthermore, the increase in the frequency components at 40, 50, 60 and 490 Hz cannot be explained by such simple reasoning.

The results presented by Delaere (2002), namely that the magnetostrictive forces can be ignored and that they do not affect the noise and vibrations of rotating electrical machines, contradict the results presented in this chapter. In Delaere (2002), the magnetostrictive forces are calculated in an equivalent manner as it is done in this work. However, the data on the magnetostriction was missing and a simple function of the square of the flux density was used. The only results from the literature that agree somehow with the presented calculations are those presented by Witczak (1996). He calculated large magnetostrictive forces in an induction machine.

In Fig. 68, the stresses in the direction parallel to that of the flux density vector \mathbf{B} at each element are plotted. These are stresses calculated in the dynamic case without taking into account the effect either of magnetostriction or of the magnetoelastic coupling. The stresses vary from -1 to 1.5 MPa. Looking at the measurement results of magnetostriction, it becomes clear that the effect of stress on magnetostriction has to be taken into account when evaluating magnetostriction forces.

Fig. 69 shows the differences in the stress component in the direction parallel to that of the flux density vector. Most of the differences are between -800 and 200 kPa. This result explains why the integration, with respect to the flux density, in the calculation of the magnetic energy and the magnetic and magnetostriction forces are made at constant stress. However, the stress induced by magnetostriction is large enough to cause some calculation error. This problem has been experienced when the calculations with both magnetoelastic coupling and stress-dependent magnetostriction were tried. The Newton iterations did not converge and the combined effect of magnetostriction and magnetoelastic coupling could not be established, except in the case of stress-independent magnetostriction.

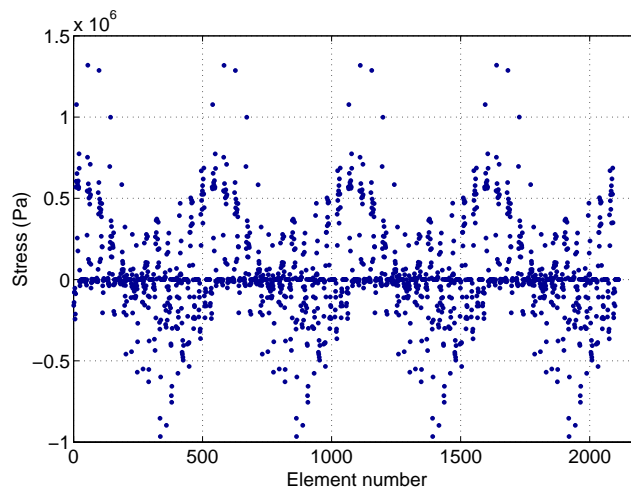


Fig. 68: Component of stress parallel to \mathbf{B} at each element.

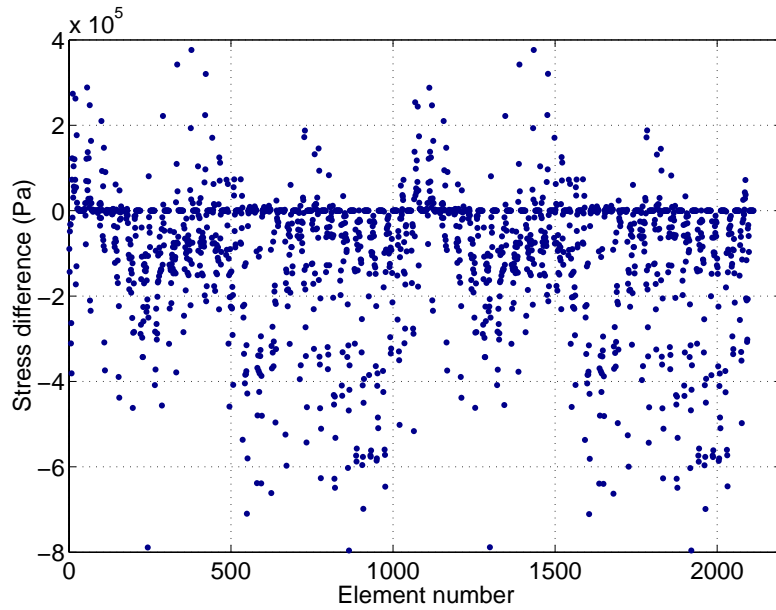


Fig. 69: Difference in stress parallel to B , due to magnetostriction.

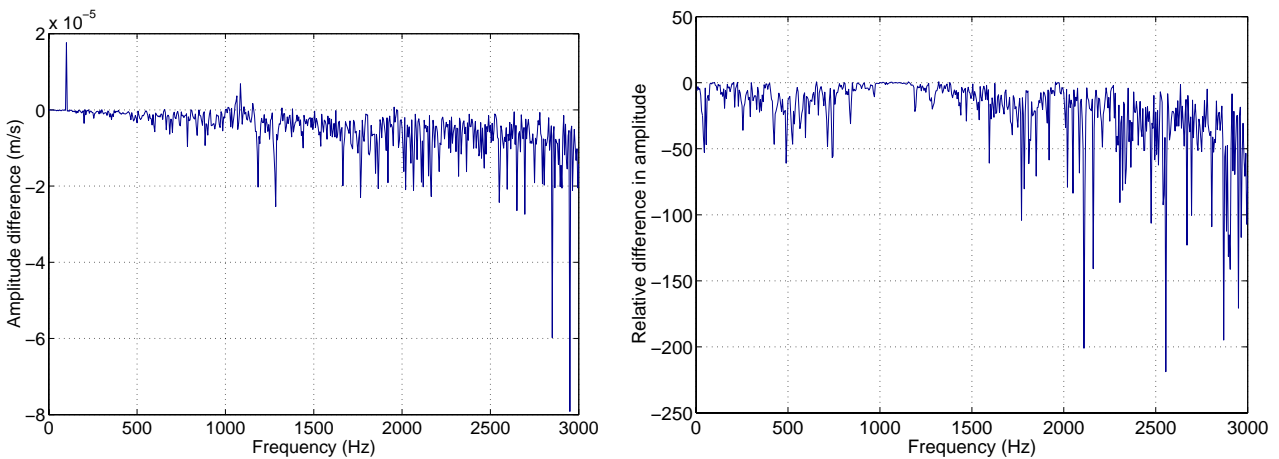


Fig. 70: Difference in frequency contents of the velocity between the stress-independent and stress-dependent cases.

To establish the effect of stress on magnetostriction, calculations have been undertaken with stress-dependent and stress-independent magnetostriction. The results of these calculations are shown in Fig. 70 as the differences in the frequency contents of the velocity of the same node on the outer surface of the stator core. The vibration velocity is increased for almost all the frequency components. However, the abundance of frequency components in the spectrum of velocity is not strictly correct. The inaccuracy of linear triangular finite elements combined with the large values of magnetostrictive forces cause the surface of the iron core to deform discontinuously. This phenomenon causes an enrichment of the spectrum. However, even if only part of these frequency components is correct, they will still affect the vibrations of the stator core.

7.3 Conclusions

Computations of two kinds of rotating electrical machines were performed to establish the effect of magnetostriction and magnetoelastic coupling on the vibrational behaviour of the stators of those machines. It has been shown that the mass greatly affects the velocities of vibrations and cannot be ignored.

It has also been shown that magnetostriction affects the velocities of vibrations of the stators of rotating electrical machines. This effect seems to be smaller at high frequencies over 1500 Hz. Moreover, the effect of stress-dependent magnetostriction has been shown to play a role in the determination of the amplitude of the velocities of vibrations.

Evidence of the existence of the magnetoelastic coupling phenomenon in rotating electrical machines is given. This phenomenon has been ignored until now and its existence has never been demonstrated. The computations performed and presented in this chapter show that magnetoelastic coupling changes the velocities of the vibrations of the stators of rotating electrical machines compared with the velocities calculated without coupling. These results show a strong coupling phenomenon in the large stator, while in the small stator this phenomenon is less pronounced.

8 Discussion and conclusions

The aim of this chapter is to summarise and discuss the results obtained in this work. Some computational aspects of the results, such as computation time and accuracy, are also discussed. Suggestions as to how this work might be developed in the future, and possible issues relating to its future applications, are also presented.

8.1 Importance of the work

The updated literature review undertaken during the years of this study shows that the problem of magnetostriction in electrical machines is still a matter of controversy. Many researchers tried, and still try, to address the question of the nature of the effects of magnetostriction on the vibrations and noise of rotating electrical machines. The model used for magnetostriction varies from one author to another, and the differences between the results remain too large to allow definitive answers.

Although the magnetostriction phenomenon by itself is well understood, a major difference between the so-called magnetostrictive forces and magnetic or reluctance forces should be emphasised. This difference resides in the effect of these forces on elastic structures. While the magnetic forces act mainly at interfaces between different materials (mostly iron-air interfaces) causing rigid body displacements and elastic deformations of the structures, the magnetostrictive forces act at different parts of the iron, only causing deformations other than rigid-body ones, and tending to stretch or shrink the iron without any major effect on the structure itself. This difference makes the effects of magnetic and magnetostrictive forces on a stator of electrical machines very different from one another. The magnetic forces act on an elastic structure with relatively low stiffness, while the magnetostrictive forces act on the material itself, which is very stiff. Although the magnetostriction forces are many times larger than the magnetic forces, their effect on the vibrations of the structures is, except at some frequencies, less important than that of the magnetic forces.

The separation of magnetic forces into the forces traditionally called magnetic (or reluctance) forces and magnetostriction forces is shown in the derivation of magnetic forces from the principle of virtual work. In this method, the magnetic forces are composed of different terms.

If the stress dependence of the magnetisation is not taken into account, the non-zero terms are demonstrated to give the same total force as the Maxwell stress tensor method. However, while the

radial component of the Maxwell stress tensor taken as force distribution gives non-zero forces only at the interface between iron and air, the nodal forces give non-zero forces inside iron also. These forces are attributed to the effect of saturation. Indeed, the magnetic reluctance (or permeability) varies from one element to the other. At the interface of the elements, the difference in reluctivity leads to forces, the directions of which are from the element with smaller reluctivity to the one with higher reluctivity.

When the stress dependence of magnetisation is taken into account, there are extra terms in the formulae of the forces. These terms, strongly related to the elasticity of the iron (or any magnetic material under consideration), are attributed to magnetostriction. Within this theory, the magnetostrictive forces can be calculated in different ways, depending on the body of data available and its accuracy.

In this work, the magnetostrictive forces used for the calculation of the effect of magnetostriction on the vibrational behaviour of the stator of electrical machines are calculated in a simple, but accurate, manner that reflects the measured magnetostriction. The derivation of the magnetostrictive forces from the principle of virtual work is presented for its theoretical importance and for completeness and consistency. Its application to the calculation of these forces in complex systems like rotating electrical machines still requires too much measurement and verification.

The effect of magnetostriction on the vibrational behaviour of the stator of rotating electrical machines is found to be more important than stated in the literature. However, the changes in the velocities of vibrations affect mainly frequencies below 1500 Hz. This range of frequencies is still large enough to cause acoustic noise problems. The effect of mechanical stress on the vibrations due to magnetostriction is also important, although exact computation of this effect needs a more accurate model that excludes the effect of the stress induced by the magnetostriction itself. This problem is possible to overcome, since the elastic problem is linear.

The effect of electromagnetoelastic coupling on the vibrations of rotating electrical machines has never been studied, except in the work of Arkkio (2001), and then only from the electromagnetic point of view. The effect of electromagnetic damping of mechanical vibrations has been interesting mainly for the studies concerned with rotor dynamics and rotor vibrations. In this work, the effect of electromagnetoelastic coupling is shown to be very important in the large stator. Its effect on the

vibrational behaviour of small-size stators is not that important. This result is logical, since the elastic displacements in large stators are much larger than those in small-size stators.

One aspect of the electromagnetoelastic coupling that has not been studied in this work is the change of magnetisation with respect to mechanical stress. This problem has been disregarded for three reasons: the low level of stress in the stator core, the lack in the knowledge of the effect of multidirectional stress on the magnetisation and the lack of time.

The main achievements of this work are the development of the theory and formula relating to magnetoelastic coupling within time stepping FE analysis and the building of the required simulation tools. The measurement of magnetisation and magnetostriction under externally applied mechanical stress is also an achievement, which produced results that have many applications, either of theoretical interest, like the determination of magnetoelastic coupling constants, or of computational interest, as in this work. Last but not least, the simulations of the two kinds of machines and the results obtained from these simulations are very important for those designers concerned with the problems of the vibrations and noise of rotating electrical machines.

8.2 Accuracy matters and computation time

The accuracy of the developed model and that of the computation are difficult to evaluate. However, some considerations have to be mentioned. First, the developed tools are based on linear triangular finite elements, the accuracy of which is not the best possible. The development of the formula for elements of a higher order is a task that can be better addressed in the next section (8.3 Future work). However, before doing so, an estimate of the computation time with second- or third-order elements is needed. Second, the magnetic field solution is based on the $A-\phi$ formulation of the magnetic field. In this formulation, the magnetic flux density is solved accurately at element level, but the magnetic field strength is not. The continuity of the tangential component of the magnetic field strength is not guaranteed within this formulation. This discontinuity results in inaccuracies of both the magnetic vector potential and the magnetic forces. These phenomena are important in the iron core, but as we have seen, the forces in the iron core are very small compared with those on its surface.

The effect of magnetostrictive stress on the total mechanical stress in iron elements also decreases the accuracy of the calculation of magnetostrictive forces when the stress-dependency of the magnetostriction is taken into account.

These remarks, and the measurements made on the validation device, allow us to say that the accuracy of the method, as well as that of the computations, are sufficiently accurate to allow us to draw the conclusions presented in this work. The only way of estimating the accuracy of the computations would be by complicated measurement of the vibrations of the computed machines as well as the magnetic flux density in the core of these machines through search coils. This measurement has not been performed on the simulated machines (synchronous and induction).

The accuracy of the measured data, on the other hand, can be considered as good. According to the specifications of the measurement devices used, and within the range of measured values, the error in measurements is less than 5 %. However, the measured values are hysteresis loops of either magnetisation or magnetostriction. These loops needed filtering and averaging to get them into a form suitable for the computations. As a result, a rough estimate of the error on these values is about 10 %.

The error on the measurement made on the validation device is estimated to be about 10 %, based again on the specifications of instruments used for these measurements.

The computations were performed on different platforms. A total of 4000 time steps with 300 steps per period of the line voltage was computed in each case. Each time step took five or six iterations, depending on whether the problem was coupled or not. On a Sun Microsystems Blade 100 workstation with an UltraSPARC-IIe processor having a clock frequency of 500 MHz, the total computation time was 10h 15min for an uncoupled dynamic case and 18h 16min for the coupled one. This is already a huge computation time, and the idea of second- or higher-order finite elements does not sound reasonable at least at this computational speed.

However, the tools developed here are for research or special analysis purposes. The program code is not optimised and a possible lowering of the number of equations by using geometrical and electrical symmetry of the machines was not used. Taking advantage of these technical considerations might reduce the computation time.

8.3 Future work

The path from vibrations to the noise level of rotating electrical machines is long and complex. Different aspects of the problem have to be studied. Among these aspects, we can mention here the structure of the machine mounting, the mechanism of vibration transfer from the stator core to the structure around it, the pre-stress of the stator core (in some induction machines the stator core is under pre-stress from the surrounding frame) and the radiation of noise by the vibrating components of the mounted machine. All these aspects require special studies that are beyond the scope of this thesis; nevertheless, the study of aspects such as these is necessary if a better understanding and quantitative establishment of the problem of noise from rotating electrical machines is to be gained.

The results and the tools built in this work give a good background for further studies. These tools can also be used to study more complex phenomena like the effect of stress on magnetisation. However, logically, the next step in this work is the systematic simulation of different types and sizes of electrical machines and the use of statistical analysis of the results to formulate general rules for the use of magnetostriction and electromagnetoelastic coupling to build and design less noisy rotating electrical machines.

Last and not least, The effect of mechanical stress on the iron losses has not been studied in this work. The mechanical stress is known to increase the magnetic losses in iron sheets. This is also a subject than needs more work an deep studies to establish how the losses are changed and whether it is possible to reduce them by any means.

Appendix A: Parameters of the validation device

The main parameters of the validation device are listed below. Figure A1 shows the geometry of the cross section of the device (only a quarter is shown), while Fig. A2 shows the geometry of a slot. Table A1 gives the electric parameters of the device and its windings. Table A2 gives the dimensions of the slot and Table A3 those of the device.

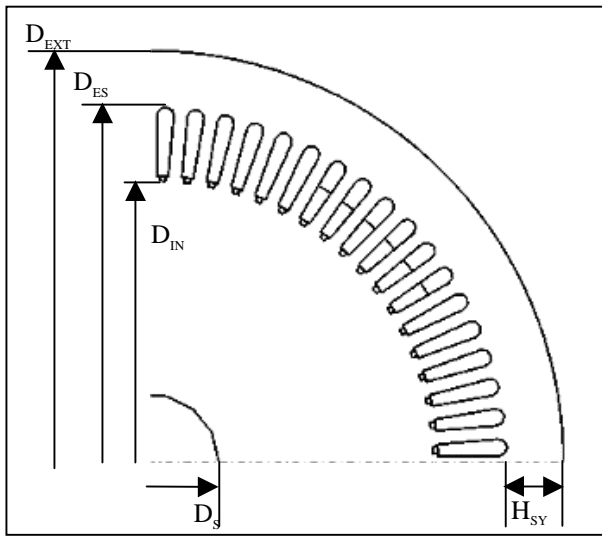


Fig. A1: Geometry of the validation device.

Table A1 Electrical parameters of the device.

Number of poles	2
Number of phases	3
Number of parallel paths	1
Number of conductors in a stator slot	8
Number of layers of the stator winding	2
Coil pitch in slot pitches	30

Table A2: Slot dimensions.

Slot data	[mm]
H_1	54
H_2	44
H_3	3
B_1	4
B_2	12
B_3	8

Table A3: dimensions of the validation device.

Stator data		[mm]
Inner diameter	D_{IN}	410
Outer diameter	D_{EXT}	600
Shaft diameter	D_S	100
Height of stator yoke	H_{SY}	41
Length of stator core	Th	100

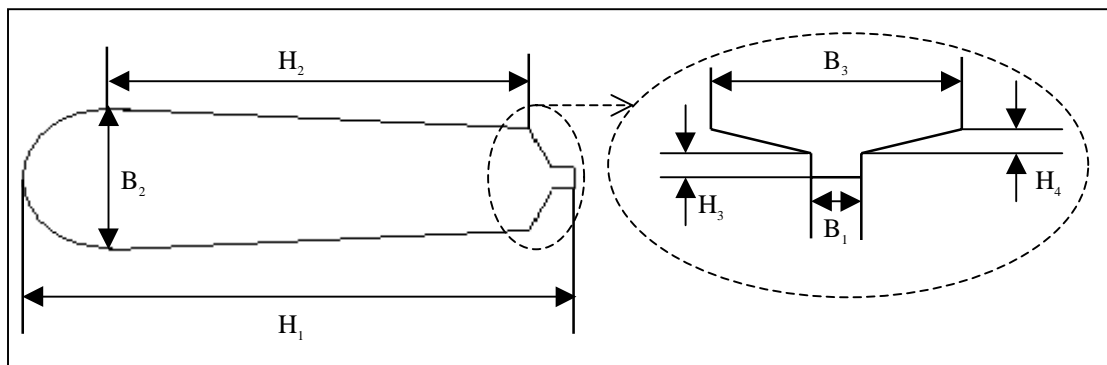
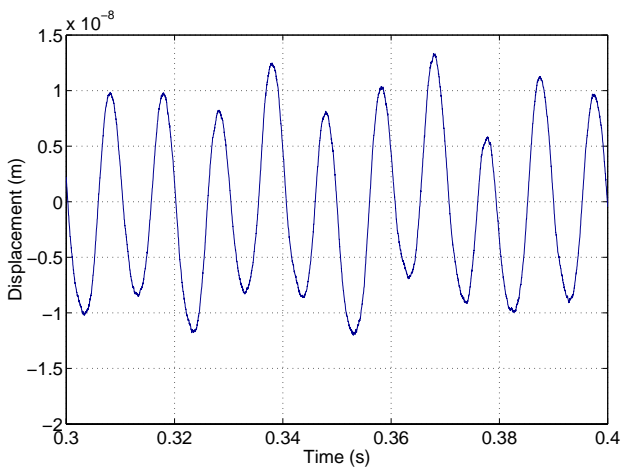


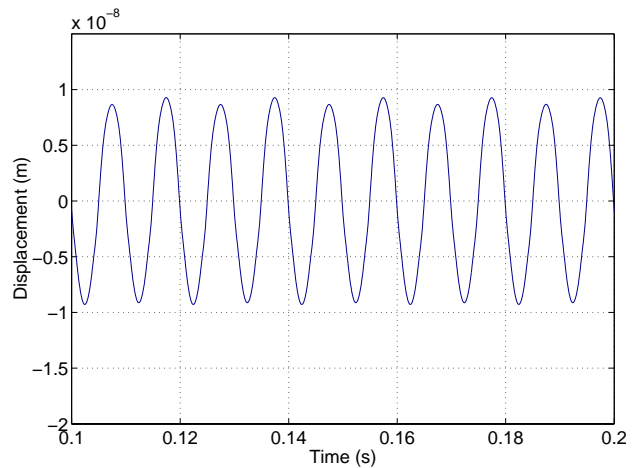
Fig. A2: Geometry of the slot.

Appendix B: Result of measurements and simulations of the test device

Some of the measured and/or simulated quantities from the validation device are presented below. Whenever the quantities are both measured and simulated, they are compared to each other. Some of the results are only measured (supply voltage of 500 V). They are presented here for completeness only.

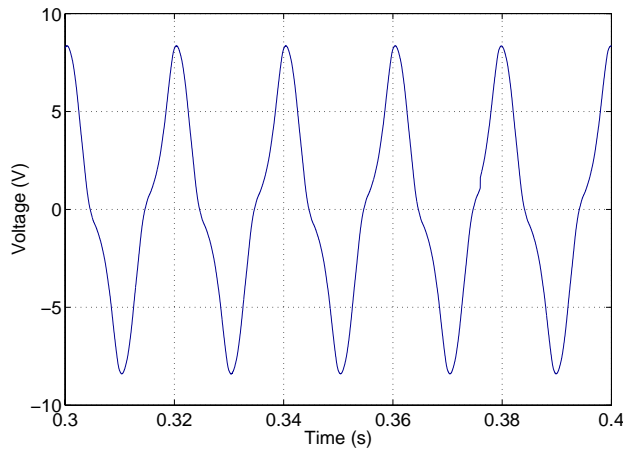


a) measured

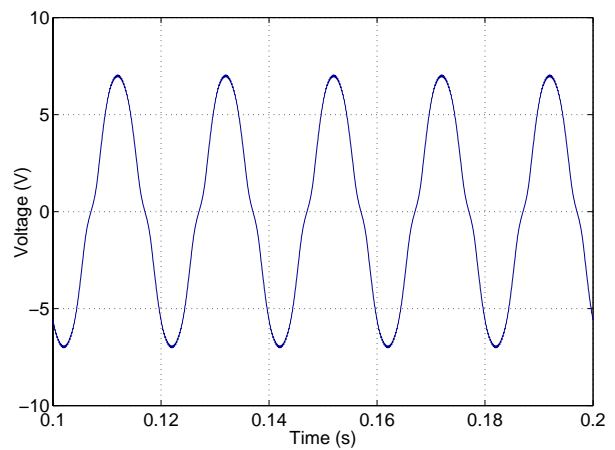


b) simulated

Fig. B1: Displacement of point A at a feed voltage of 300 V 50 Hz.

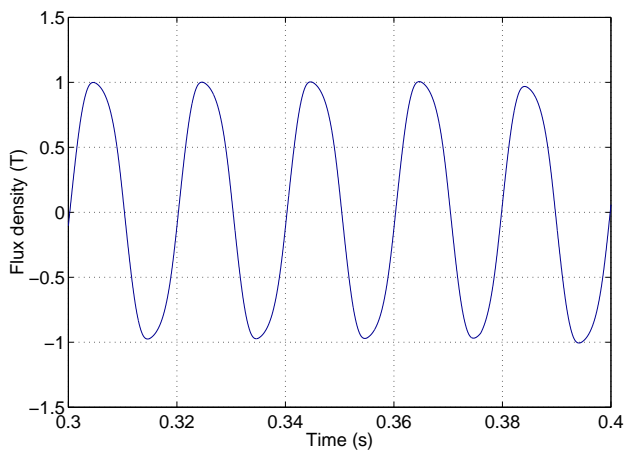


a) measured

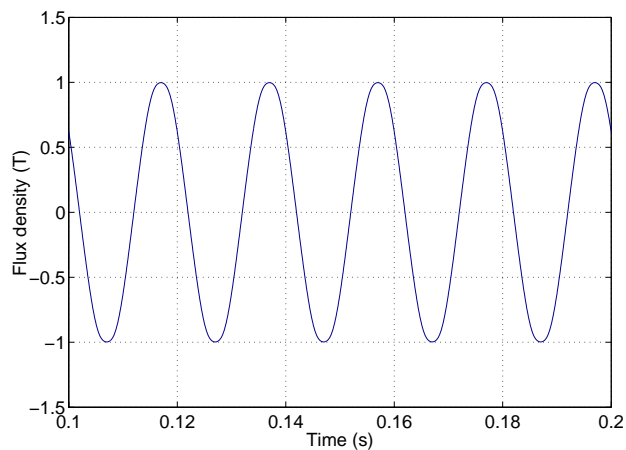


b) simulated

Fig. B2: Voltage of the search coil at a feed voltage of 300 V 50 Hz.

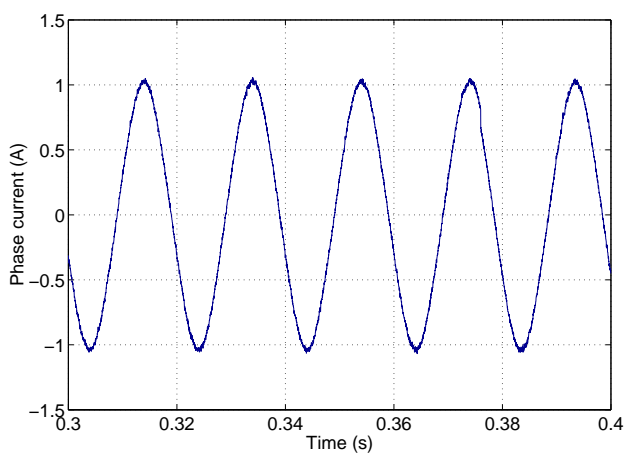


a) measured

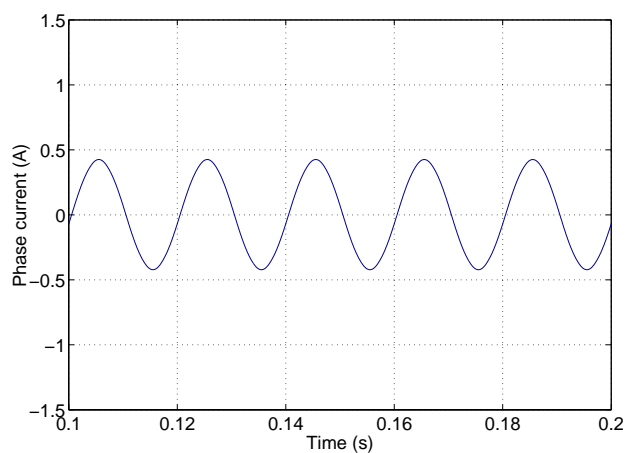


b) simulated

Fig. B3: Flux density across the search coil at a feed voltage of 300 V 50 Hz.



a) measured



b) simulated

Fig. B4: Phase current at a feed voltage of 300 V 50 Hz.

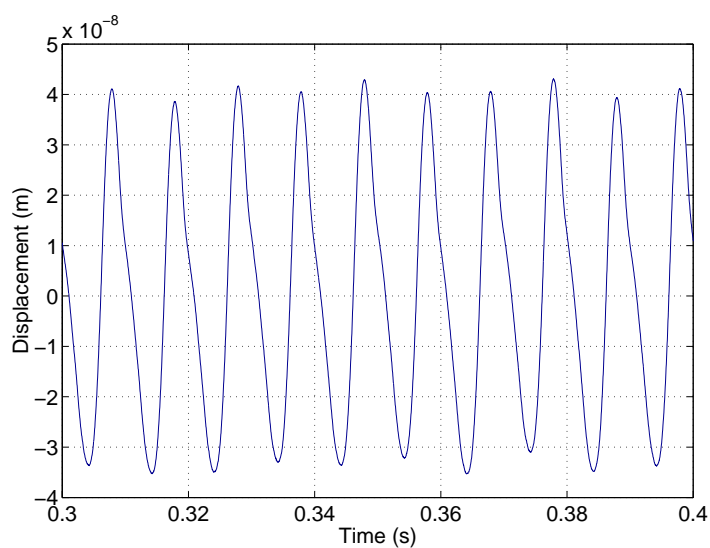


Fig. B5: Measured displacement of point A at a feed voltage of 500 V 50 Hz.

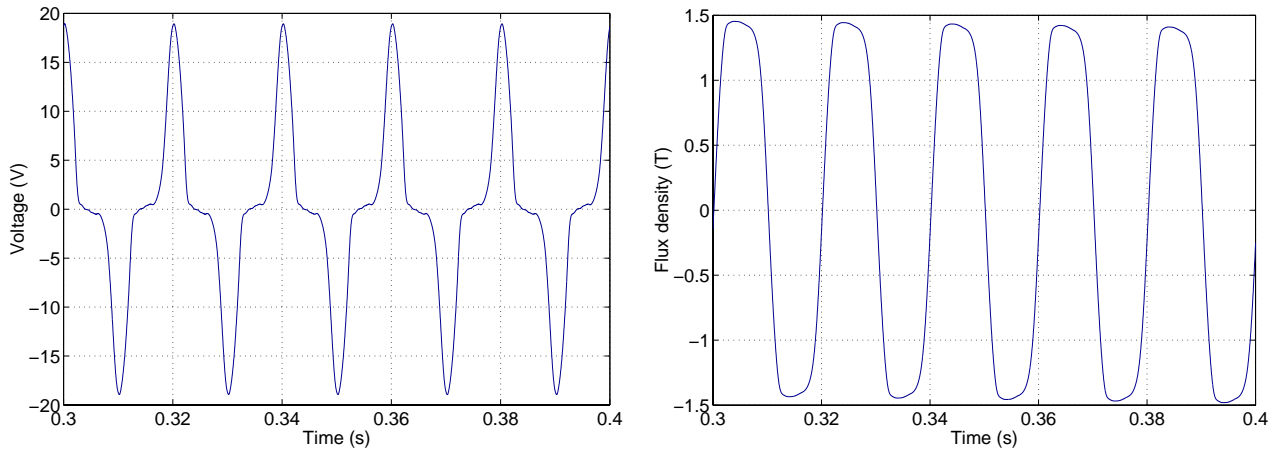
*a) voltage**b) flux density*

Fig. B6: Measured voltage of the search coil and flux density across it at a feed voltage of 500 V 50 Hz.

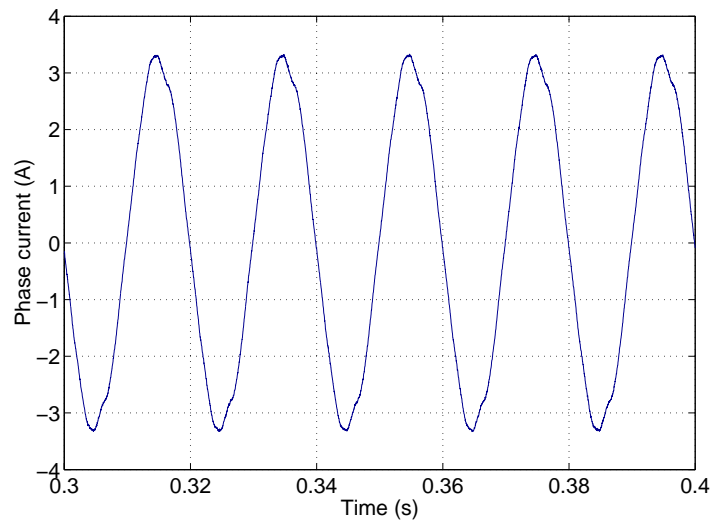


Fig. B7: Measured phase current at a feed voltage of 500 V 50 Hz.

Appendix C: Parameters of the analysed synchronous machine

The rated values and geometry of the synchronous machine simulated and analysed in Chapter 7 are given in table C1.

The synchronous machine was simulated at the rated power. The field current was 100 A and the terminal current 300 A. The power factor was 0.80 and the displacement factor 0.80 capacitive. The shaft power was 2.78 MW.

Table C1: Rated and geometrical values of the synchronous machine.

Rated power	3,025 MVA	Number of stator slots	96
Rated voltage	6600 V	Stack length	1200 mm
Frequency	60 Hz	Stator outer diameter	1200 mm
Number of phases	3	Stator inner diameter	950 mm
Number of poles	10	Damping bars/pole	4
Power factor	0.80 Cap.		

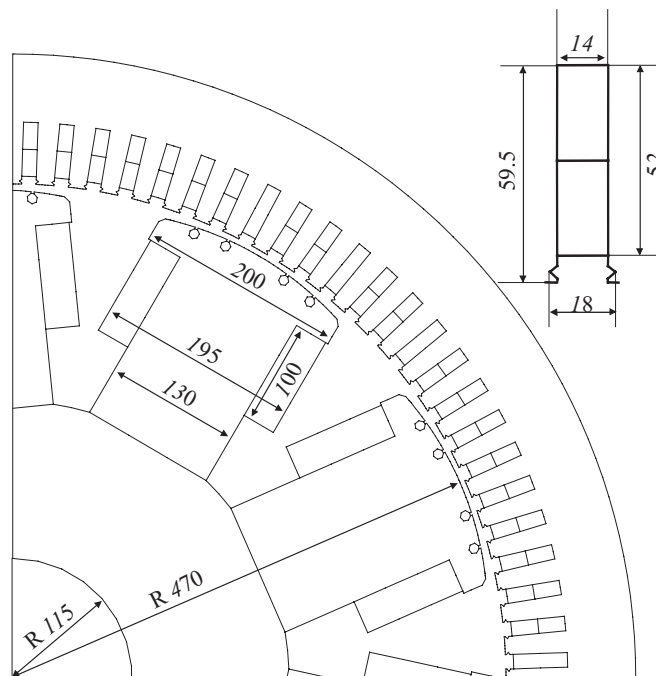


Fig. C1: Geometry and dimensions (in mm) of the synchronous machine.

Appendix D: Parameters of the analysed induction machine

The rated values and geometry of the induction machine simulated and analysed in Chapter 7 are given in table D1.

The induction machine was simulated at the rated power. The terminal current was 68.2 A, shaft power 36.2 kW and the power factor 0.83.

Table D1: Rated and geometrical values of the induction machine.

Rated power	37 kW	Stator outer diameter	310 mm
Rated voltage	380 V	Stator inner diameter	200 mm
Connection	Star	Stack length	289 mm
Slip	1.7 %	Number of stator slots	48
Frequency	50 Hz	Rotor outer diameter	198.4 mm
Number of phases	3	Rotor inner diameter	70 mm
Number of poles	4	Number of rotor slots	40

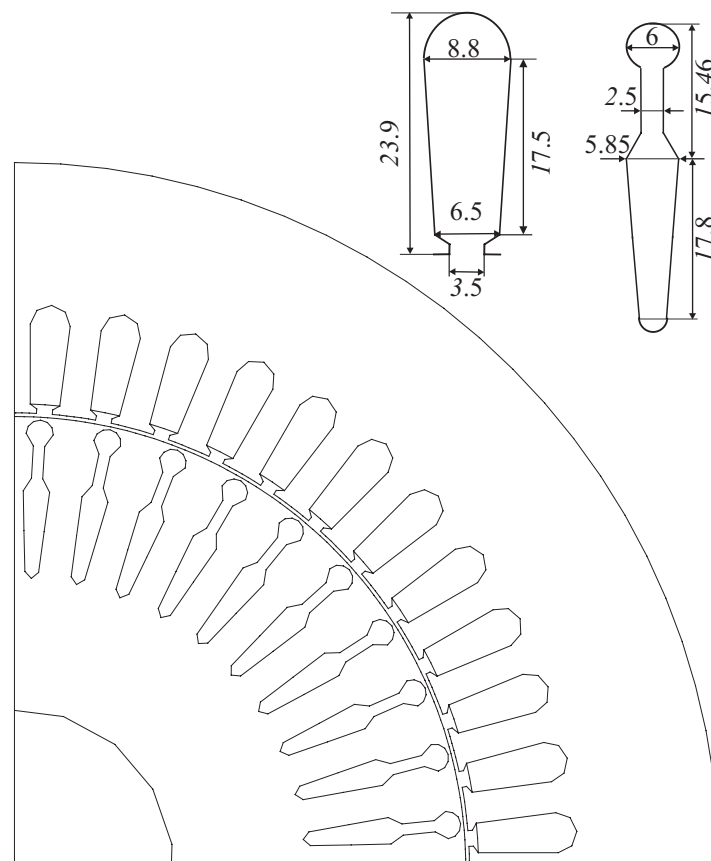


Fig. D1: Geometry and dimensions (in mm) of the induction machine.

References

Arkkio, A. 1987, "Analysis of Induction Motors Based on the Numerical Solution of the Magnetic Field and Circuit Equations", doctoral thesis, Acta Polytechnica Scandinavica, Electrical Engineering Series No. 59, 97 p. <<http://lib.hut.fi/Diss/198X/isbn951226076X/>>

Arkkio, A. 1995, "Unbalanced Magnetic Pull in a Four-Pole Induction Motor with an Odd Number of Rotor Slots", Proceedings of CICEM'95, Hangzhou, 31 Aug. - 2 Sept. 1995, China, pp. 343–348.

Arkkio, A. 2001, "Electromagnetic Damping of Stator Vibrations in a Cage Induction Motor", VTT SYMPOSIUM 209, Espoo 2001, pp. 25–44.

Bath, K. J. 1982, "Finite Element Procedure in Engineering Analysis", Prentice-Hall International, New Jersey, 1982, 735 p.

Belahcen, A., Arkkio, A., Klinge, P., Linjama, J., Voutilainen, V., Westerlund, J. 1999 "Radial Forces Calculation in a Synchronous Generator for Noise Analysis", Proceedings of CICEM'99, Xi'an, China, 29-31 August 1999, pp. 119–122.

Belahcen, A. 2001, "Review of the Methods for Local Forces Calculation in Electrical Apparatus", Proceedings of Xth International Symposium on Electromagnetic Fields, 20-22 September 2001, Cracow, Poland, pp. 339–342.

Benbouzid, M. E. H., Spornic, S. A., Body, C. 1997, "Computer-Aided Design of Magnetostrictive Devices Using Terfenol-D", ETEP, Vol. 7, No. 5, September 1997, pp. 351–159.

Besbes, M., Ren, Z., Razek, A. 1996, "Finite Element Analysis of Magneto-Mechanical Coupled Phenomena in Magnetostrictive Materials", IEEE Transaction on Magnetics, Vol. 32, No. 3, May 1996, pp. 1058–1061.

Besbes, M., Ren, Z., Razek, A. 2001, "A Generalized Finite Element Model of Magnetostriction Phenomena", IEEE Transaction on Magnetics, Vol. 37, No. 5, September 2001, pp. 3324–3328.

Body, C., Reyne, G., Meunier, G. 1997, "Nonlinear Finite Element Modelling of Magneto-Mechanical Phenomena in Giant Magnetostrictive Thin Films", IEEE Transaction on Magnetics, Vol. 33, No. 2, March 1997.

Bossavit A., 1992, "Edge-element Computation of the Force Field In Deformable Bodies", IEEE Transaction on Magnetics, Vol. 28, No. 2, March 1992, pp. 1263-1266.

Bozorth, R. M. 1951, "Ferromagnetism", Toronto, Van Nostrand, 968 p.

Carpenter, C. J. 1959, "Surface-Integral Methods of Calculating Forces on Magnetized Iron Parts", The Institution of Electrical Engineers Monograph, No. 342, pp.19-28.

Cester P. 2002, "Magnetostriction as Source of Noise and Vibration: Design, Construction and Measurements on an Experimental Electrical Machine", Università Degli Studi di Padova, Tesi di Laurea (Master's thesis), 61 p.

Coulomb J. L. 1983, "A Methodology for the Determination of Global Electromechanical Quantities from a Finite Element Analysis and its Application to the Evaluation of Magnetic Forces, Torques and Stiffness", IEEE Transactions on Magnetics, Vol. MAG-19, No. 6, November 1983, pp. 2514-2519.

Dapino, M. J., Smith, R. C. and Flatau, A. B. 2000, "Structural Magnetic Strain Model for Magnetostrictive Transducers", IEEE Transaction on Magnetics, Vol. 36, No. 3, May 2000, pp. 545-556.

Delaere, K., Belmans, R., Hameyer, K., Heylen, W., Sas, P. 1999, "Coupling of magnetic analysis and vibrational modal analysis using local forces", Xth International Symposium on Theoretical Electrical Engineering ISTET'99, Magdeburg, Germany, 6-9 September 1999, pp.417-422.

Delaere, K. 2002, "Computation and Experimental Analysis of Electrical Machine Vibrations Caused by Magnetic Forces and Magnetostriction", doctoral thesis, Publication of the Katholiek Universiteit Leuven, 223 p.

Du Tremolét de Lacheisserie, E. 1993, "Magnetostriction, Theory and Applications of Magneto-Elasticity, CRC Press, Florida, 1993, 409 p.

Garvey, S. D., 1999, "Magnetostrictive Excitation of Vibration in Machines – A Modal Approach", Proceedings of the 9th Conference on Electrical Machines and Drives, IEE Conference Publication No. 468, pp. 169–173.

Gros, L., Reyne, G., Body, C. Meunier, G. 1998, "Strong Coupling Magneto Mechanical Methods Applied to Model Heavy Magnetostrictive Actuators", IEEE Transaction on Magnetics, Vol. 34, No. 5, September 1998, pp. 3150–3153.

IEC 60027-1 1992, "Letter symbols to be used in electrical technology", Corrected and reprinted 1995-03-31, - Part 1: General, 111 p.

IEC 60404-2 1996, "Magnetic materials - Part 2: Methods of measurement of the magnetic properties of electrical steel sheet and strip by means of an Epstein frame", 37p.

Jiles, D. C. and Devine, M., K. 1994, "Recent Developments in Modeling of The Stress Derivative of Magnetization in Ferromagnetic Materials", Journal of Applied Physics, Vol. 76, No. 10, November 1994, pp. 7015–7017.

Jiles, D. C. 1995, "Theory of the Magnetomechanical Effect", Journal of Physics D: Applied Physics, Vol. 28, 1995, pp. 1537–1546.

Kameari, A. 1993, "Local Calculation of Forces in 3D FEM with edge elements", International Journal of Applied Electromagnetics in Materials, Vol. 3, 1993, pp. 231–240.

Kashiwaya, K. 1991, "Fundamentals of Nondestructive Measurement of Biaxial Stress in Steel Utilizing Magnetoelastic Effect under Low Magnetic Field", Japanese Journal of Applied Physics, Vol. 30, No. 11A, November 1991, pp. 2932–2942.

Lundgren, S. A., Bergqvist, A. and Engdahl, S. G. 1997, "A Rate Dependent Magnetostrictive Simulation Method for Silicon Iron Sheets under Harmonic Excitation", IEEE Transaction on Magnetics, Vol. 33, No. 2, March 1997, pp. 1674–1677.

Låftman, L. 1995. "The Contribution to Noise from Magnetostriction and PWM Inverter in an Induction Machine", doctoral thesis, IEA Lund Institute of Technology, 94 p.

Melcher, J. R. 1981, "Continuum Electromechanics", MIT Press, Cambridge, MA, 1981, 640 p.

Mohammed, O., Calvert, T., and McConnell, R. 1999, "A Model for Magnetostriction in Coupled Nonlinear Finite Element Magneto-Elastic Problems In Electrical Machines", Proceedings of the International Conference on Electric Machines and Drives, pp.728–735.

Mohammed, O., Calvert, T., and McConnell, R. 2001, "Coupled Magnetoelastic Finite Element Formulation Including Anisotropic Reluctivity Tensor and Magnetostriction Effects for Machinery Applications", IEEE Transactions on Magnetics, Vol. 37, No. 5, September 2001, pp. 3388–3392.

Mohammed, O., Calvert, T. E., and McConnell, R. 2002, "Transient Modeling of Coupled Magnetoelastic Problems in Electric Machines", Proceedings of the Power Engineering Society Summer Meeting, 21-25 July 2002, Vol. 1, pp. 281–287.

Rafinéjad, P. 1977, "Adaptation de la Méthode des Eléments Finis a la Modélisation des Systèm Electromécanique de conversion d' Energie", doctoral thesis, Grenoble.

Ren Z., Razek A. 1992. Local Force Computation in Deformable Bodies Using Edge Elements. IEEE Transaction on Magnetics, Vol. 28, No. 2 March 1992. pp. 1212–1215.

Reyne, G. 1987, "Analyse Theorique et Experimentale des Phenomenes Vibratoires d'Origine Electromagnetique", doctoral thesis, Grenoble, 1987, 267 p.

Ruuskanen, P. 1987, "Magnetomechanical Effect in Polycrystalline Iron and Nickel During Cyclic Stressing", doctoral thesis, Tampere University of Technology, publication 48, 126 p.

Sablik, M. J. and Jiles, D. C. 1993, "Coupled Magnetoelastic Theory of Magnetic and Magnetostrictive Hysteresis", IEEE Transactions on Magnetics, Vol. 29, No. 3, July 1993, pp. 2113–2123.

Sablik, M. J. and Burkhardt, G. L. 1995, "Biaxial Stress Effects on Magnetization Perpendicular to the Stress Plan", IEEE Transactions on Magnetics, Vol. 31, No. 6, November 1995, pp. 3665–3667.

Schneider, C. S. and Richardson, J. M. 1982, "Biaxial Magnetoelasticity in Steels", Journal of Applied Physics, Vol. 53, No. 11, November 1982, pp. 8136–8138.

Silvester, P. P., Ferrari R. L. 1991. "Finite Elements for Electrical Engineers". 2nd edition, Cambridge University Press, 344 p.

Takahashi, N., Nakata, T., Suhartono and Morishige, H. 1994 "Investigation of a Model to verify Software for 3-D Force Calculation", IEEE Transactions on Magnetics, Vol. 30, No. 5, September 1994, pp. 3483–3486.

Thompson J. E., Wilkins J. T. 1963. Harmonics in Transformer Noise, Electrical Times, 14 November 1963.

Vandeveld, L., Gyselinck, J. J. C., Melkebeek, J. A. A. 1998, IEEE Transactions on Magnetics, Vol. 34, No. 5, September 1998, pp. 3540–3543.

Vandeveld, L., and Melkebeek, J. A. A. 2001, "Magnetic Forces and Magnetostriction in Magnetic Material", COMPEL, Vol. 20, No.1, pp. 32–51.

Witczak, P. 1995. "The Magnetostriction Forces in the Induction Motor", COMPEL, Vol. 14, No. 4, pp. 229–232.

Witczak, P. 1996, "Calculation of Force Densities Distribution in Electrical Machinery by Means of Magnetic Stress Tensor", Archive of Electrical engineering, Vol. XLV, No. 1, pp. 67–81.

Zienkiewicz, O. C. 1977, "The Finite Element Method", London, McGraw-Hill, 787p.